DOCTOR OF PHILOSOPHY

Investigation of the structural changes in LDPE and XLPE induced by high electrical stress.

Sayers, Paul William Charles

Award date:
2001

Awarding institution:
Bangor University

Investigation of the Structural Changes in LDPE and XLPE Induced by High Electrical Stress

Paul William Charles Sayers

Thesis submitted to the University of Wales in candidature for the degree of Doctor of Philosophy
September 2001

School of Informatics
University of Wales
Bangor

PLEASE SCAN AND INCLUDE AS PART OF THE DIGITISED TEXT, THE LIST OF EXCLUSIONS INSERTED AFTER THE THESIS TITLE PAGE

Third party material to be excluded from digitised thesis:

Appendix A, Appendix B and Appendix C (not numbered)

Please return thesis to:

ETHOS RETURNS
Collection Management
Main Arts Library
Bangor University
College Road
Bangor, Gwynedd LL57 2DG

Summary

High voltage electrical cables play an immensely important, although largely unseen, part in the lives of everybody in the world today. They are mostly buried underground and provide trouble free operation for the majority of their operational lives. However, the polymer based insulation that is used for a large number of high voltage cables is subject to long term ageing which can eventually lead to electrical breakdown. This ageing manifests itself as the appearance of tree like structures in the bulk polymer insulator. The growth of a tree frequently starts on the boundary of the polymer at the so-called "polymer-semicon" interface.

This thesis is concerned, however, with the changes that must take place in the polymer before the tree is formed.

Previous investigations of field induced changes occurring within polymer insulation have involved cutting the polymer to expose the region of interest: this is not a satisfactory as the cutting process can produce changes in the polymer. To avoid this a novel technique was developed whereby the polymer-semicon interface can be exposed without cutting the polymer.

The interface region of the polymer in contact with the plane electrode was examined and even though the field in this region is less than at the point, it can be sufficiently large to induce structural change in the polymer, readily detectable by Raman spectroscopy.

In studies of both LDPE and XLPE, we find evidence of structural change within the polymer and most significantly of considerable Raman fluorescence which is indicative of defect states in the polymer. The latter becomes modified as the polymer structure approaches electrical failure.

The observations reported are set in context by the examination of the work of relevant authors and some conclusions deduced. The evidence supports a model in which the forces induced by the electrical field lead to failure by the mechanisms of local yield, microvoid craze and crack formation commonly invoked for the mechanical fracture of polymeric solids.

Acknowledgements

I would like to thank the School of Informatics, University of Wales, Bangor for all the help and assistance provided not only through the period of this PhD but also during my degree course. I would like to thank the people who worked at BICC Cables Limited before it became BICC General and then was sold to Pirelli Cables who closed BICC down. I would also like to thank the EPSRC for funding this work through a Co-operative Award in Science and Engineering (CASE) studentship.

As a result of these connections I have had the pleasure and honour of working with Professor T.J. Lewis and Doctor J.P. Llewellyn both of whom continue to astound me with their ability to absorb new ideas, generate original ideas and furthermore to critically review those ideas and theories. Doctor Carl. Griffiths, previously of BICCGeneral provided invaluable critical appraisal of the work, results and interpretations presented here. I would also like to thank Dr Steven Betteridge, also previously of BICCGeneral, for his help and insight especially in the area of Scanning Probe Microscopy. Doctor Stephen Hobdell and Mr Albert Rees for their help and invaluable assistance in the laboratory during the first year or two of this project. I offer a general word of thanks to the staff of the BICC Cables Energy Technology Centre at Wrexham (now ceased operations); the world of cables research is a poorer place for its demise.

I dedicate this thesis to the following people:

Above all to my wife Innys.

To my daughters Claire, Eleanore and Nicola and to my sons William, Keith and Paul (all of whom fortunately share my sense of humour).

Also to my friends, Dave Thomas [Amazing Cyclist] in the world of Cycling and Hugh Roberts 4th Dan in Shukokai Karate for dragging me away from the laboratory and back to the real world.

A special thanks to our close family friend, Janet Lancaster, for her care and support.

I thank them for their help and support.

1. Introduction

High voltage cables play an extremely important, if unseen, part of everyday life for most people. They are buried beneath the infrastructure of all urban conurbation's no matter how small and when they fail, not only is it very difficult to identify the point of failure, it is also very expensive and usually disruptive to correct the fault. It is also a fact that many of the cables installed in the last fifty years are coming to the end of their reliable operating life and replacement or failure is becoming overdue.

The long term electrical performance and ageing of these cables is still, despite much research in the area, poorly understood. There are many theories and models [Dang, et al., 1996; Parpal, et al., 1997; Ding, et al., 1994; for example], but no real consensus on how the ageing of cables, and in particular the insulating system, takes place or what the cause is. In general electrical ageing refers to a spectrum of effects that manifest themselves in HV cables with time, for example;

- Electrical Breakdown
- Electrical Discharge
- Tree Initiation and Propagation

Ageing of insulation is defined in IEC Publication 505 as "....irreversible deleterious change to the service ability of insulation systems. Such changes are characterised by a failure rate which increases with time". This definition demonstrates the lack of a real understanding of ageing in the very open

nature of the wording. A better definition for extruded HV cables is, perhaps, provided by Dang, et al. (1996), " .. any physical or chemical phenomena occurring under continuous HV application which would ultimately lead to electric breakdown of an actual HV cable (i.e. rated at greater than or equal to 69 kV)..".

The ageing and breakdown of electrical cables has been the subject of extensive research over many years and there are many theories as to the mechanism involved which will be discussed in this thesis. It is clear, however, that the development and growth of a tree in polymeric insulation subjected to electrical stress must be preceded by a number of stages in which the physical and chemical structure of the polymer is considerably reorganized and modified. The nature of these changes is only poorly understood but is the key to understanding the mechanism of electrical breakdown and hence to improving the performance of polymeric insulation.

Shimizu and Uchida *et al* (1991, 1992) have made extensive studies of treeing phenomena in Low Density Polyethylene (LDPE), using a point plane electrode geometry and have shown that deterioration occurs in the high-field region adjacent to the point before tree initiation. Using Fourier Transform Infra Red (FTIR) spectroscopy and Raman spectroscopy they were able to show that this region is characterized by enhanced concentrations of carbonyl C=O and carbon double bond C=C groups above those present in unstressed polyethylene. There was also evidence to support destruction of the lamella structure and an increase in the amorphous content of the polymer. To expose the deteriorated region near the tip electrode so that spectroscopic

study could be made, it was necessary to cut the sample into 100-micron thick slices. This introduces physical damage and may have influenced the results, especially as it is known that mechanical working of polymers can generate free radicals [Zhurkov *et al* (1974)].

The present study makes use of a point-plane electrode geometry but the region examined using Raman spectroscopy, FTIR and Scanning Probe Microscopy (SPM) is the interface between the polymer and the plane electrode. In this situation there is the considerable advantage that the plane electrode may be easily removed to expose the polymer interface for investigation without disturbing the sample. Even though the field in this region is less than at the point, it can be sufficiently large to induce structural change in the polymer, readily detectable by Raman spectroscopy. Furthermore a planar electrode interface is likely to be more representative of those obtained in practical high voltage equipment. For example, as will be shown, it is possible to examine the changes induced in the polymer at a carbon-loaded (semicon) electrode-polymer boundary corresponding to that in a high-voltage cable.

In studies of both LDPE and Cross Linked Polyethylene (XLPE), evidence is presented, not only for the generation of C=C and C=O bonds, but most significantly for considerable fluorescence which is indicative of defect states in the polymer. The latter becomes modified as the polymer structure approaches electrical failure.

Uchida and Shimizu *et al* (1991) have suggested that the double bonds created in the high field region arise from free-radical production as a

consequence of polymer chain scissions. They proposed that electrons injected from the cathode cause the scissions, either by direct collisions or indirectly via electron induced electroluminescence.

An alternative view, suggested here, is that the evidence supports a model in which the forces induced by the electrical field lead to failure by mechanisms of local yield, microvoid craze and crack formation that are commonly invoked for the mechanical fracture of polymeric solids. This model does not require direct electron intervention.

2. Power Transmission Cables

The primary objective of this thesis is to investigate electrical breakdown originating at the interface between the bulk polymeric insulator and the inner semi-conducting layer surrounding the main conducting core. This requires an outline understanding of power transmission cable construction together with the morphology and rheology of the component parts and the nature of the interface between these components. This is necessary in order to appreciate the approach taken during the course of the experimental work and in order to properly evaluate the results presented.

2.1. Basic Construction

Power transmission cables have developed into a complex structure produced by a triple extrusion production process. The main components of a modern power cable consist of a low resistance conducting core, a semi-conducting screen, a cross-linked low-density polyethylene (XLPE) insulator and an outer semi-conducting screen. Depending on the intended application there may be a metal sheath for moisture protection and armouring or even external cooling systems.

The use of the semi-conducting screens around both the conducting core and the XLPE insulator is incorporated to reduce local field enhancement, primarily in the neighbourhood of the interface between the conductor core and bulk XLPE insulator. The XLPE insulator will usually have a range of additives introduced at the manufacturing stage. These will include anti-oxidant and ultra-violet radiation damage inhibitors in addition to cross-linking

agents. The semi-conducting screening material will typically be a carbon-loaded polyethylene. The cable models examined in these experiments were constructed in this manner from cross-linked polyethylene insulator and carbon loaded polyethylene semi-conducting screening material. These individual components will be discussed further in the following sections.

The basic construction of a power transmission cable is shown in figure 2.1.

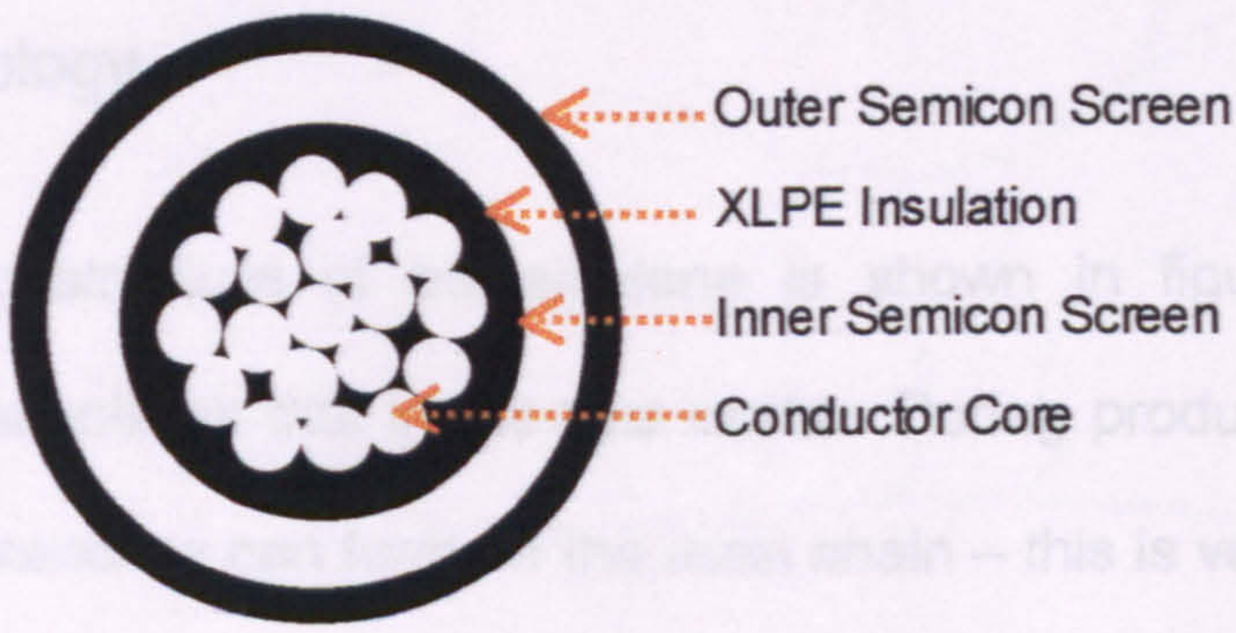

Figure 2.1 Cross-section of a typical triple extruded power transmission cable.

2.2. Polyethylene

Polyethylene is a long chain macromolecule having repeating monomer units of ethylene arranged as shown in figure 2.2.

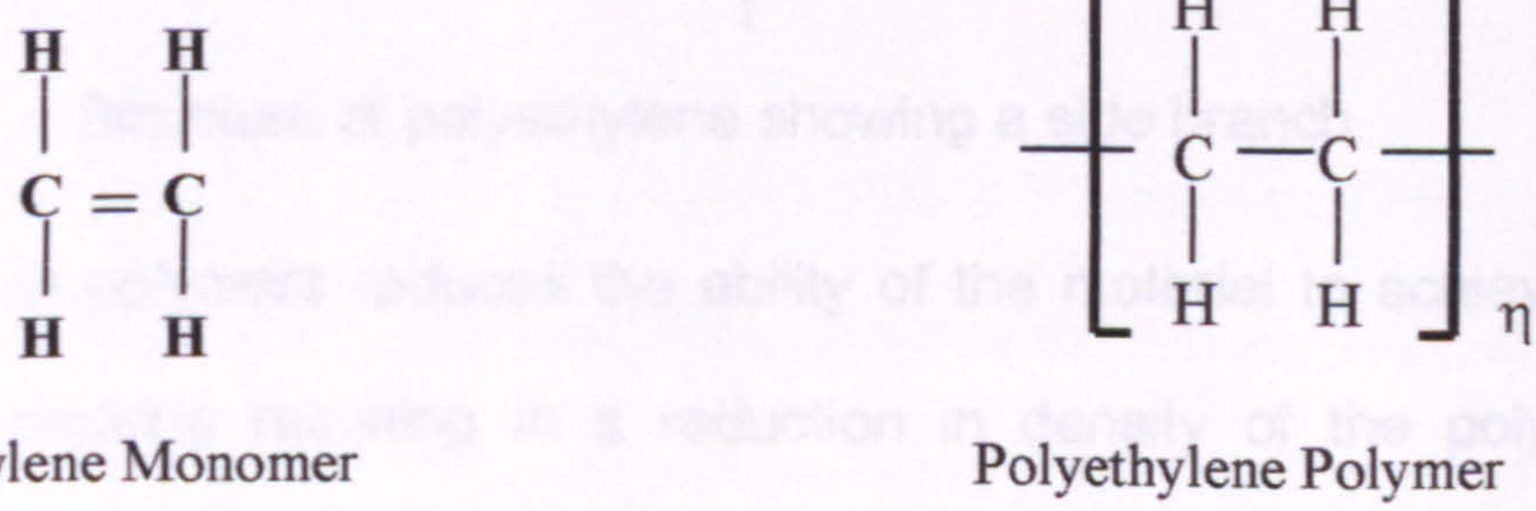

Figure 2.2 Ethylene Monomer and Polymer, η is the degree of polymerisation and is, in general, very large typically in the order of 10^3 to 10^5.

Polymers have found wide acceptance as cable insulation materials because they offer extremely good insulation properties (high electrical breakdown strengths - typically ~10^9 $V.m^{-1}$ together with being easy to include in mass production techniques. Additionally they show good resistance to corrosion and are available with a wide range of stiffness and mechanical strength specifications.

2.2.1. Morphology

Although the basic structure of polyethylene is shown in figure 2.2 the situation is not as simple as that in the real world. During production of the bulk polymer side branches can form off the main chain – this is very common in polyethylene, the resulting structure being shown in figure 2.3.

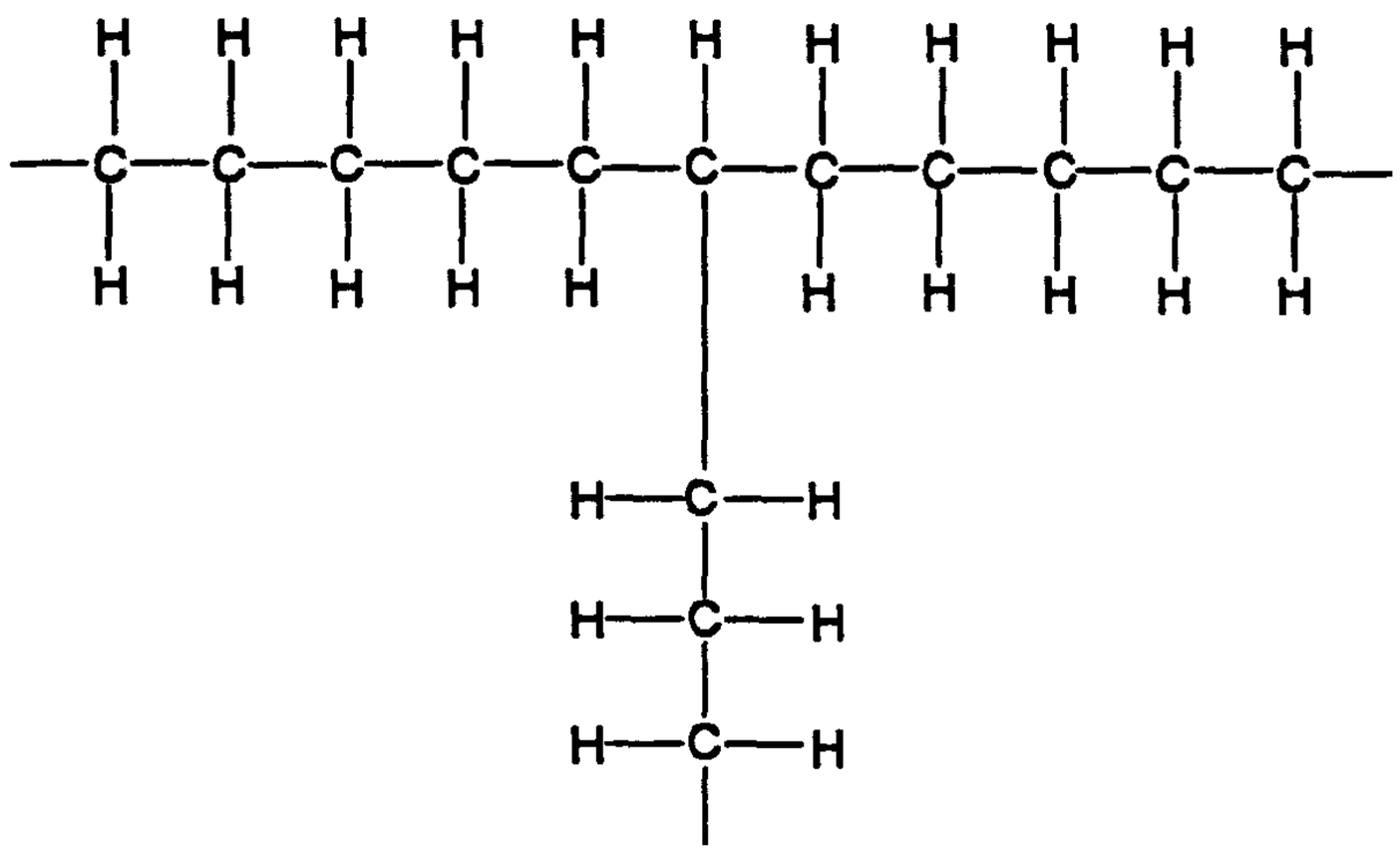

Figure 2.3 Structure of polyethylene showing a side branch.

Branching in polymers reduces the ability of the material to achieve regular molecular packing resulting in a reduction in density of the polymer. In polyethylene this results in Low Density Polyethylene or LDPE.

Another form of branching known as cross-linking can take place in a polymer. This involves the generation of links between the long polymer chains as shown in figure 2.4.

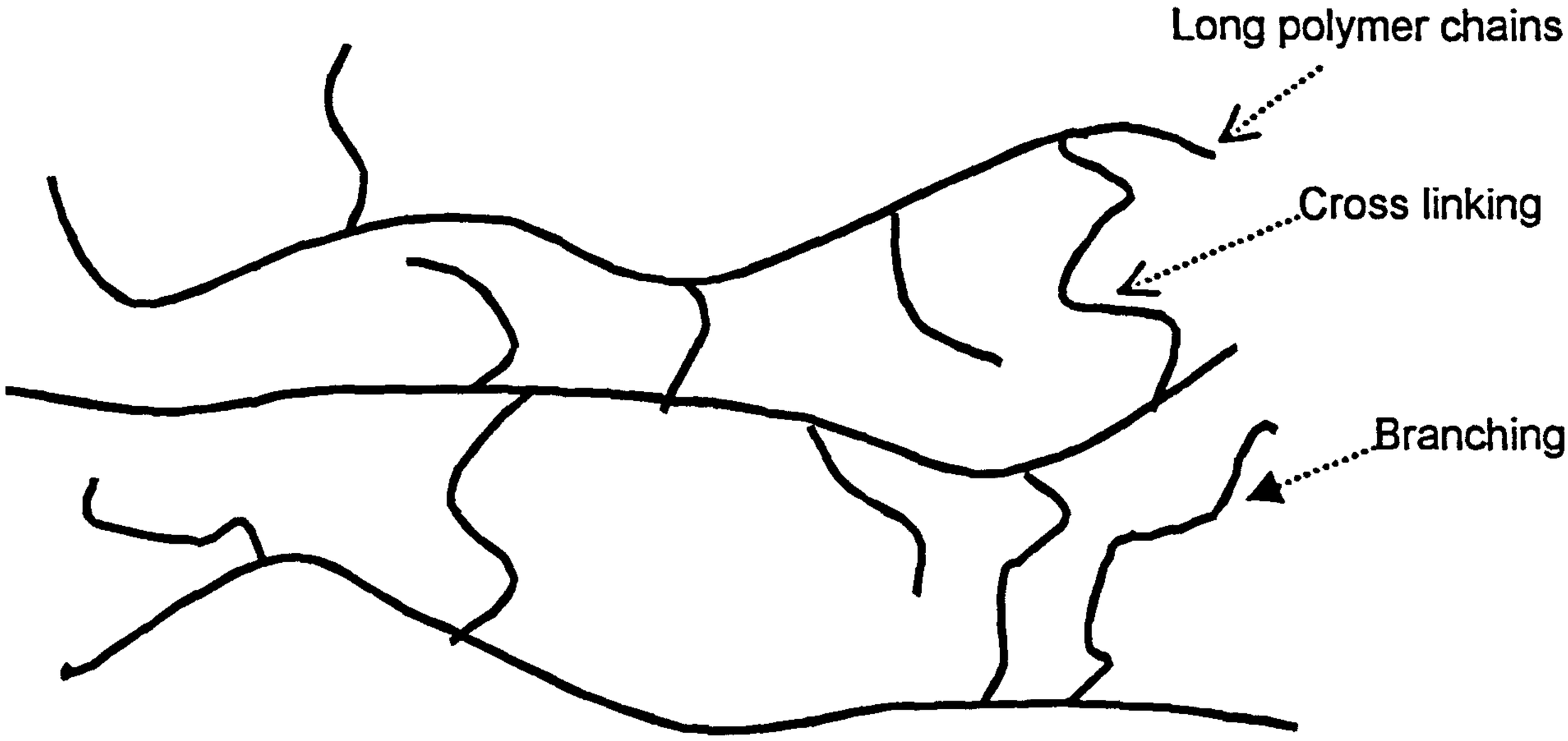

Figure 2.4 Sketch showing long polymer chains with branches and cross-links between the chains.

Cross-linking improves the structural strength of the polymer and has the added advantage of increasing its melting point. Cross-linked PE insulation has an operating temperature of 80 to 90°C as opposed to the operating temperature for LDPE of 70°C. Cross-linking is usually achieved by the addition of 1-2% of dicumyl peroxide, which does not react until the manufactured cables are treated using high pressure nitrogen gas at elevated temperatures.

The above description relates to the situation at the molecular level, however to view the morphology of bulk polyethylene one must step back and observe how these individual molecules behave when they are part of the bulk material. When the polyethylene melt cools the individual polymer chains tend to arrange themselves into lamellar crystals. The polymer strings will be

folded many times within a single lamella, some of the them leaving one crystal and entering another forming tie molecules between the lamellar crystals. The material between the individual lamella lacks order and is known as the amorphous region. This generally accepted view of how the individual polymer chains organise themselves within bulk polyethylene is shown in figure 2.5.

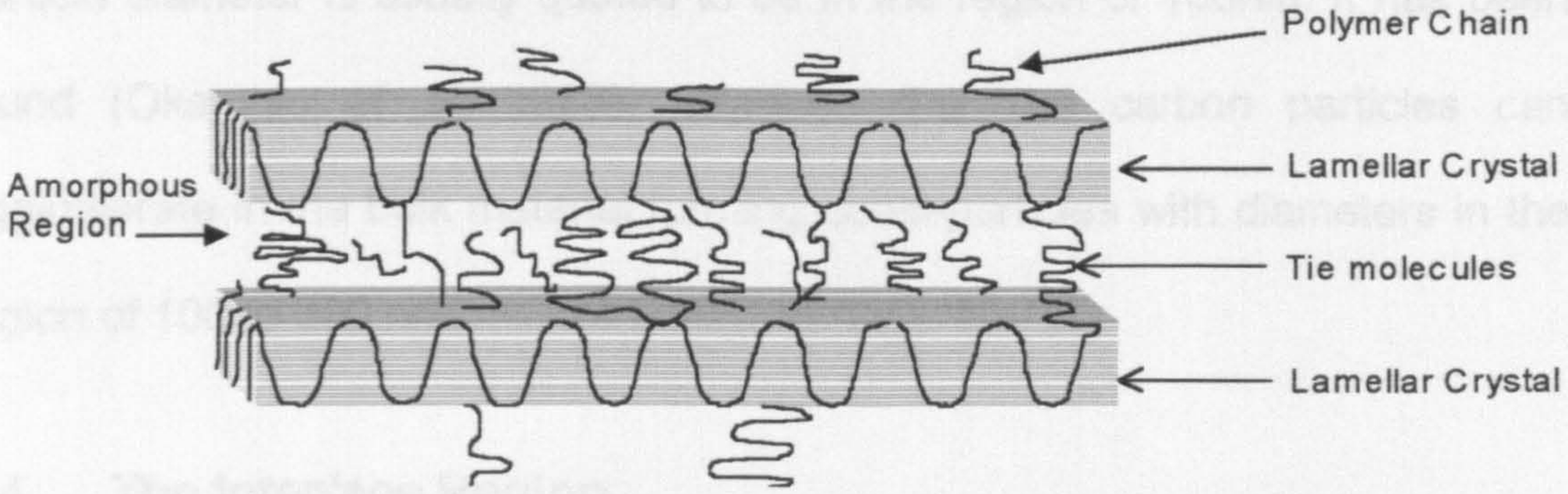

Figure 2.5 Schematic showing two lamellar crystals and the tie molecules binding them together.

The amorphous and crystalline phases are often considered to be different materials. They will possess for instance different electrical and and mechanical properties. The amorphous phase has a lower density than the crystalline phase and therefore has a higher free volume. Free volume, in relation to LDPE is the difference between the specific volume of the actual material and that of the close packed equilibrium form at the same tempreture. In the case of amorphous polymers the free volume arises from the fact that the chain structure and steric hinderances prevent all potential lattice sites from being occupied.

The amorpous region is a volume of material where defect sites are likely to be created during electrical stressing of the polymer because of the greater potential for mobility of the individual polymer chains.

2.3. Semi-con Screening Material

The semi-conducting screens around both the core conductor and the XLPE insulator consist of a polyethylene base material with the addition of fine carbon particles in order to increase its conductivity. Furnace black and acetylene black are the two most common forms of carbon in use today: the particle diameter is usually quoted to be in the region of 100nm. It has been found (Okamoto *et al*, 1988), however, that the carbon particles can agglomerate in the bulk material forming quasi-particles with diameters in the region of 100 to 300 nm.

2.4. The Interface Region

The interface between the semicon screening material and the bulk insulator has a major influence in determining the performance of XLPE cables. It is a boundary where local electrical fields are likely to be intense, across which space charge can be injected and the region in which electrical trees are likely to be initiated. It is also the transition region between the bulk XLPE and the carbon-loaded semicon producing a region of changing morphological, rheological and chemical structure.

During electrical stressing of cable structures, such as occurs during normal operational usage, this interface is subjected to varying degrees of electrical stress and, according to the Electro-Mechanical model of ageing as proposed by Lewis *et al,* 1996, mechanical stress. A key feature of this model, which will be discussed later, is the degradation of the polymer by this electrically–induced mechanical stress. This is predicted to happen at an early stage in

the pre-electrical failure scenario well before any gross physical signs would manifest themselves.

The change in the structure of the materials involved is exacerbated by the less than ideal conditions that exist at the interface region. The actual interface region presents, at the micron level, a volume full of micro protrusions as shown in figure 2.6 these can lead to field enhancement taking place.

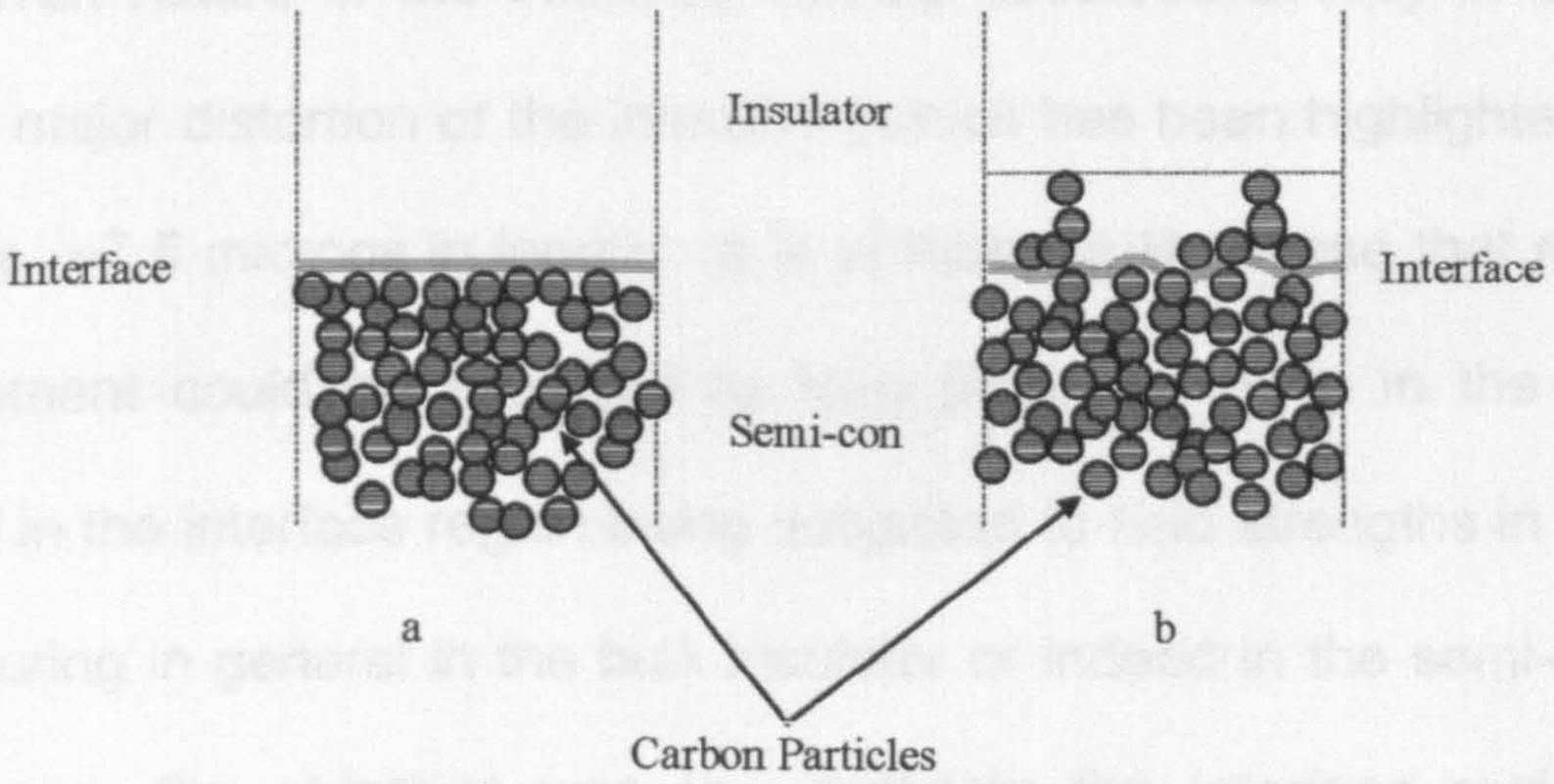

Figure 2.6 Diagram showing diffusion of carbon particles into insulator layer. (a) Shows an ideal interface whilst (b) shows a typical interface layer. Note the sharp semi-con points in (b).

The ideal interface, a in figure 2.6, presents a regular even interface between the carbon-loaded polyethylene and the bulk polyethylene insulator which avoids the possibility of any field enhancement at the edges of any protuberances. The interface region in the real world however has been found to resemble the situation shown in figure 2.6 b. (Betteridge *et al*, 1998.) These findings were confirmed by the author using the Scanning Probe Microscope as shown in figure 2.7.

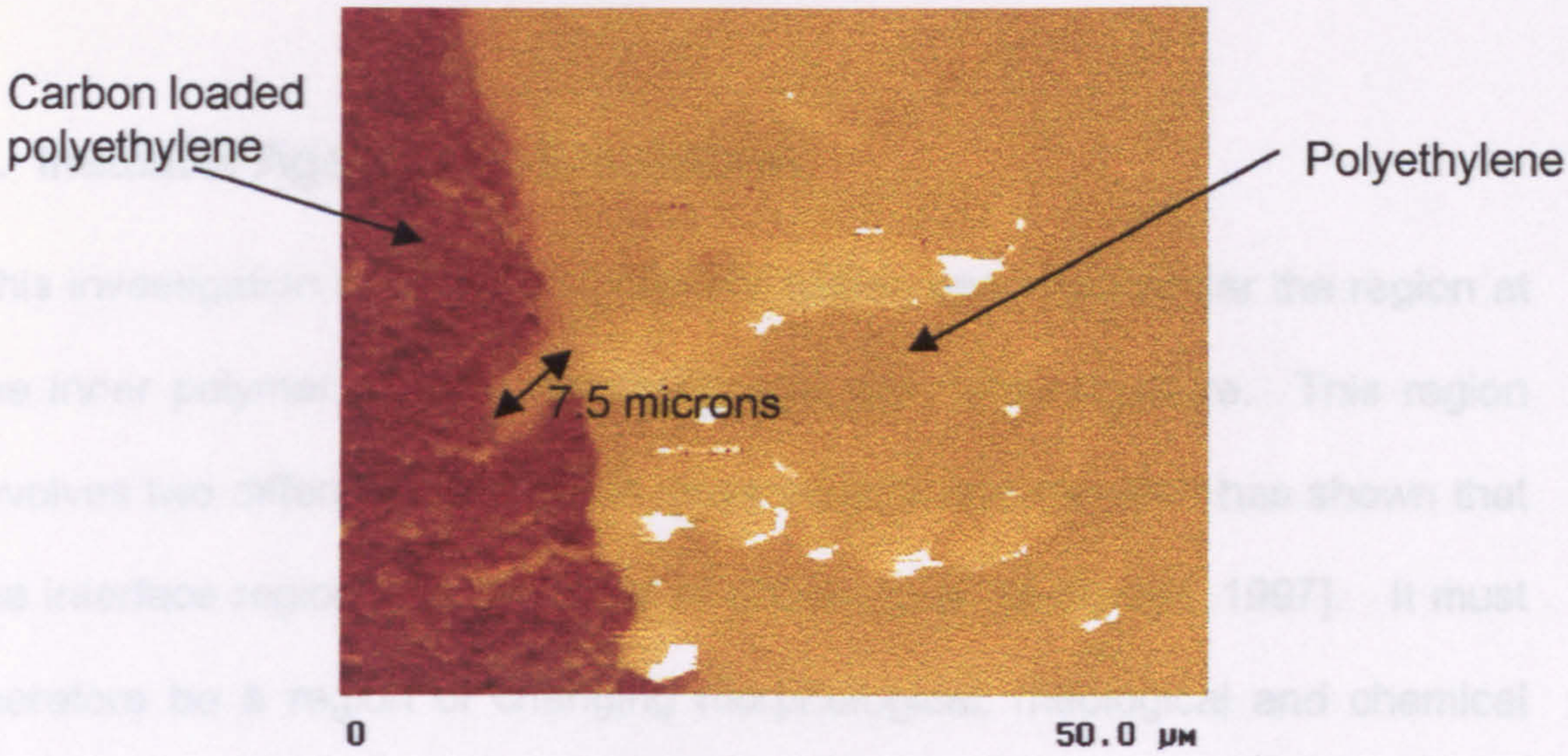

Figure 2.7 Showing the interface region between the bulk insulator and the carbon loaded polyethylene.

The uneven nature of the interface can be observed directly in this image where a major distortion of the interface (which has been highlighted) can be seen it is ~7.5 microns in length. It is at features like these that major field enhancement could be expected to take place, resulting in the materials involved in the interface region being subjected to field strengths in excess of that occuring in general in the bulk insulator or indeed in the semi-con layer.

In this work the objective was to duplicate the interface region in the laboratory so that the effect of enhanced electrical fields on the bulk insulator could be observed both as a function of time and field strength.

3. Insulator Ageing and Breakdown.

This investigation is concerned with HV cables and in particular the region at the inner polymer – semi-con interface of the cable structure. This region involves two different materials in close contact and research has shown that the interface region is of the order of 600nm wide. [Bettridge, 1997]. It must therefore be a region of changing morphological, rheological and chemical structure and this was confirmed in part by the work of Bettridge. On one side of the interface is a relatively homogeneous material, the polymer insulator, whilst on the other side the semi-con is basically a polymer with contaminants (in this case carbon particles) deliberately introduced. The ideal interface region between the two materials would be smooth with no mixing between the two materials. However when the cables are extruded they are at a temperature of approximately 100° C and this must inevitably lead to softening of the materials and mixing at the interface region.

When electrical breakdown of HV cables has taken place and electrical trees have been identified as the cause it has been found that the major initiation site is the interface region. There has been very little investigative work into this region especially involving actual cable samples at the point of breakdown initiation.

3.1. Tree Initiation

Insulator degradation manifests as the appearance of treelike structures in the bulk` material. However before these structures develop there is an initiation phase when there are no changes taking place in the material, visible to the naked eye. Partial discharges were considered by many (Dissado et al 1992) to be the initial indicators of impending tree growth and subsequent electrical breakdown of the material. However with improved manufacturing techniques the inclusion in the bulk material of defects likely to give rise to stress enhancement is largely eliminated reducing the occurrence of partial discharges. In manufacturing terms this means that the insulator size can be reduced resulting in lower costs. This leads to higher power densities in cables and prebreakdown phenomena, previously not considered, to possibly become the main factor leading to tree growth. These phenomena are more difficult to detect than partial discharge effects and more sensitive detection techniques are required to deduce the chemical and structural changes that could be taking place.

Electroluminescence is one method being used to attempt to detect the occurrence of prebreakdown changes in the material. Several researchers have investigated this method to detect the initiation phase of tree structures, Laurent et al 1999, Bamji 1999, Mary et al 1997 and Champion et al 1995 for example.

Bamji et al (1991) showed by embedding semicon protrusions into XLPE and applying high electrical fields at these points would lead to

electroluminescence at the semi-con tip. It was also shown that the application of electrical stress lead to degradation of the polymer and the formation of electrical trees. Bamji et al (1999) also demonstrated that the presence of oxygen in the free volume of the XLPE plays an important role in the degradation of the polymer.

Laurent et al (1999) used a flat electrode arrangement to monitor the electroluminescence seen whilst applying electrical stress across the sample. Laurent makes some important observations, that ageing is a localized process and that ageing proceeds through the molecular dissociation of some of the original constituents of the material and the formation of new chemical bonds. The latter observation, as Laurent points out, necessitates the mediation of electronically excited states.

It is important to be aware that in both of the specific cases discussed above and in the more general research being undertaken elsewhere the emphasis is on the observation of electroluminescence whilst the electrical stress is applied. As will be explained in chapter 5 the techniques applied to produce the results seen in chapter 6 enable the observation of field induced fluorescence but after that field has been removed.

3.2. Insulator Degradation through Treeing.

Treeing is a phenomenon observed in electrically stressed polymers. During the early stages of development trees are small dendritic like growths consisting of voids in the polymer which may be only ~ 10^{-4}m long. As ageing progresses these tree like structures grow until at the point of electrical breakdown one of them spans the polymer from one electrode to the other. The main branches of the tree are usually ~30-100 nm in diameter. (Hozumi *et al*, 1988)

Insulator degradation through treeing has been accepted as one of the most important mechanisms responsible for the ultimate electrical breakdown of insulators and in particular in polyethylene when used as an insulator in HV cables. [Dissado, *et al.*, 1992]

There are two main categories of trees, Water Trees and Electrical Trees. It is possible that a water tree may initiate an electrical tree and that on the occurrence of either of these breakdown of the insulator is likely but not inevitable. Indeed electrical trees have been observed to cross the insulator without breakdown occurring whilst it is also possible for breakdown to occur without the electrical tree completely crossing the insulator. The appearance of treeing structures in polymers is a gross indicator of insulator damage occurring but not necessarily the prime cause of electrical failure.

3.2.1. Water Trees

Water trees can be generated in an environment where the insulator has direct access to an aqueous electrolyte and they can be conveniently split into two types, vented trees and bow tie trees. Vented trees are initiated at the surface layer of the insulator and have direct access to a moisture source.

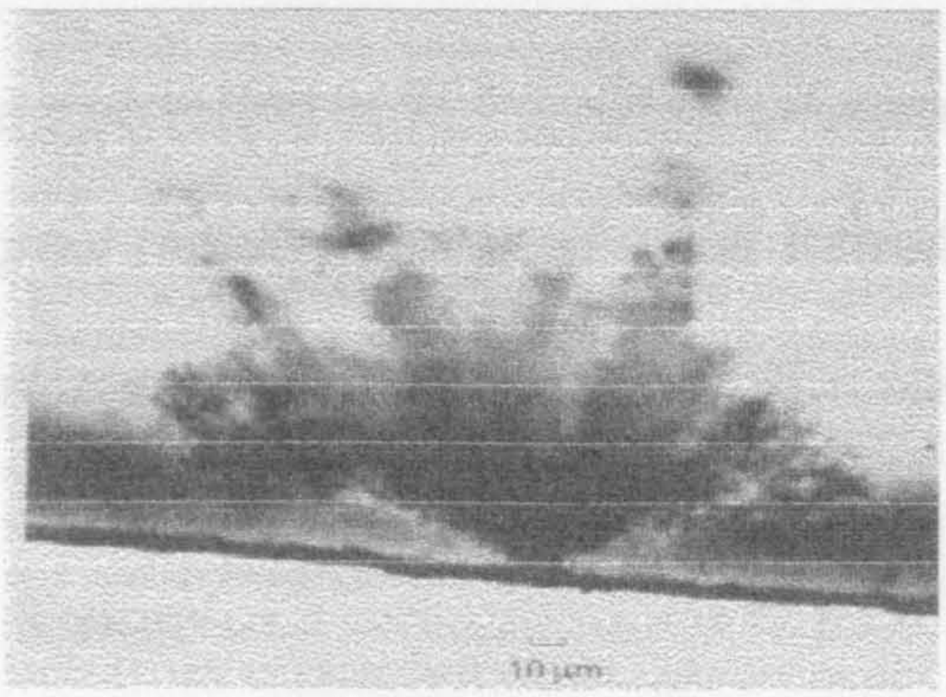

Figure 3.1 Typical vented water tree in XLPE cable.

As can be seen in figure 3.1 vented water trees exhibit no distinct structure but rather have a diffuse bush like appearance with a definite link to the surface layer. Vented trees are thought to grow more or less continuously in an applied field once initiated and may therefore reach the other side of the insulator providing a possible path for electrical breakdown.

Bow tie trees are initiated at the site of imperfections, contaminants or cavities in the bulk material. They grow in a roughly symmetrical fashion along the line of the applied electric field.

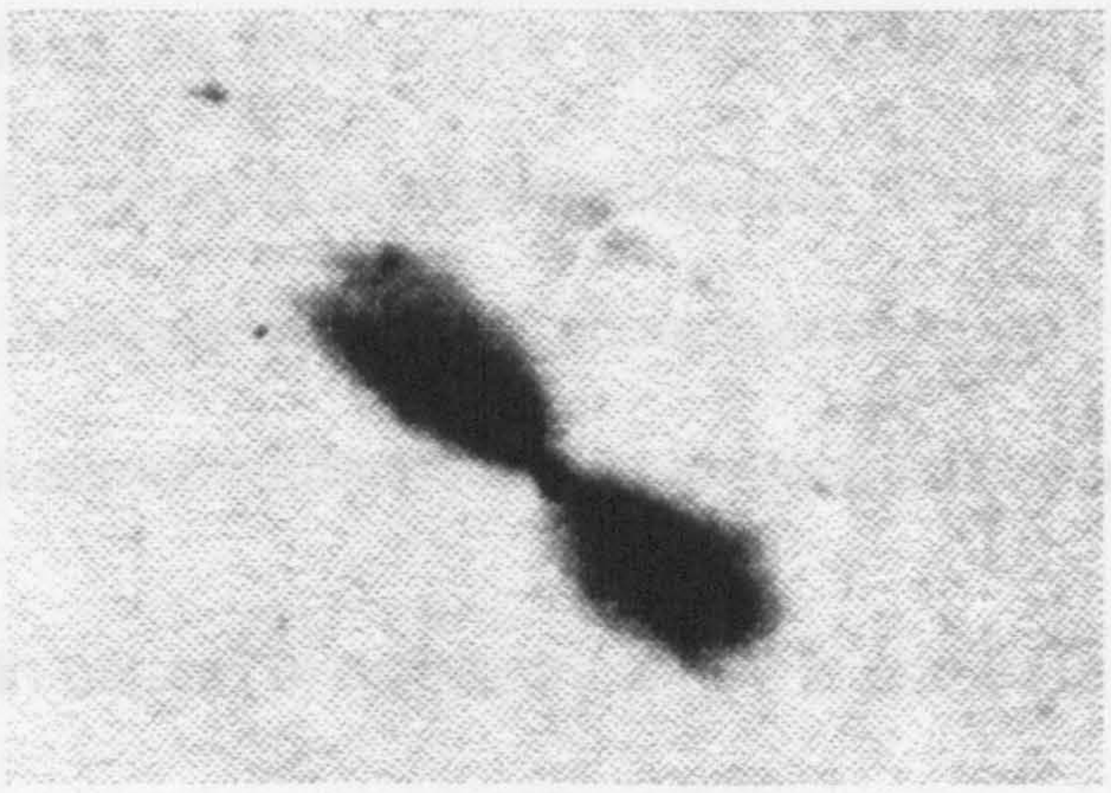

Figure 3.2 A bow tie tree found in XLPE cable. Dissado et al. (1992).

Bow tie trees at first grow rapidly after their initial formation but they stabilise after reaching a certain length usually at ~10^{-12} m. [Dissado, *et al.*, 1992]

3.2.2. Electrical Trees

Electrical trees, in general, have a much more clearly defined tree like structure than water trees and some researchers consider that they originate in areas of the bulk material having defects, contaminants or structural irregularities (e.g. voids or microcavities).

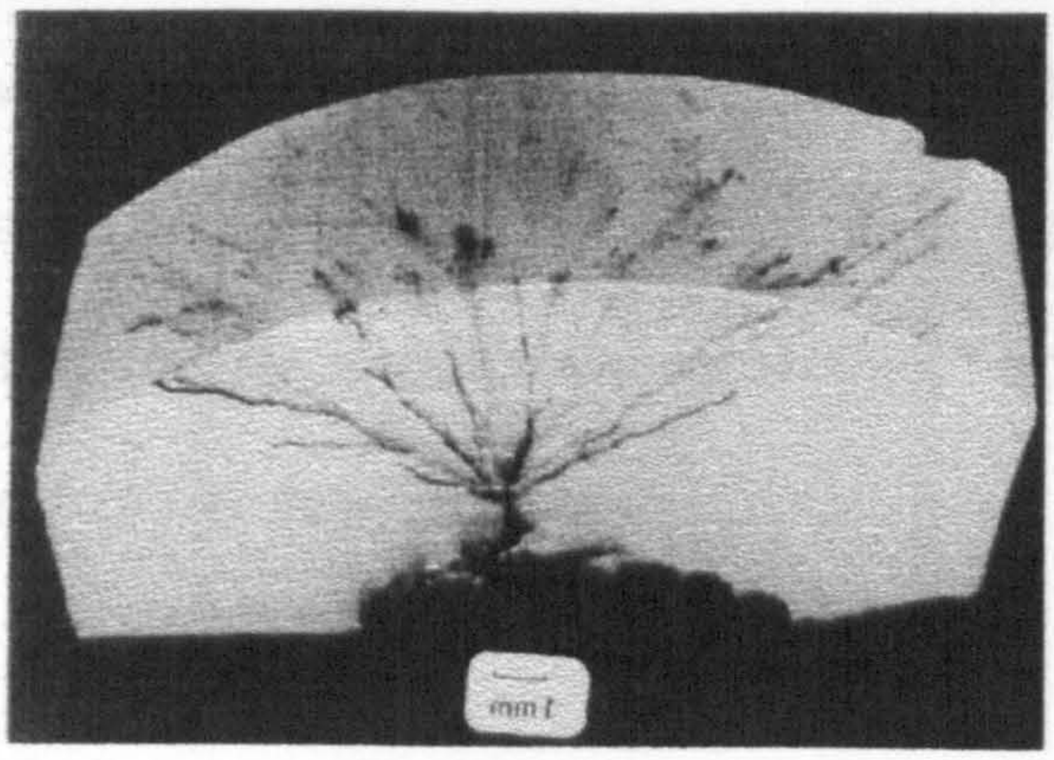

Figure 3.3 Electrical Tree in XLPE cable. [Dissado, *et al.*, 1992]

Electrical trees may also be initiated at the site of an electrode in which case they are known as vented electrical trees. Trees initiated in the bulk material

are orientated along the lines of the applied electrical field. Electrical trees have been found to grow at a decelerating rate [Dissado, *et al.*, 1997] until a certain point is reached when an acceleration of the growth rate occurs (resembling an avalanche effect) leading to electrical breakdown.

The typical growth pattern of an electrical tree is shown in figure 3.4,

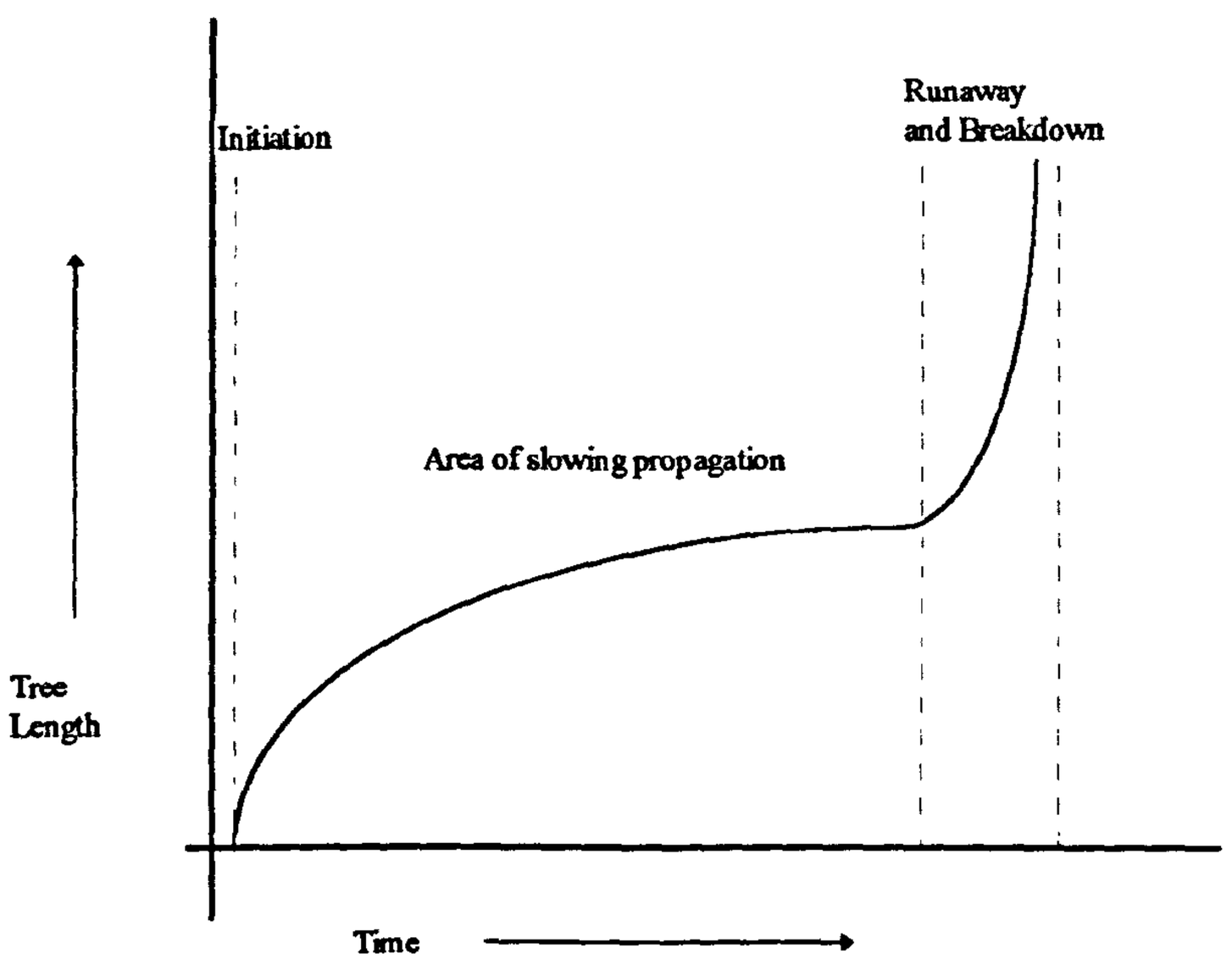

Figure 3.4 Schematic representation of electrical tree growth showing the decelerating growth rate and then the runaway or avalanche breakdown. [Dissado, *et al.*, 1992].

Dissado, (1997) however postulates that the "...electrical trees in solids which demonstrate a fractal structure and decelerating growth rate are a consequence of a deterministic breakdown mechanism operating in a regime of deterministic chaos, rather than runaway".

3.2.3. Review of Ageing and Breakdown Models

There are a large number of theories and models which attempt to give a scientific basis for the ageing of extruded HV cables, both as functions of time and applied electrical stress. Dang, *et al.* (1996), review over 200 papers covering the period 1965 to 1996. They found that most data presented was obtained under conditions that did not allow comparison and in any case were different from actual operating conditions. They list over 20 papers giving details of twelve theories which relate to the ageing of extruded HV cables, whilst Scarpa (1995) and Dissado *et al*, (1992), categorize the ageing models into three groups, Physical Ageing, Chemical Ageing and Electrical Ageing. It should be appreciated that all these mechanisms can be expected to play their part in the ageing of insulators depending on the operating conditions. Dissado describes this as "combined mechanical and electrical ageing".

The degradation of the polymer insulation with time in terms of its physical and chemical properties will eventually lead to the electrical breakdown of that polymer. Scarpa (1995) defines electrical breakdown as "when the applied voltage can no longer be maintained across an insulator in a stable manner without excessive flow of current and physical disruption." When this happens the material is said to have failed, however the exact failure mechanism has not as yet been established. What is certain, however, is that all breakdown in polymeric insulators is irreversible and catastrophic.

Dissado, *et al*, (1992), making a distinction between ageing and breakdown suggest that breakdown mechanisms can be divided into four categories,

"Electrical Breakdown", "Thermal Breakdown", "Electromechanical Breakdown" and "Partial Discharge Breakdown". There is usually assumed to be a link between the ageing and electrical breakdown of the insulator and the popular models seek to combine these aspects. Scarpa (1995)' and Dissado (1992) agree that models of ageing and breakdown mechanisms may be conveniently divided into three categories: -

I Low Level (Molecular) Degradation Models

In these models the insulator characteristics at the molecular level are deleteriously affected by an applied electric field possibly in combination with other factors.

II Deterministic Models

These models attribute the final electrical breakdown of the insulator to the direct effect of an earlier event or condition produced when a critical electrical field value is exceeded.

III Stochastic Models

Here there is considered to be a finite probability that at any time the breakdown may occur following local changes in the physical conditions or electric fields caused by an inhomogeneous material.

The most recent research has been conducted in areas of I and III whilst deterministic models have not been as productive in terms of possible life prediction models.

3.2.4. Low Level Degradation Models

3.2.4.1. Physical Ageing

This model of the ageing process is also known as the free volume model, as it proposes a reduction in the free volume of a material. "Free volume" is defined as the difference between the specific volume (inverse of specific gravity) of the actual material and that of the close packed equilibrium form of the same material at the same temperature. The free volume is made up of "structural holes" formed when some potential lattice sites remain unoccupied due to inefficient molecular packing. These holes are different to the microscopic cavities or voids already discussed (3.2.2) which have a radius of ~0.1μm or larger and smooth surfaces.

This process is self-retarded as the segmental motion that accounts for chain rearrangement slows down as the free volume itself is reduced. Struik (1978) proposed that mechanical stresses driving segmental motions could also generate free volume. Other researchers [Lustiger, *et al*, (1986)] pointed out that since segmental motions can be driven electrically as well as mechanically such process allows for electric coupling between free volume degradation and dielectric processes on a molecular scale. Indeed, Barlow, (1983), found that one effect of a high level of stress on polyethylene was to increase the microvoid density and size. The sample in this case originated from a virgin cable.

Another problem which can occur in physical ageing is that the number of interfaces between amorphous and chain fold regions can increase [Dissado

(1992)] giving rise to an increasing density of traps and defects and therefore an increase in local space charge concentration. [Nath , *et al*, (1989), Perlman, *et al*, (1986)].

Other problems include the thermal variations in operating conditions experienced by power cables, due to I^2R losses which can generate temperatures up to 90° C, far in excess of ambient temperatures. As many of these cables are buried underground heat dissipation becomes a major problem. This can cause thermal disarrangement of the molecular structure including the acceleration in the production of microcavities [Smit, (1984)] which can be deleterious to the cable.

3.2.4.2. Chemical Ageing

This model of ageing [Reich, *et al.* (1971) takes place following the formation of polymer free radicals (R*),

$$X + R_{a+b} \longrightarrow R^{\bullet}_{a} + R^{\bullet}_{b} \qquad (3.1)$$

where X is an initiation step.

Free radicals are very reactive chemically, this can produce chain reactions resulting in chain scission, [Ross, *et al.* (1992)]. The formation of these free radicals can be initiated thermally, mechanically or may result from oxidation, ionising radiation or UV absorption.

In addition when talking about chemical ageing it must be understood that some chemical processes, such as cross-linking (Section 2.2.1), remain active for some time after being initiated artificially. [Struik (1978); Bhateja (1983)].

Bhateja noted that in the case of HDPE cross-linking initiated by radiation continued for up to 2.5 years. Other chemical changes can continue in this fashion and unlike cross-linking in polyethylene they are not advantageous to the properties of the polymer, some for instance lead to oxidation and crystallisation of the polymer. Changes resulting from continued chemical processes such as this can be expected to lead to increased susceptibility of the material to electrical breakdown and degradation.

The use of additives in the polymer must also be mentioned. Barlow et al (1983) observed that antioxidants added to polyethylene could actually migrate out of the material leaving voids or aggregate into clusters about 25μm in size [Thue, *et al.* (1983)]. Such clusters have led to stress cracking, oxidation (instead of suppressing it) and evidence has been reported [Thue, *et al.* (1983)], linking their formation with that of treeing failure in cables in service.

3.2.4.3. Electrical Ageing

The physical and chemical processes described above can occur whether there is an applied electric field or not. However, the presence of an electric field can accelerate, initiate and drive those physical and chemical processes.

Electric fields can also promote the following effects:-

- Dissociation and transport of ionized and ionizable by-products, this can cause an increase in local stress patterns with a subsequent deterioration in insulation performance.

- Water Trees; these require the presence of moisture to be initiated and can lead to complete electrical failure.

- Partial Discharges. There is published work proposing that these can occur within micro-cavities or voids when the electric field exceeds a threshold value, the actual threshold value depending on void size and local gas pressure, [Bahder, *et al* (1982).; Mason, (1981)].

- Electrical Trees as discussed in section 3.1.

3.2.5. Deterministic Models

As already discussed, deterministic models attribute the final electrical breakdown of the insulator to the direct effect of an earlier situation when a critical electrical field value was exceeded. The various forms of breakdown will be discussed using the categorization suggested by Dissado (1992).

3.2.5.1. Electronic Breakdown

Zener breakdown and avalanche breakdown are the two best known examples of electronic breakdown. However for polymers where the band gap is large (>~8eV) then electric fields exceeding ~ $1x10^{10}V.m^{-1}$ would be required to produce Zener breakdown. In the case of avalanche breakdown although the required conditions have been shown to exist [Ritsko (1982); Zeller, *et al* (1984)] for polyethylene the average applied field is unlikely to be high enough for breakdown to occur in the bulk material. It is possible that localised electric breakdown of this form may occur at the tips of electric trees or as a result of space charge build up near electrodes due to very high localised fields.

In terms of an electrode-polymer interface it has been shown, Jonscher and Lacoste (1984), that tunnel-injection of electrons from the electrodes can limit the breakdown field to magnitudes of about $1x10^{9}V.m^{-1}$.

3.2.5.2. Thermal Breakdown

Thermal breakdown occurs when cumulative heating effects, specifically joule heating, lead to increased carrier numbers and mobility giving rise to

increased conduction and ultimately "thermal runaway". This has been observed to be a bulk phenomenon, Klein (1969). However this form of breakdown usually leads to a localised filamentary breakdown path.

3.2.5.3. Electrically Induced Mechanical Breakdown

Dissado (1992) describes this as "the electrostatic attraction of the electrodes which decreases the width of the insulation by an amount depending on Young's modulus." This reduction in insulation width increases the field, thereby increasing the attraction, local heating and softening then exaggerate this.

Dissado, therefore, is talking of a bulk process and he makes the point that even if polyethylene insulated power cables are operated above the softening point "...then they are usually cross-linked and sufficiently thick for this effect to be negligible."

3.2.5.4. Partial Discharge Breakdown

Within the bulk material of a polymer insulator there will inevitably exist small voids or cavities and these will contain gas and therefore have a lower permittivity than the bulk polymer. Depending on the gas and the local pressure the applied field may cause breakdown or discharge within the void. This effect is usually local and is therefore termed Partial Discharge Breakdown.

Cavities are an unavoidable consequence of manufacture. In particular the various processes which are applied in order to improve one or another attribute of the insulator may themselves introduce voids. For instance, cross-

linking can introduce voids and the introduction of impurities (such carbon particles from the semicon interface) may also create voids or cavities.

Partial discharge breakdown can also promote the formation of electrical trees which themselves can lead to breakdown of the bulk material.

3.2.6. Stochastic Models

Stochastic models use empirical statistical distributions to develop predictions of physical breakdown.

Scarpa (1995), lists the following stochastic models,

- The Fluctuation Model [Dissado, *et al* (1987)]
- Fractal Models [Barclay, *et al* (1990).; Dissado, *et al* (1987).]
- Cumulative Defect Models [Lloyd, *et al.* (1977); Jonscher, *et al.*(1984)]

3.2.6.1. The Fluctuation Model

The Fluctuation models assume that the material is divided into small local structural units. These units or clusters are composed of atoms, molecules, chain segments and other structural elements whose displacement motions are connected. [Dissado, *et al.* (1992)] Under the influence of an applied electric field the intrinsic fluctuations of the system will cause the aggregation or fragmentation of the clusters. When an electric field is applied to the bulk those clusters possessing a polar charge will modify the magnitude of the local electric field by polarisation or depolarisation. These intrinsic fluctuations of the local fields within the bulk system will be spread over a range of values

with a probability that at some point the field of a particular cluster will exceed the breakdown value.

3.2.6.2. Fractal Models

The Fractal models explain the tree like discharges as examples of branched stochastic fractals [Barclay, *et al* (1990) Niemeyer, *et al.*(1984); Dissado, *et al.*(1987)].

3.2.6.3. Cumulative Defect Models

The cumulative models assume that the eventual breakdown of an insulator is not linked to a single event, but rather to individual processes that combine to generate new defects and extend existing defects until breakdown is inevitable.

3.2.7. Space Charge Considerations

Space charge accumulation in insulating materials is widely recognised as being one of the causes of deterioration in HV cables and several methods are available for the measurement of space charge. [Abou-Dakka, *et al.* (1997)]

Stucki (1994) proposed a model based on space-charge injection under high fields leading to cumulative effects. A critical total injected charge density Q_c is suggested as being necessary prior to any permanent damage occurring. Using this concept he postulates that a critical total charge injected or de-trapped per unit area leads to micro-voids and subsequently tree formations.

Zebouchi [Zebouchi, *et al.*, 1997], also considered the effects of pressure and temperature on space charge. Their model combines thermal and electronic breakdown models taking into account the charge carrier hopping transport mechanism and local field distortions due to space charges.

The effect of heat treatment and vacuum treatment on the formation of space charge in XLPE cables is discussed by Wang *et al* (1995). They discovered that if the cable was heat-treated, space charge previously formed under an applied voltage, disappeared. If electrical stress was applied once again space charge reformed, however if they then degassed the sample and heated it for a long time not only did the space charge disappear but also the re-application of a dc voltage failed to create space charge in the cable. These results may well be related to those of Bamji et al (1991) where they

relate the presence of oxygen in the free volume of insulators to the eventual degradation of that insulator.

Different mechanisms of charge trapping are discussed by Dissado *et al.* (1995) and incorporated into a life model "..through an alteration to the free energies of the reacting system." They show that trapped charge can contribute to the ageing of insulators when conditions exceed suitable temperature or field threshold values. They also make a tentative suggestion that the "...stored mechanical energy used in the degradation mechanism is released in a co-operative manner along a polymer chain." Coudray *et al* (1996) also discuss the electromechanical energy stored in a dielectric containing trapped charges and also attribute the degradation of dielectric materials to the release of this energy following the de-trapping. They also arrive at a value for the energy released of 5 - 10 eV per trapped charge dependent on crystal structure and location of trapped charge, either at an atomic site or inter site. They also state that this energy around a trapped charge, spread over less than 100 atoms, is sufficient to produce molecular level damage when it is released on the de-trapping of the charge.

Summary

It is possible that all of the above processes may occur independently. However in the real world there is likely to be a combination of these forms of ageing taking place together with an additional factor which must represent the interaction of these processes, for instance the presence of an electric field will accelerate some processes or initiate others.

A generally accepted model that will predict and explain all of the various processes experimentally observed in the generation and propagation of tree structures in the degradation of electrical insulation has still to be put forward. Such a model will probably encompass many aspects of other theories and models already proposed. A recent paper for example [Parpal, *et al.* (1997)] proposes a model to describe a wide range of experimental observations that were described in an earlier paper [Dang, *et al.*(1996)]. In this paper they state ".the proposed model described relies on simple thermodynamic arguments (Crine 1990), on part of the free-volume breakdown theory of Artbauer (1996) on the formation of sub-micron sized cavities observed by Zhurkov (1972) during the mechanical ageing of polymers and on the molecular ageing model of Crine and Vijh (1985)

3.3. The Electro-mechanical Model of Breakdown.

Electromechanical breakdown in polymers has attracted much less attention in published works on insulating material failure. It is quite possible, however, that it is a common breakdown mechanism, the generally accepted view that an increase in temperature is accompanied by a decrease in breakdown strength tends to support this view. When it is discussed, however, the aspect that is usually being examined is that of electrostriction. This is defined as the expansion or contraction of a dielectric in the presence of an electric field. This can occur when there is a potential across two electrodes leading to an electrostatic attractive force. This manifests itself as a mechanical compressive force, breakdown occurs when this force can no longer be balanced by the dielectric elasticity.

There is also a transverse stress on the dielectric. Lewis et al (1996) explain this effect in terms of the Lippmann electro-chemical equation which states that a change in interfacial tension $\Delta\gamma$, generated by a change in potential difference across an interface ΔV is given by

$$\Delta\gamma = -q\Delta V \qquad \textbf{(3.2)}$$

where q is the surface charge density on the electrode.

In polyethylene, being a bulk insulator, the field is present through out the material and there may well be trapped charges in the bulk material, not just at the interface region. This situation was addressed by Sanfield *et al* (1968)

resulting in a generalised Lippman equation predicting an increase in the transverse stress σ, in a dielectric between metal electrodes, of magnitude

$$\sigma = \varepsilon E^2 \qquad \textbf{(3.3)}$$

where ε is the permittivity of the dielectric and E is the electric field strength.

In the case of an alternating electric field ($E = E_o \text{ Sin } \omega t$) the stress εE^2 will result in an alternating strain of frequency 2ω. (Lewis *et al* (1996))

Lewis *et al* explored the consequences of invoking this model in the case of electrical failure of polyethylene used as a bulk insulator in power transmission cables. They argue that the stress εE^2 acts to reduce the activation energy for thermally-induced bond scission in the molecular structure of the polymer accelerating the rate of bond scission and leading to the ultimate failure of the material. By assuming that failure of the insulator occurred when 10% of the bonds were ruptured their model predicted "time to failure" characteristics in reasonable agreement with experimental results.

In addition Lewis at al discussed the possibility that the mechanical stress would lead to a propagating crack process based on the Griffith model (1920). The transition from bond breakage to crack development and subsequent tree generation depends on the release of stored mechanical energy. Figure 2.5 shows a representation of the inter-lamella space; it is important to note the presence of tie molecules across this inter-lamella or amorphous region. These tie molecules maintain the structural integrity of the polymer stabilising the individual lamella and therefore the bulk material. The tie molecules offer

resistance to any stress that might act to move the lamella apart, this resistance is limited however by a process known as reptation whereby the tie molecules unravel themselves from the crystalline lamella. The tie molecules may become completely disassociated from one or other of the lamella or may reach a limit due to entanglement of the ends of the tie molecules. In the latter case the tie molecules still bridging the amorphous region may eventually experience bond scission due to the continued application of the mechanical stress. Lewis *et al* suggest that these ductile creep processes of reptation and disentanglement in the polymer are likely to correspond with the α process of relaxation in polyethylene in which a chain twist propagates through the crystalline structure by a thermally-activated stepping mechanism.

Lewis *et al* therefore suggest that the process of crack initiation and propagation could commence by a process of fibril thinning due to tie molecule reptation induced by the electromechanical transverse stress. This would lead to craze and crack nucleation, these sub-microscopic cracks and crazes would grow further by way of reptation processes, continuing to be driven by the externally generated transverse electromechanical force. Eventually the strain on the remaining tie molecules would drive them beyond their breaking point leading to active fractures of the material and electrical failure. Lewis at al assume that any applied stress would be shared equally by a certain concentration of taut tie molecules and that the reptation velocity depends on this stress. Using this approach an expression is derived for the rate of craze growth $d\delta/dt$ the activation energy involved in this expression is of the form shown in equation 3.4.

$$Q = Q_o - \lambda \varepsilon E^2 \qquad (3.4)$$

The activation energy given by Lewis *et al* is of the order of 1.2 eV, which is reasonably in agreement with experimental evidence (Amelin et al (1971) and Masyo (1976)).

It is evident that for any given tie molecule there will be an initial entanglement length *l* and that there will therefore be a finite time *t* for a particular molecular chain to move out of the lamella by reptation. The possible stress will depend on *l* and there will be a critical value of *l* beyond which the chain will fail by molecular scission rather than reptation. The rate of increase of stress $d\sigma/dt$ will therefore become an important factor.

When molecular scission happens it is likely that oxygen will be an important feature of the process. There will always be some oxygen present in XLPE even in the presence of anti-oxidants and crucially this oxygen will be concentrated in the amorphous region since it is relatively insoluble in the crystallites. It is known, for instance, that oxygen is capable of hydrogen abstraction from a polymer chain to form chain-side and hydroperoxy radicals and that the activation energy for this reaction is in the range 1.3 to 1.95 eV. [Kagiya, V.T. et al (1979)] Moreover the hydrogen atoms most vulnerable to abstraction are those at carbon sites or where cross-linking or chain-branching occur; XLPE therefore being particularly susceptible. During bond scission highly reactive polymer free radicals will be produced and the stored elastic energy in the broken parts of the polymer chain will be released. The release of this energy at the free radical sites can take part in a cyclic process

resulting in continuous polymer decomposition and further free radical generation.

The effects of bond scission therefore are likely to be several, including an increase in the number of end-groups, an increase in the number of shorter polymer chains, resulting from the scission of the longer chains. The increase in end-groups will potentially increase the number of CO, CH_3 and C=C end groups as these are all possible end groups for polyethylene. The change in the ratio of shorter polymer chains to longer polymer chains should be detectable by using Raman spectroscopy in particular by concentrating on the Disordered Longitudinal Acoustic Mode peak which shows at around $200cm^{-1}$ for polyethylene. The change in end-group concentration should show up in peak development, the relevant peak for the CO end group is at $1725cm^{-1}$ in the FTIR spectrum of polyethylene, for CH_3 and C=C at 1373 and $1600cm^{-1}$ respectively in the Raman spectrum. In particular the peak due to the stretching vibration of the C=C group is, when present, one of the most intense peaks in the Raman spectrum. (Hendra *et al*, 1991) Therefore the appearance of or increase in concentration of any end-groups of this configuration should result in a significant change in the resultant spectrum.

Figure 3.5 summarizes these concepts; the lamella being under an electromechanical strain, reptation taking place resulting in the remaining tie molecules being placed under greater individual strain resulting in eventual rupture. The role of oxygen and free radicals are also introduced resulting in the growth of end-groups one possible type being shown.

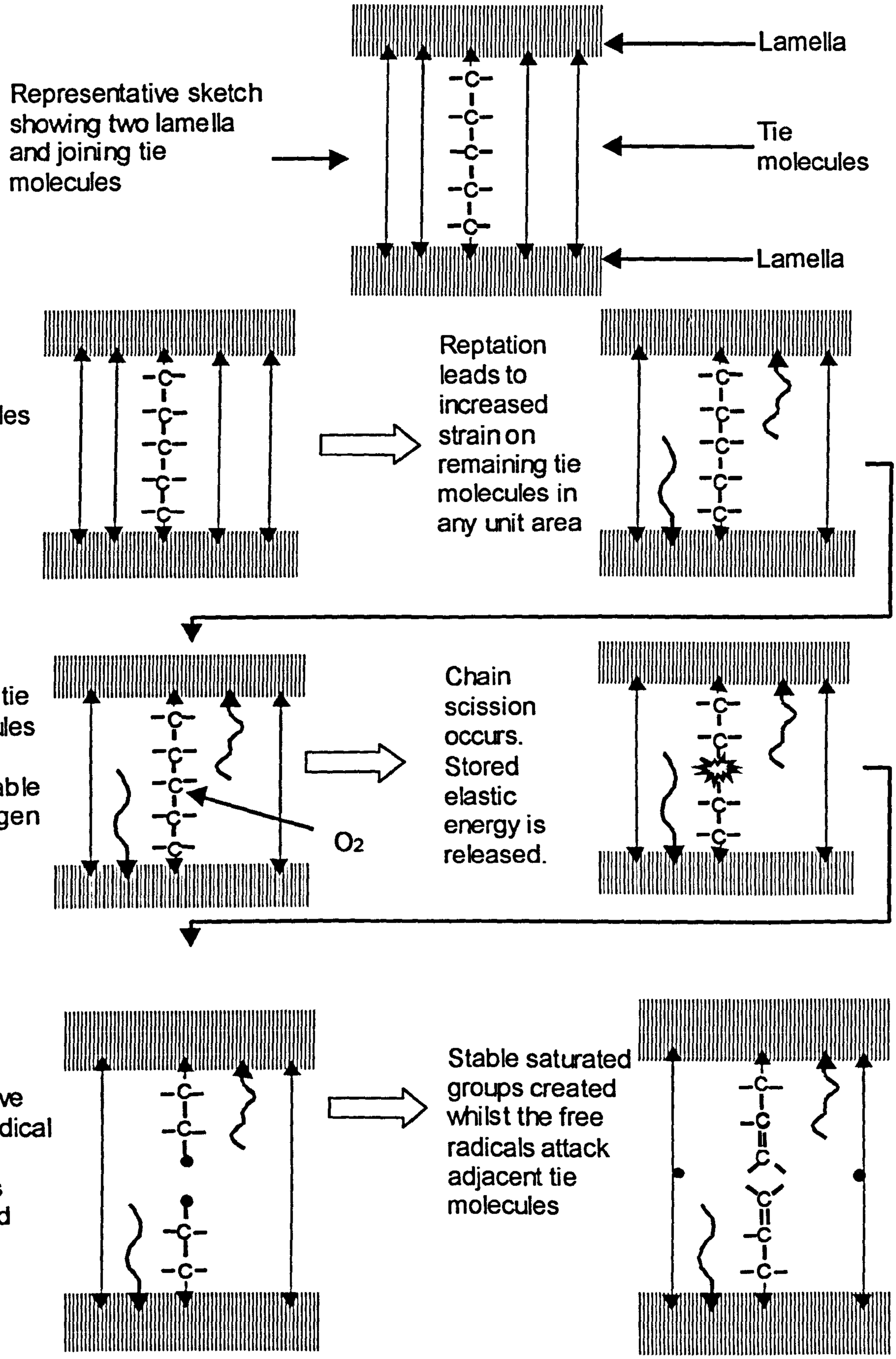

Figure 3.5 Showing the progressive nature of electromechanically induced reptation and bond scission.

4. Surface Investigation Techniques

4.1. Vibrational Spectroscopy

4.1.1. Raman Spectroscopy

When monochromatic light is incident upon a transparent target, most of that light is transmitted unaffected. A proportion however is scattered by the molecules of the target. The scattered radiation mostly consists of photons with the same frequency, ν, as that of the incident radiation; this is called Rayleigh scattering. However a small proportion of photons with frequencies $\nu+\nu_1$ or $\nu-\nu_1$, where ν_1 is a vibration frequency of the scattering molecule. The photon frequency is therefore shifted and this implies a change in photon energy; this process is therefore called inelastic scattering. This effect was first observed by C.V. Raman in 1928. The lines due to photons with frequency, $\nu+\nu_1$ are known as Anti-Stokes lines whilst those due to photons with frequency $\nu-\nu_1$ are known as Stokes lines. Since the ratio of the intensity of the Stokes to Anti-Stokes lines is approximately 10:1, it is usual to concentrate experimental work on the Stokes lines especially as the Raman shift is the same.

4.1.1.1. Origin of Raman Scattering

According to the classical theory of Raman scattering a molecule in an electric field of strength E has an induced dipole moment $P = \alpha E$ where α is the polarizability. This polarization can be affected by incident photons, which are equivalent to a varying electric field, and it is this that gives rise to inelastic

scattering. On the other hand the quantum mechanical mechanism of Raman scattering can be envisaged by reference to figure 4.01.

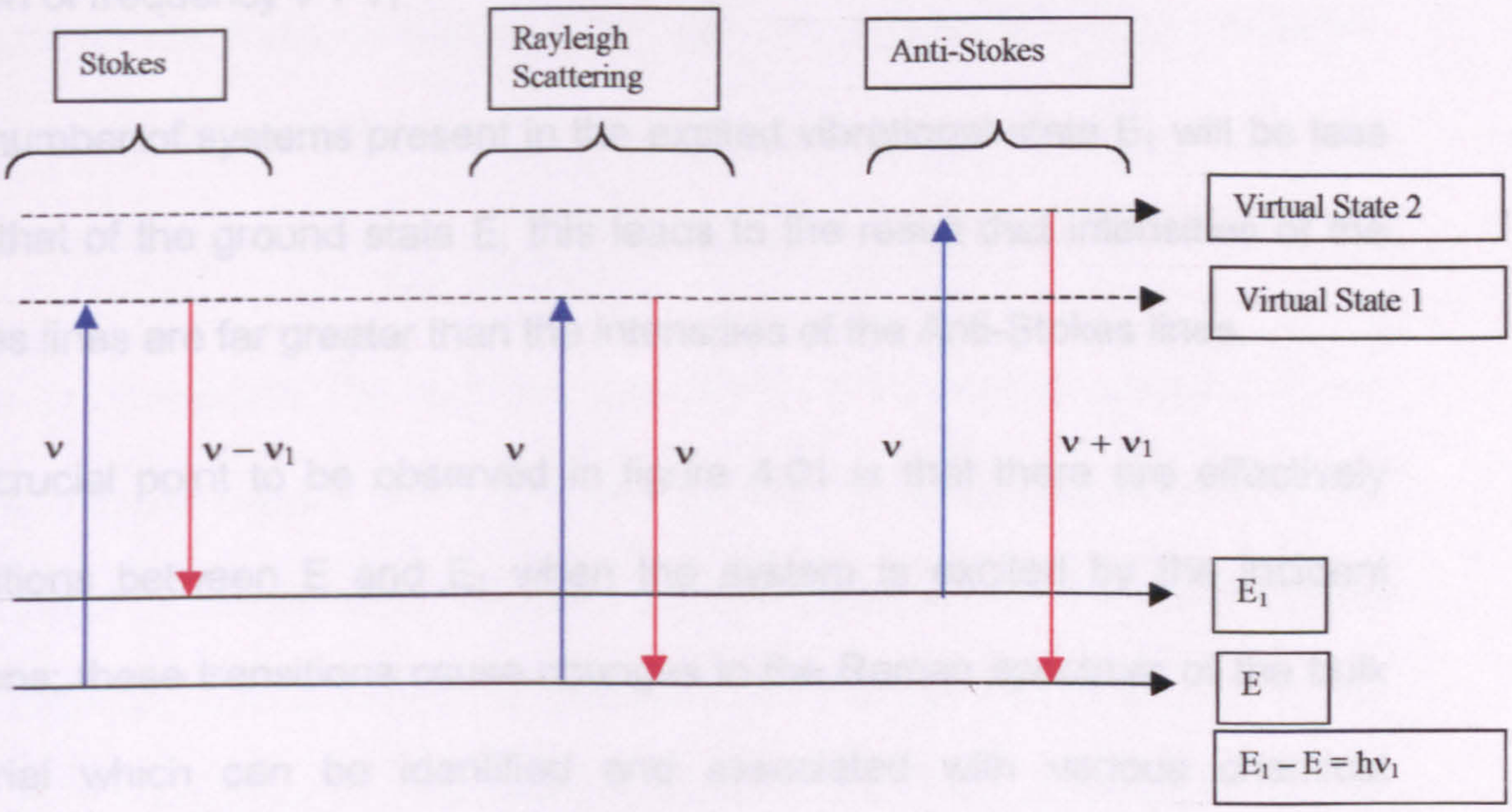

Figure 4.01 Energy level diagram showing the raising of the molecule to a 'virtual state' and then that energy being lost, resulting in the production of the Stokes and anti-Stokes lines. The population of the excited vibrational state, E_1, is less than that of the ground state and as a result the Anti-Stokes lines are weaker than the Stokes lines.

In each case the incident photon (of frequency ν) interacts with the system and is leading to an upward transition in the energy of the scattering molecule.

In the case of Stokes lines there is an upward transition between energy level E and virtual state 1; there is then an immediate downward transition[1] to energy level E_1 resulting in the generation of a new (scattered) photon with frequency $\nu - \nu_1$. In the case of Rayleigh scattering the system starts and finishes at the same energy level, E, and the annihilation of the incident photon, with frequency ν, is therefore accompanied by a new scattered

[1] Virtual States are used merely to simplify the explanation; there are no real energy levels at this excited condition which is why there is an immediate downward transition from these states.

photon, of frequency ν. For Anti-Stokes lines the incident photon, of frequency ν, is absorbed, and the system is excited to virtual state 2; the immediate downward transition to E is accompanied by the emission of a photon of frequency $\nu + \nu_1$.

The number of systems present in the excited vibrational state E_1 will be less than that of the ground state E, this leads to the result that intensities of the Stokes lines are far greater than the intensities of the Anti-Stokes lines.

The crucial point to be observed in figure 4.01 is that there are effectively transitions between E and E_1 when the system is excited by the incident photons; these transitions cause changes in the Raman spectrum of the bulk material which can be identified and associated with various chemical species.

4.1.1.2. Changes in the Raman Spectra

The Raman spectrum obtained is dependent on the bonds between atoms and the masses of the atoms involved. Considering the molecules in a crystal structure as harmonic oscillators their resonant frequency can be modelled approximately by using the formula for SHM.

$$\Omega = \sqrt{(B/M)} \qquad (4.1)$$

Where Ω represents the resonant frequency, B the spring constant of the bond and M the mass of the molecules involved. It can be seen therefore that any change in the resonant frequency can be related to a change either in the bond strength (representing the spring constant in our simple model) or the mass of the molecules. Therefore if the electrical field applied affects the structure of the material either by breaking bonds or in some other way then this should cause a change in the Raman Spectrum.

4.1.1.3. Interpretation of Raman Spectra

4.1.1.3.1. Vibrational Assignments in Raman Spectroscopy

A Raman spectrum obtained from a sample consists of many peaks and to interpret a spectrum one must assign those peaks; that is to understand the origin of each peak. The line or peak may be assigned at various levels of detail. These are to a chemical species or molecular configuration, to a crystalline or amorphous region, to a specific molecular conformation, to a symmetry species or to a specific normal mode. Raman spectroscopy has become an easily accessible technique due to the introduction of the laser as an intense monochromatic light source and computers to ease the analysis and spectrum production. Reported Raman investigation into the structure of cables and in particular the physical changes taking place due to the presence of stress, whether mechanical or electrical, is somewhat limited. However, there is significant literature [Nielson and Woolett, 1957: Snyder, 1967: for example] on the investigation of the structure of polymers using Raman spectroscopy and in particular polyethylene which, of course, forms the basis of the insulator in XLPE HV cables. The assignment of the various peaks in the spectrum of PE is the subject of much discussion in the literature. Figure 4.02 summarises the currently accepted main vibrational assignments for polyethylene.

Vibration	Assignment	Description of Vibration	Symbol	Frequency (cm^{-1})
ν_1	CH_2	Symmetric stretch	$\nu_s(CH_2)$	2848
ν_2	Skeletal	Chain Stretch		1133
ν_3	CH_2	Asymmetric stretch	$\nu_a(CH_2)$	2883
ν_4	CH_2	Wagging motion	$\gamma_w(CH_2)$	1370
ν_5	CH_2	Rocking motion	$\gamma_r(CH_2)$	1170
ν_6	CH_2	Bending motion	$\delta(CH_2)$	1440
ν_7	CH_2	Twisting motion	$\gamma_t(CH_2)$	1296

Figure 4.02 Raman active vibrational modes for polyethylene after Bower and Maddens (1989). Skeletal modes, ν_2, are associated with the molecular framework rather than with specific atomic groups.

In addition to the seven main peaks indicated, overtones[2] of other Raman peaks or IR peaks can be found. For instance weak peaks at 2926 and 2946cm-1 have been assigned to overtones of the 1463 / 1473cm^{-1} IR active doublet in Fermi resonance with the $\nu(CH_2)$ stretching fundamentals. In addition combination[3] frequencies may occur.

4.1.1.3.2. End Group Identification

The long chain molecules that make up any polymeric substance are terminated by a variety of chemical groups these are known as end groups. These end groups differ significantly from the repeat unit of the polymer and they are detectable by vibrational spectroscopy even though their concentration must by definition be far lower than the repeat unit of the

---

[2] Integral multiplies of the fundamental frequencies

[3] Sums or differences of integral multiples of the fundamental frequencies of two or more modes.

polymer. Obviously where one is looking for signs of increased bond breakage (and therefore the appearance of end groups) this is a great advantage. This is especially true since the rupture of chemical bonds has been shown to lead to the appearance of free radicals and that the appearance of free radicals has been linked to end group formation. In addition it has also been shown that ruptured bonds can localise into micro regions forming sub-microvoids which have been found to lead to the physical breakdown of the polymer. [Zhurkov et al. (1974)]

4.1.1.3.3. Crystallinity

There has been a significant amount of published work carried out with Raman spectroscopy on the crystallinity of polymers and particularly PE. This has resulted in the identification of the three main spectral regions that give structural data relating to the degree of crystallinity of the polymer [Mandelkern et al. (1993), (1990) and others]. The so-called internal modes or fingerprint region, in the range 900 – 1500cm^{-1} give quantitative information on the elements of the phase structures. The longitudinal acoustic modes (LAM), which lie in the range of about 5-50 cm^{-1}, give the ordered sequence length[4]. Because of the low frequency of these vibrational modes these proved impossible to examine with the equipment available for the present study.

On the other hand the disordered longitudinal acoustic modes (DLAM), in the region of 200cm^{-1}, were observable. These modes give a measure of the

---

[4] Ordered sequence lengths i.e. the length of the straight chain segments in the crystal lamella.

long-range conformational disorder and are the dominant feature in the low frequency spectrum of a liquid *n*-alkane longer than about C_9. [Snyder et al. (1986); Mandelkern et al (1993)]

Looking first at the internal modes Strobl and Hagedorn (1978) showed that the integrated intensity of the band at 1416cm^{-1} (which they linked to CH_2 bending – since assigned to 1440cm^{-1}) is related to the degree of orthorhombic crystalline material present. They also related the broad shoulder of the 1296 cm^{-1} band at 1303 cm^{-1} and the band at 1080cm^{-1} (integrated intensities) to the amount of amorphous material present in the sample.

LAM vibrations arise as a result of the molecular chains vibrating along their length in an accordion like fashion and the frequency of these vibrations depends on their molecular length. These bands are therefore used to measure the physical size of the lamellae in polymers which is closely related to the degree of crystallinity in the material.

The DLAM mode was identified by Snyder et al. (1986) at 206 cm^{-1} for a semi-crystalline PE and by a broader band at 202 cm^{-1} in molten PE. Snyder also examined the use of the DLAM band in the determination of the crystallinity of polyethylene. They found that the frequency and the shape of the DLAM peak were dependent on the average number of carbon atoms in the chain and on the ratio of trans to gauche bonds. In particular they established that the DLAM band could be detected in solid polyethylene at ambient temperatures and was in fact found to be present in all samples with a crystallinity of less than about 90%. They also concluded that the fraction of

the sample consisting of highly disordered chains, as measured by the DLAM intensity, is linearly related to the degree of crystallinity.

The DLAM peaks were observable in the experiments reported here by fitting a baseline to the spectra to remove the fluorescence background and then comparing the resultant spectra.

4.1.2. Fourier Transform Infra-Red Spectroscopy

Infra-Red spectroscopy is the measurement of the wavelength and intensity of the absorption of infrared light by a sample. The infrared light is energetic enough to excite the molecular vibrations of the sample to higher energy levels. The wavelength of IR. absorption bands are characteristic of specific types of chemical bonds and therefore this technique has found wide usage in the determination of the chemical structure of samples.

Fourier Transform InfraRed (FTIR) spectroscopy involves the production of a spectrum by taking the Fourier Transform of a two-beam interference pattern. In order to do this a "white" source of light is used to produce radiation over a broad range of infrared wavelengths.

Light coming from the source is split into two paths using a half silvered mirror (a beamsplitter); the light is then reflected back from two mirrors, one of which is movable, to the beamsplitter where it recombines. If the distance from the beamsplitter to each individual mirror is not exactly the same then when the two beams recombine there will be difference in phase, which will lead to either destructive or constructive interference (the superposition principle). In FTIR spectroscopy the intensity of the light is measured and then plotted as a function of the distance to the movable mirror, the resultant graph is the Fourier Transform of the intensity of the light as a function of the wavenumber (cm^{-1}).

4.1.3. Fluorescence and Phosphorescence

Molecular fluorescence originates when molecules that have been excited to higher electronic energy levels decay to the ground state releasing energy as they do so. The three main decay processes, fluorescence, delayed fluorescence and phosphorescence are best discussed by reference to a Jablonski diagram as shown in figure 4.03.

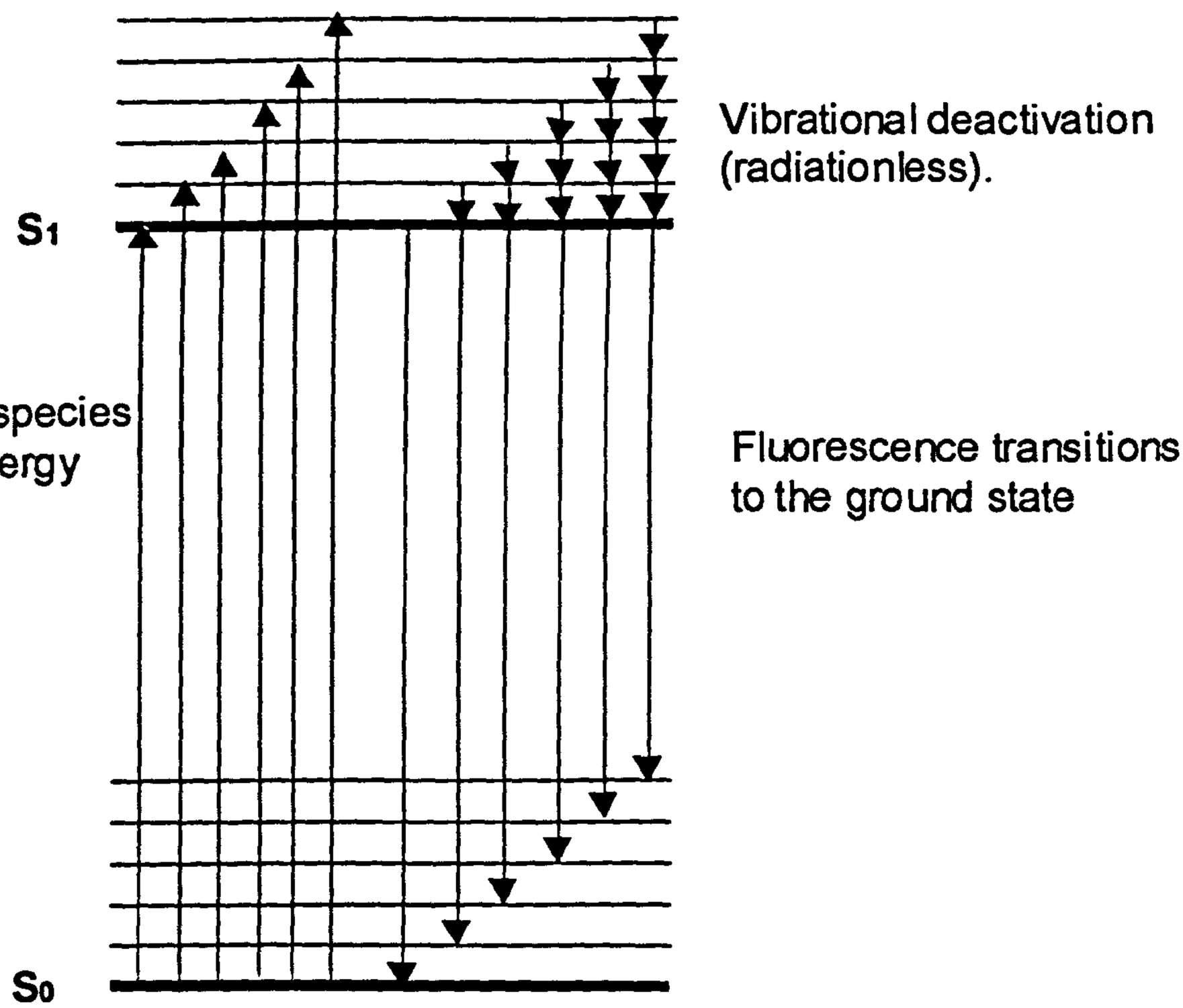

Figure 4.03 Basic Jablonski or state diagram showing the excitation of species from a ground state (S_0) to a higher energy state (S_1) and the subsequent decay to the ground state giving up energy in the downward transition as fluorescence.

For every molecule the associated electrons occupy orbitals forming the framework of the molecule. Each electron therefore possesses a definite energy and momentum due to its motion. The electrons also possess angular momentum due to their spin; the units used to measure the electron spin are

such that each electron possesses ½ unit of angular momentum. The Pauli exclusion principle states that any one molecular orbital can possess a maximum of two electrons of opposite spin, one of + ½ and one of – ½. In the ground state, S_0, the electrons are arranged so that the net spin of the electrons is zero; such states are known as singlet states. If an electron in the ground state is excited to a higher energy level, S_1, it will normally retain its original spin: the total spin is therefore still zero and the system is still in a singlet state. Decay from a singlet state is called fluorescence. It is possible however for the excited electron to undergo spin inversion and this leads to the so-called triplet state, which possesses a spin of 1; decay from this state is called phosphorescence.

There are a number of energy levels to which the excited electrons or excitons can be promoted. At first radiationless decay between these levels[5] takes place yielding a relaxed singlet state from which the electrons can subsequently decay to the ground state emitting energy as fluorescence in the process.

---

[5] The energy is usually lost through collisions with other species, although intersystem crossing can occur, where a change in spin state of the electron takes place leading to the creation of so called triplet states giving rise to phosphorescence.

4.1.3.1. Fluorescence

Looking more closely at luminescence in polymer solids, and in particular how this may be affected by distortions in the molecular framework it is useful to consider transitions in terms of the energy as a function of molecular configuration co-ordinates. Luminescence involves the excited (electronic) states of the molecular solid in the generation of excitons by the incoming photons. Consider figure 4.04.

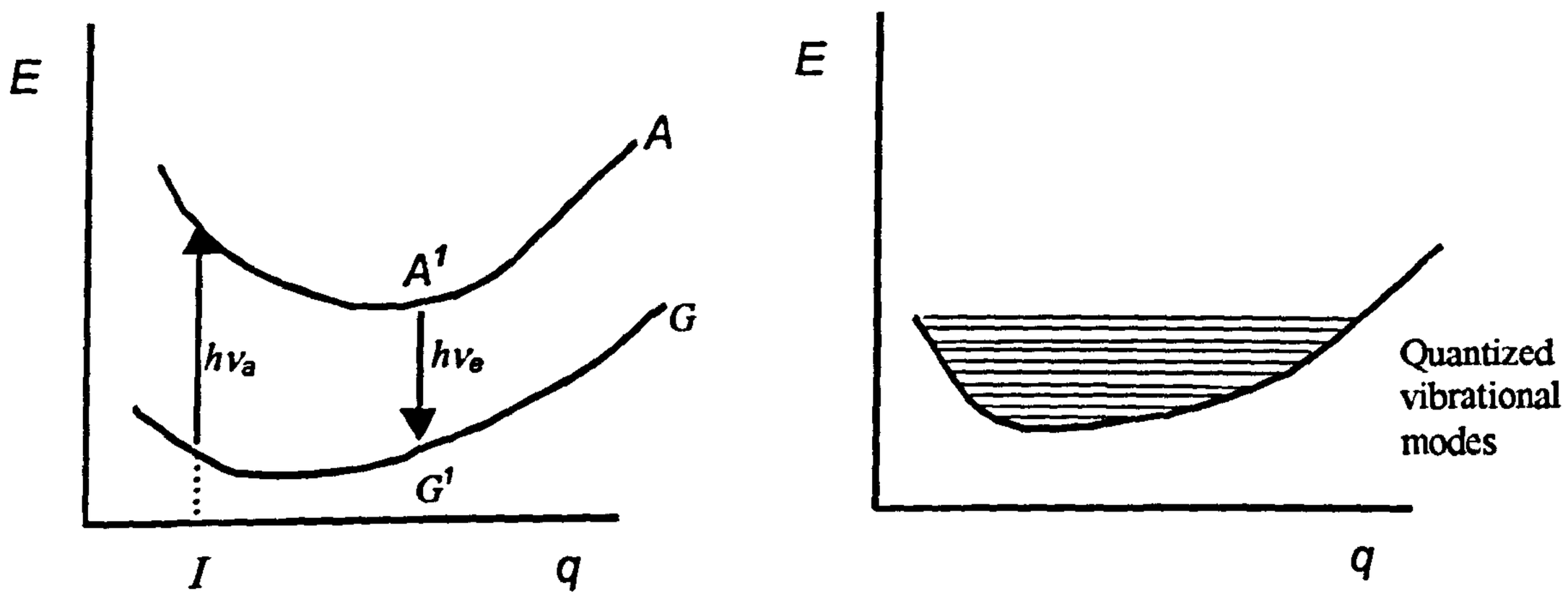

Figure 4.04 Showing a plot of the energy of a molecular unit of a solid as a function of the molecular configuration co-ordinate *q*. [In practice molecular configuration might be determined by a set of position co-ordinates of the individual atomic centres.]

Curve *G* shows how the ground state electronic energy *E* changes as a function of *q*; i.e. as the molecular bonds are distorted. The minimum represents the equilibrium configuration. At a given temperature the system is capable of vibrational excursions about the minimum and a series of quantized energy levels result involving the electronic plus vibrational energy. In a similar manner curve *A* represents the energy of an excited electronic state of the molecular system, i.e. of an exciton. Note that the minimum of A is

shifted from that of G; the molecular configuration is changed and the vibrational modes will be different from those of the ground state.

Consider now an incoming photon which excites the system causing an electronic transition from *G* to *A* at a moment when the molecular configuration is as shown at *I*. The transition is vertical because according to the Franck-Condon principle[6], the nuclei effectively remain at rest during the very short time of the transition. The transition requires an energy $h\upsilon_a$. Because of molecular vibrations there will be a band of possible transition energies $h\upsilon_a$. After the transition, the nuclei move to their preferred positions for the excited state with molecular vibrations in the neighbourhood of the minimum at A^1. Subsequently it will be possible for a reverse transition to occur from the excited state near A^1 back to the ground state at G^1 (a vertical FC transition) with the emission of a photon of energy $h\upsilon_e < h\upsilon_a$. This is the process of luminescence. In general the excitonic state may be expected to last for up to 10^{-8} seconds. When the system is in the triplet state the lifetime can be very much longer; in which case the process is known as fluorescence.

It is clear that since the states *G* and *A* depend on molecular configuration and therefore on the environment, they will be susceptible to mechanical (structural) changes in the material. Structural defects and impurity centres could well give rise to exciton behaviour and therefore to luminescence which would be sensitive to thermal annealing and mechanical strain. This

---

[6] The Franck-Condon principle states that an electronic transition is so fast that a vibrating molecule does not change its inter-nuclear distance appreciably during the transition. This concept is applied to the interpretation of molecular spectra.

behaviour has been demonstrated for anthracene crystals, which were mechanically deformed by bending (Sillinsh (1980)). Deformation introduced additional bands of fluorescence associated with structural defects. Thermal treatment lowered the general continuous background fluorescence (which decreased towards longer wavelengths) and allowed certain discrete bands to become prominent. Exciton states associated with structural imperfections in the crystallites and with impurity states in the amorphous regions are very likely and we can therefore expect similar behaviour for PE.

4.1.3.2. Quenching or Photo-Bleaching

Quenching refers to the process whereby fluorescence in virgin polymers can be removed or quenched by exposure of the sample to a high intensity light source. This involves a collisional process whereby excited molecules return to the ground state via collisions or other non-radiative processes.

This process takes a relatively short period of time during the preparatory work carried out during this study this was established to be ~ twenty minutes to remove 90% of the fluorescence.

4.1.4. Vibrational Spectroscopy Equipment

The Raman equipment available at Bangor is the Renishaw 1000 Raman Spectrometer; the maximum spectral resolution is $1cm^{-1}$ whilst the spectral range is <100 to $4000cm^{-1}$. The lateral spatial resolution is given as 2 μm using a 50 X objective on the microscope whilst depth of field in confocal[7] mode is 5 μm.

Two FTIR spectrometers were used: one being a Bio-Rad 175C with a spectral range of 6000 – 400 cm^{-1} and a maximum resolution of 2 cm^{-1} whilst the other was a Bomen MB100 with a maximum resolution of $2cm^{-1}$.

The Bio Rad machine was fitted with a Diamond ATR attachment – this device enables a spectrum to be captured without any special preparation of samples. The sample is pressed against a diamond "window" and the infra red beam is refracted through the sample by the diamond on which the sample rests.

---

[7] Confocal mode – the ability of the microscope to focus on a particular volume element within the sample as determined by the diameter of the beam and the depth of focus.

4.2. Scanning Probe Microscopy

The Scanning Probe Microscope (SPM) was invented in 1981 (Binnig et al.1982) and the term SPM now covers a whole family of instruments all based around the concept of scanning the sample surface with a very sharp mechanical probe

All types of Scanning Probe Microscope contain the same basic components, shown below in figure 4.05.

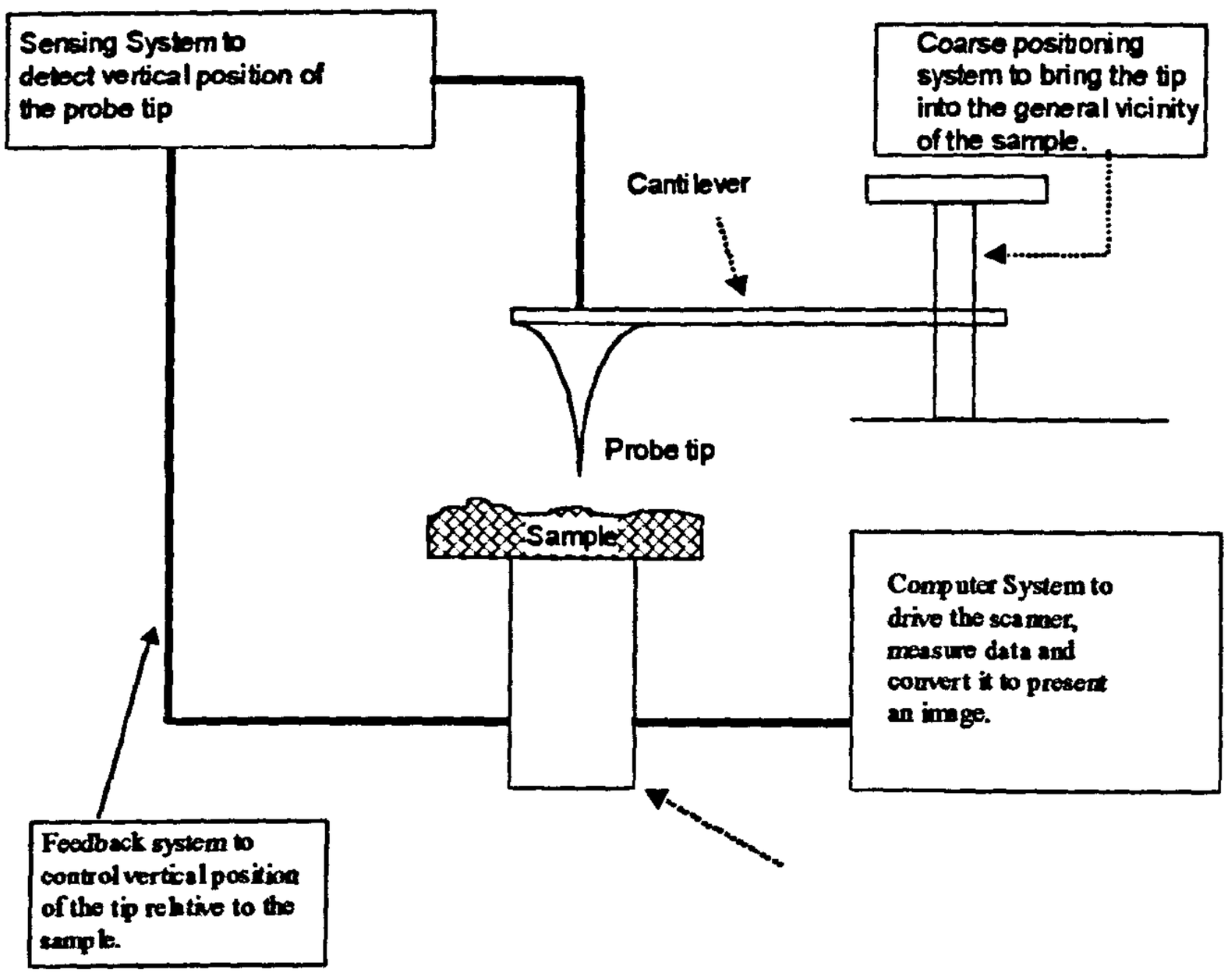

Figure 4.05 Generalised schematic of an SPM showing the principal components – individual elements are necessarily not to scale.

The probe tip mounted near the end of a flexible cantilever - usually vibrating - is brought into the region of the sample surface by the coarse positioning system. At this point the computer system takes over control of the three-dimensional spacing between tip and surface.

The Sensing system detects the position of the probe tip; this is usually done by means of a laser based sensing system as shown in figure 4.06.

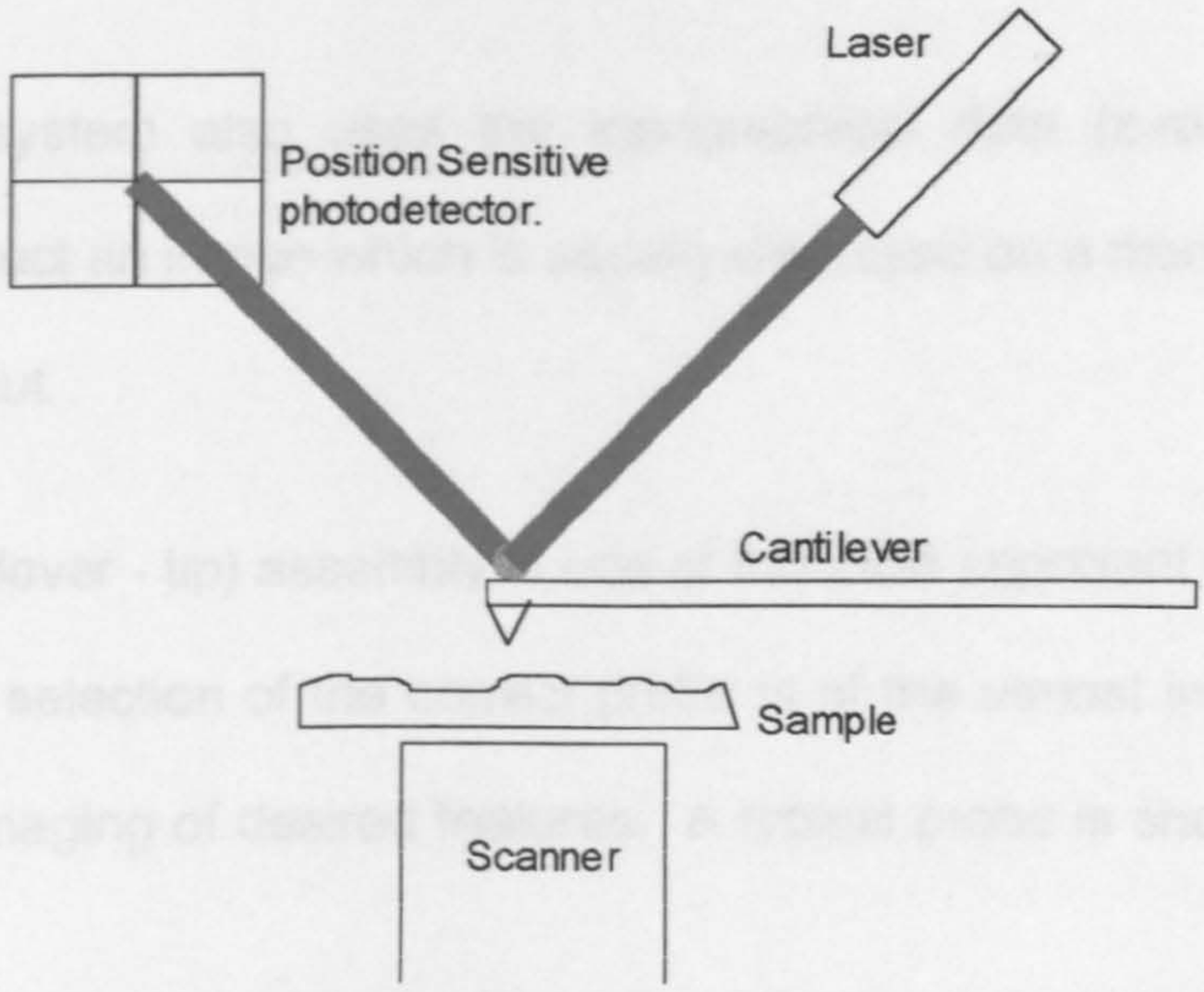

Figure 4.06 Schematic of laser sensing system showing the laser beam directed onto the back of the cantilever and subsequently being reflected to the quadrature photodetector.

Here a laser beam is shone onto the cantilever just behind the probe tip, and is reflected to the quadrature-type position sensitive photodetector (PSPD). As the sample is scanned beneath the probe the forces (which depend on the mode in operation) between the sample and the probe deflect the cantilever. The deflection of the cantilever thus moves the position of the laser beam incident on the PSPD and this change in position is detected and fed back to the computer system. The feedback is used by the computer system to drive the piezoelectric scanner on which the sample rests. The scanner moves the sample in a raster fashion whilst adjusting for variances in surface topology in order to maintain the same tip to sample distance. Using a piezoelectric transducer allows extremely fine positioning of the sample surface beneath the probe tip. The whole system is typically able to detect vertical movements

of less than 10^{-10} meters (< 1 angstrom). The scanner moves in the x, y and z directions with z relating to vertical movements. Throughout this thesis references to z-range relate to these vertical scanner movements.

The computer system also uses the topographical data (z-range) of the sample to construct an image which is usually displayed on a monitor but may also be printed out.

The probe (cantilever - tip) assembly is one of the most important components of the SPM and selection of the correct probe is of the utmost importance to the successful imaging of desired features. A typical probe is shown in figure 4.07

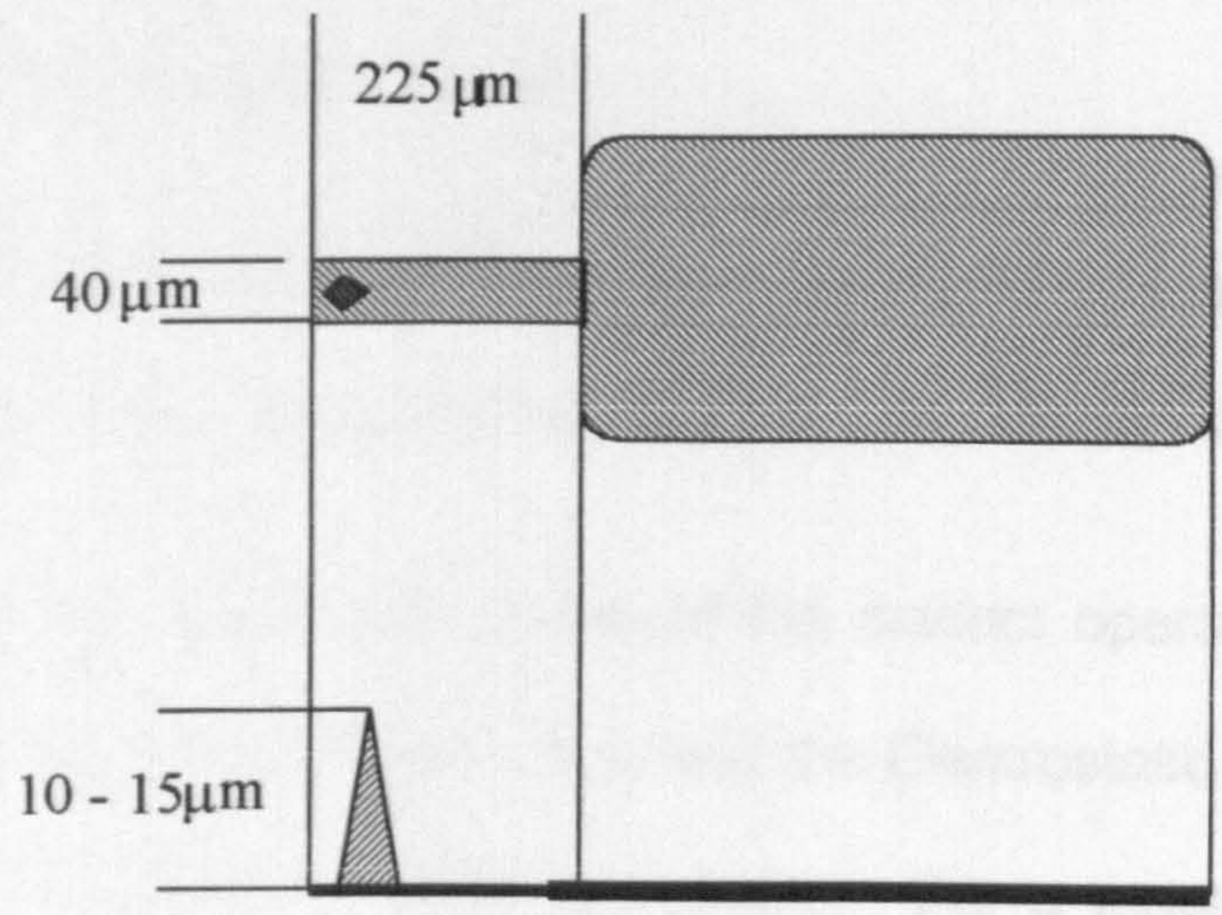

Figure 4.07 Plan and Elevation of a typical probe assembly used for Electrostatic Force Imaging

The cantilever assemblies used had a resonant frequency of ~70KHz and a quoted spring constant of about 2.8N/m. In order to have an instrument capable of high sensitivity, a relatively large deflection of the assembly is required for any given force. This requirement implies a soft spring i.e. a spring having a very low spring constant. In addition to minimise interference

from mechanical vibrations a high resonant frequency is required whilst scanning. The resonant frequency ω_0 of the cantilever system is given by,

$$\omega = (c/m)^{1/2} \qquad 4.2$$

(Weisendanger, 1994) where c is the spring constant and m the effective mass loading the cantilever. From equation 4.2 it can be seen that the only way that a large resonant frequency can be achieved whilst at the same time having a soft spring (low c) is to maintain m at as small a value as possible. This means that the physical size of the sensor must be as small as possible. Microfabrication techniques are used to enable production of reliable cantilevers of similar dimensions. L.O.T Oriel Ltd supplied all cantilever assemblies used during this project.

The sharpness of the tip and the shape of the tip determine the probe's ability to faithfully follow the contours of the sample - see section 4.3.3.

In this project use was made of two of the distinct operating modes of the SPM, namely the Atomic Force mode and the Electrostatic Force mode. The following sections describe these two modes. For a wider discussion of the SPM the reader is directed to the standard texts Magonov, 1996 and Wiesendanger, 1994.

The instrument available at the School of Informatics, Bangor is a Digital Instruments Nanoscope III A with Extender electronics.

4.2.1. Atomic Force Mode

This section describes in particular the Atomic force mode (AFM) of the Scanning Probe Microscope; this mode was invented by G. Binnig, C.F. Quate and Ch Gerber in 1985, it combines the principles of the scanning tunnelling microscope and the stylus profilometer.

The AFM uses a microscopic force sensor (the cantilever - figure 4.07) to probe the surface of the sample with a very sharp tip. The cantilever can be between 100 to 500 μm long and approximately 0.5 to 5.0 μm thick, the tip is no more than a few μm's long and usually less than 10 nm in diameter.

The AFM gathers data by interpreting the changes in the resonance of the cantilever caused by the forces present between the tip and the surface of the sample. These changes are measured and interpreted by a computer system and are used to generate an image of the surface topography. The minimum force that the AFM can detect is of the order of a few piconewtons. The forces usually detected during AFM operation are the so-called Van der Waals (VDW) forces or London forces. The magnitude and direction of these forces depends on the separation between the tip and sample as shown in figure 4.08.

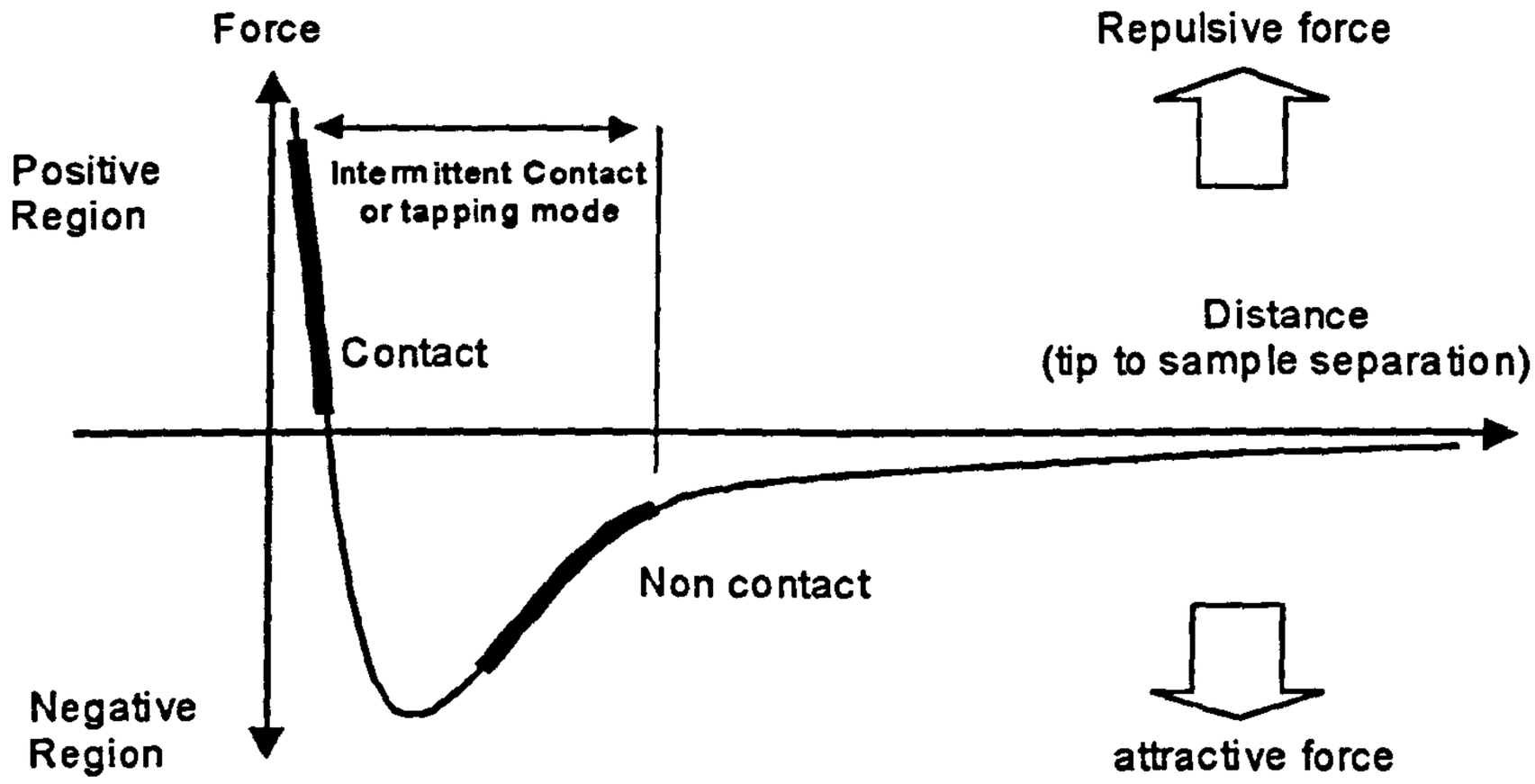

Figure 4.08 Sketch showing Force-Vs-Distance between the tip and sample. The main operating regions of the SPM are indicated.

Contact mode imaging is carried out in the positive region of the graph where the force is repulsive. Non-contact imaging is carried out in the negative region where the forces are attractive. Tapping mode operation can take place across the boundary between the two regions.

These are the three main modes of operation and the forces detected by the AFM are the result of the particular mode in which the instrument is operated. These modes are discussed below in the following order:-

- Tapping Mode.
- Contact Mode
- Non-contact Mode

(a) Tapping Mode

In tapping mode the cantilever is oscillated at or near its resonant frequency by a biomorph (or piezoelectric crystal) attached to the end of the cantilever opposite to the tip. The amplitude of these oscillations can be greater than 20nm whilst the resonant frequency can be between 50 KHz to 500 KHz. The tip is moved close to the surface and becomes subject to the attractive VDW forces. These cause a shift in the resonant frequency of the cantilever and a change in both the amplitude and phase of the oscillations as shown in figure 4.09.

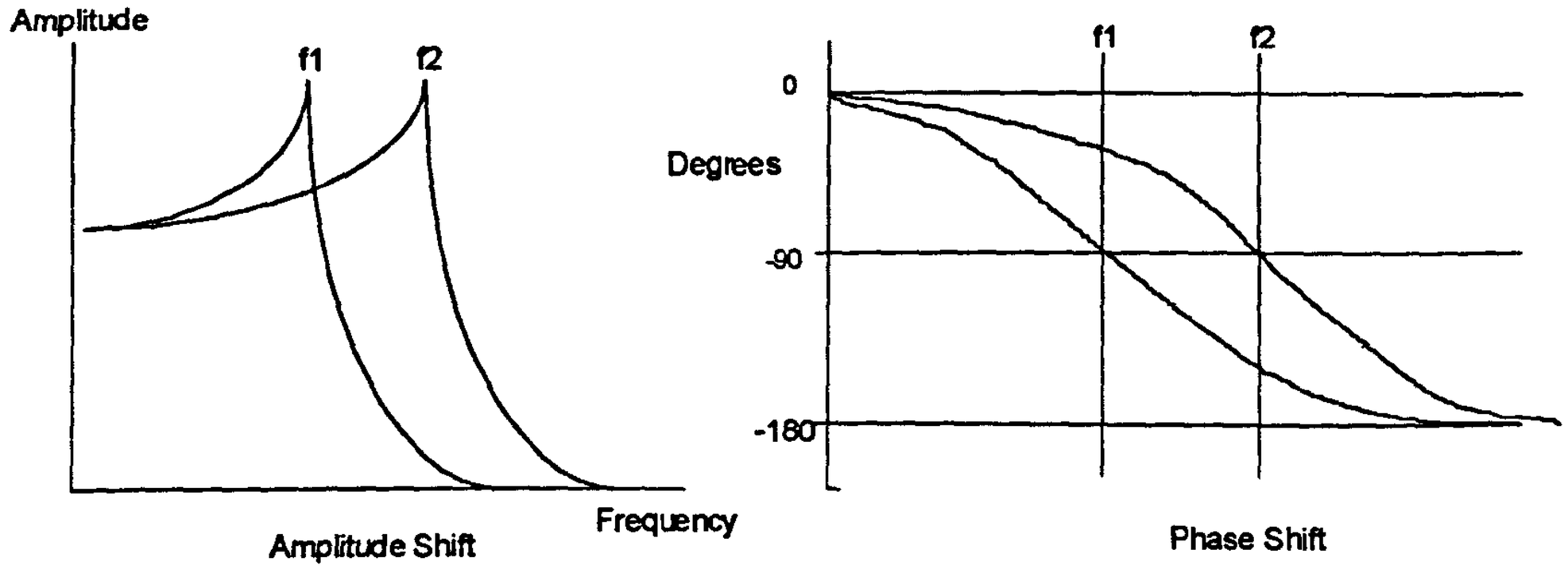

Figure 4.09 Sketch showing frequency dependence. Frequency f1 is for a tip far from the sample and f2 is for the tip and sample close together.

The sensor system monitors the resonant frequency of the cantilever and the feedback system maintains either the phase or amplitude at a constant level by movement of the sample surface in the z direction. The piezoelectric scanner on which the sample rests provides this movement. The feedback system generates an image by monitoring the driving voltage supplied to the piezoelectric scanner.

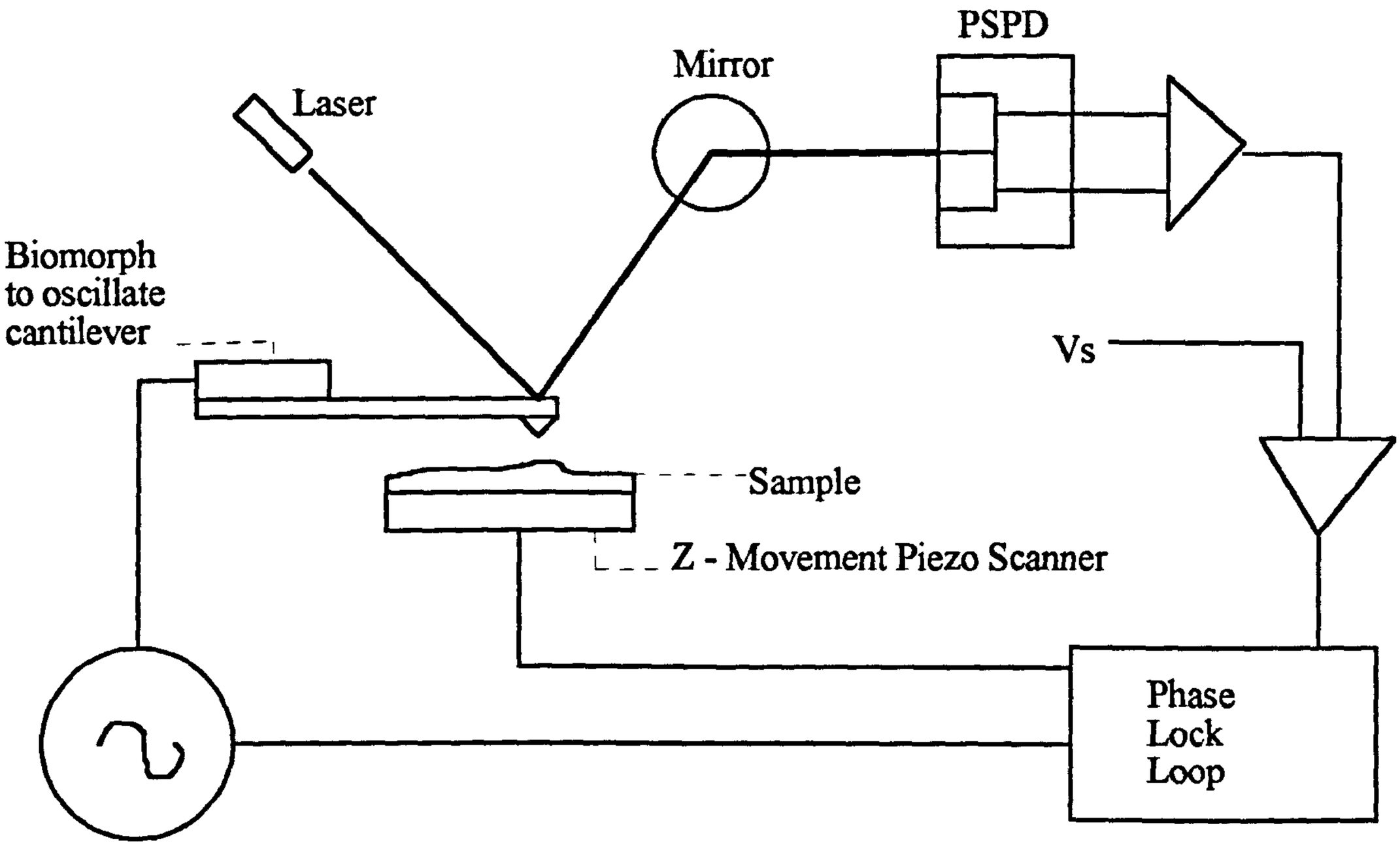

Figure 4.10 Schematic showing feedback loop operative during tapping mode.

One of the main advantages of tapping mode is the low surface force to which the sample is subjected during imaging. This is because during tapping the cantilever is oscillated at its resonant frequency and when this has been stabilised (at the setpoint) the sample is only subjected to the small force resulting from any increase in amplitude during a single oscillation. In addition, the tapping mode of operation does not subject the sample to lateral forces, as does Contact Mode when the tip is dragged across the sample surface. Therefore the tapping mode of operation was particularly suitable for the experimental work (§ 6.3), where relatively soft polymer surfaces were repeatedly scanned.

During tapping mode operation data is available on either the height change due to topographical details or the phase change in the cantilever vibrations due to these same details. The two types of data, height and phase, have

been found by other researchers (Magnov, 1996) to be suitable for quite different applications.

Height imaging is the mode most often used for topographical features and uses the Z – piezo modulation to provide the data. Height data usually gives a superior topographical image on most surfaces, but for polymer samples phase imaging has been found to provide superior imaging, probably due to the lack of lateral forces on the relatively soft sample. Phase Imaging during tapping mode operation has been found especially useful in the detection of changes in the physical properties of the sample. Such as surface viscoelasticity, friction, adhesion or areas of differing hardness.

(b) Contact Mode

Turning now to Contact mode, here the forces detected are the repulsive VDW forces, the tip is extremely close to the surface and the atoms of the tip and sample surface are so close together that they repel each other. The force - distance curve shown in figure 4.08, shows that the slope is very steep in the repulsive (positive) region of the graph - this means that the VDW force is sufficient to overcome any force applied by the AFM. The cantilever therefore bends as the tip is dragged across the surface of the sample. This deflection is measured by the sensing system to gather topographical data, which is used to drive the piezoelectric scanner and the imaging system. Due to the constant contact between sample and tip; the resultant forces mean that this mode of imaging was not suitable for these experiments (§ 6.3), as the amount of surface damage caused could have influenced the results.

(c) Non-Contact Mode

In non-contact mode the cantilever is oscillated near its resonant frequency close to the surface of the sample in the region of attractive VDW forces. These forces are much smaller than those experienced by the tip in the region of repulsive VDW forces. The practicalities of non-contact imaging also mean that a stiffer, and therefore less sensitive, cantilever must be used. A sensitive ac detection system is needed to detect the much smaller changes in the resonant frequency of the cantilever which are then used to drive the piezoelectric scanner and the imaging system.

This mode of operation is generally found to give lower resolution than either contact mode or tapping mode with the additional risk of sample damage as the tip can be pulled into contact with the sample surface. For these reasons this mode was not used to produce the results shown in section 6.3.

4.2.2. Electrostatic Force Mode

In the Electrostatic Force mode the instrument being used offered two types of electric force imaging: -

- Electric Field Gradient Imaging
- Surface Potential Imaging

In both of these operating modes for each scan line the probe makes two passes across the sample surface. In each pass the tip makes a trace and then a retrace as shown in figure 4.11.

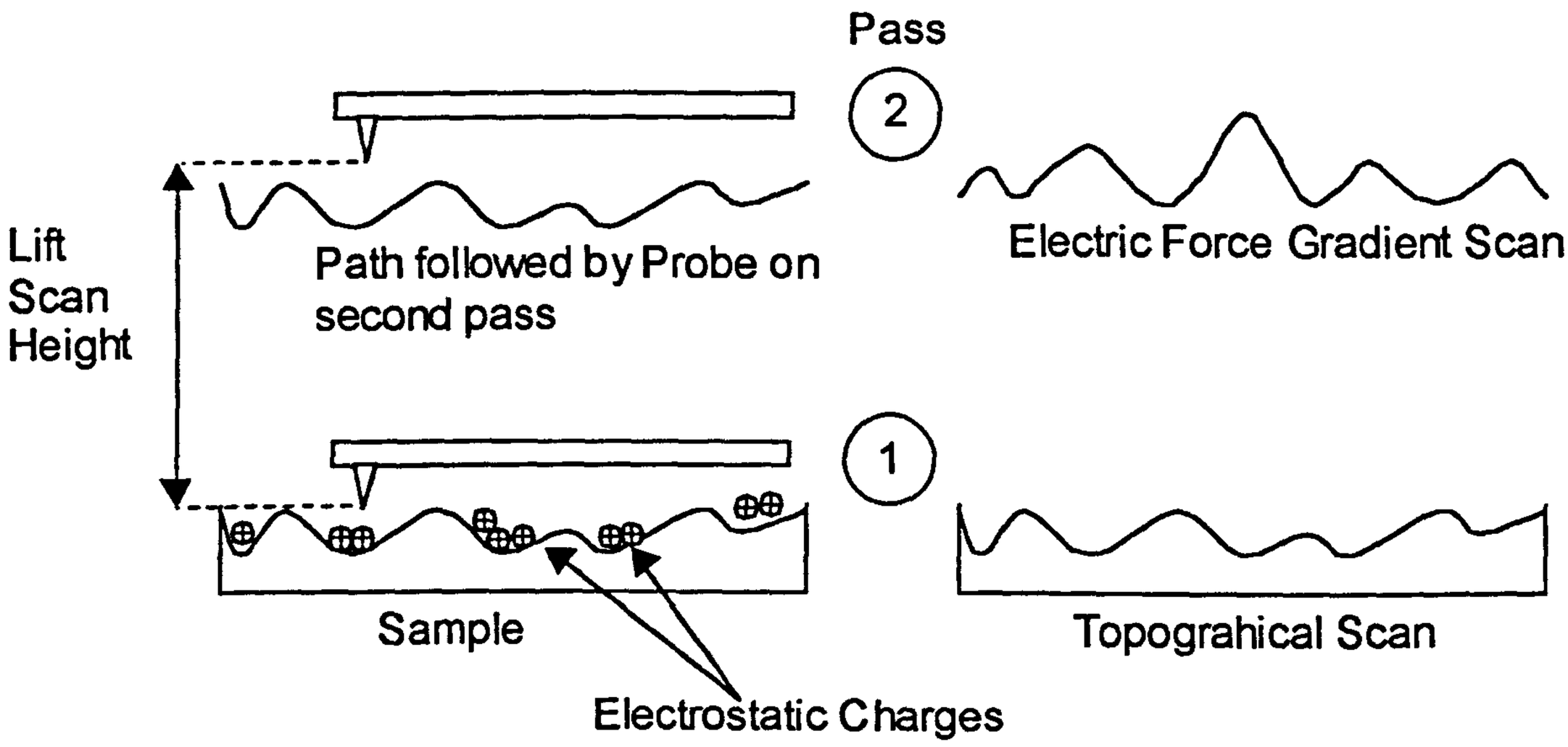

Figure 4.11 Basic Operation of Lift Mode Scanning

1 During the first pass, in tapping mode, topographical data is obtained by the system. This is used to provide a topographical image and also to drive the z axis scanner during the second pass.

2 On the second pass the probe is raised to the lift scan height and is maintained at this height above the sample surface by the microscope during

the whole of this scan. It does this by using the topographical data gathered on the first pass to maintain a constant tip to sample distance. In this way the probe detects only the relatively weak but long range coulomb or electrostatic forces.

(a) Electric Field Gradient Imaging

In electric field gradient (EFG) imaging the electrostatic force gradient between two areas is the source of the data being collected by the probe system. The cantilever assembly is oscillated at or near its resonant frequency and electrostatic forces on the sample surface modify the resonant frequency of the cantilever. The forces between tip and sample can be modelled as a spring attached to both tip and sample, figure 4.12.

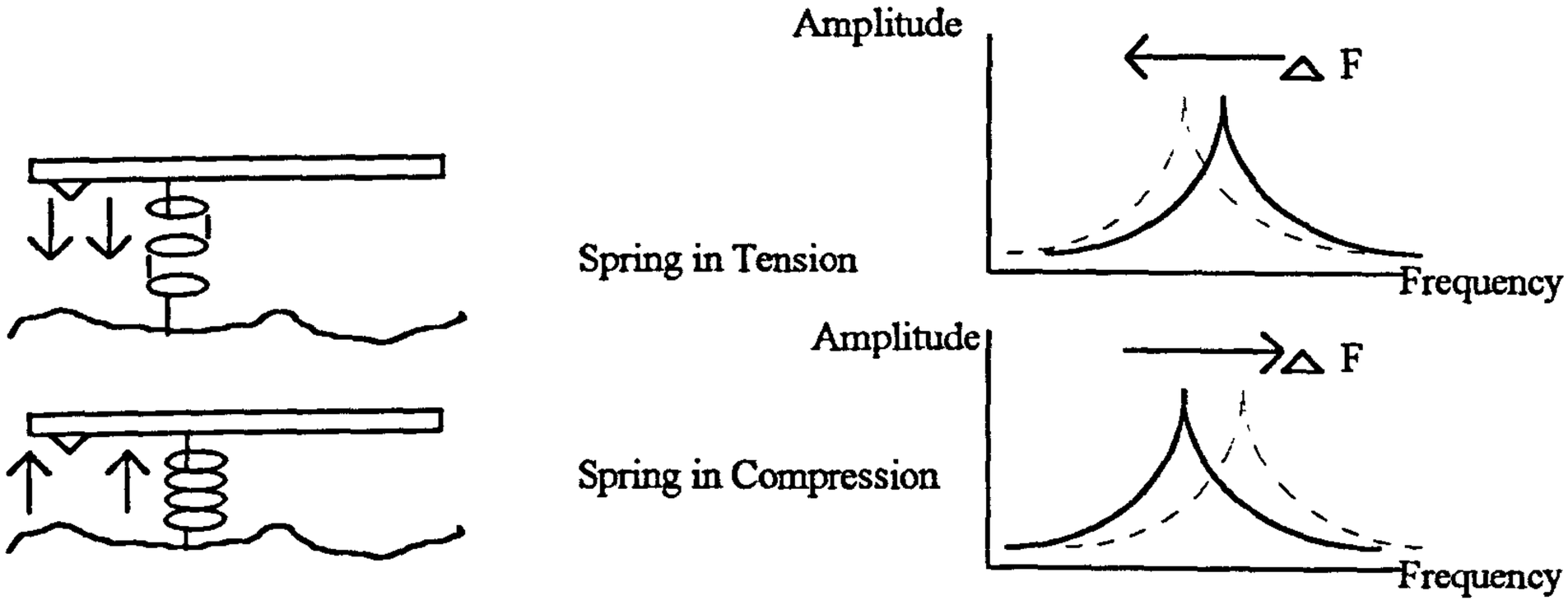

Figure 4.12 Attractive and repulsive forces on a probe tip modelled as a spring

The case of an attractive force between tip and surface can be modelled as a spring under tension. This reduces the resonant frequency of the cantilever. Conversely the case of a repulsive force can be modelled as a spring under compression this will increase the resonant frequency of the cantilever.

These changes in the cantilever resonant frequency can be detected in three ways by the microscope, Phase Detection, Frequency Modulation and Amplitude Detection.

Of the three methods Amplitude detection is not recommended (DI - Support Note #231, Rev.A) due to the appearance in images of artifacts (see section 4.2.3 for description of artifacts) whilst frequency detection has been not been found useful due to a limited contrast variance range (Z- range).

Phase detection is the method recommended (DI - Support Note #231, Rev.A) by the manufacturers and is the method used throughout this project. For details of the amplitude and frequency methods the reader is referred to Digital Instruments Inc. Support Note #231. When using phase detection the cantilever is tuned so that it reflects the phase difference between the drive voltage and the cantilever response as shown in figure 4.13.

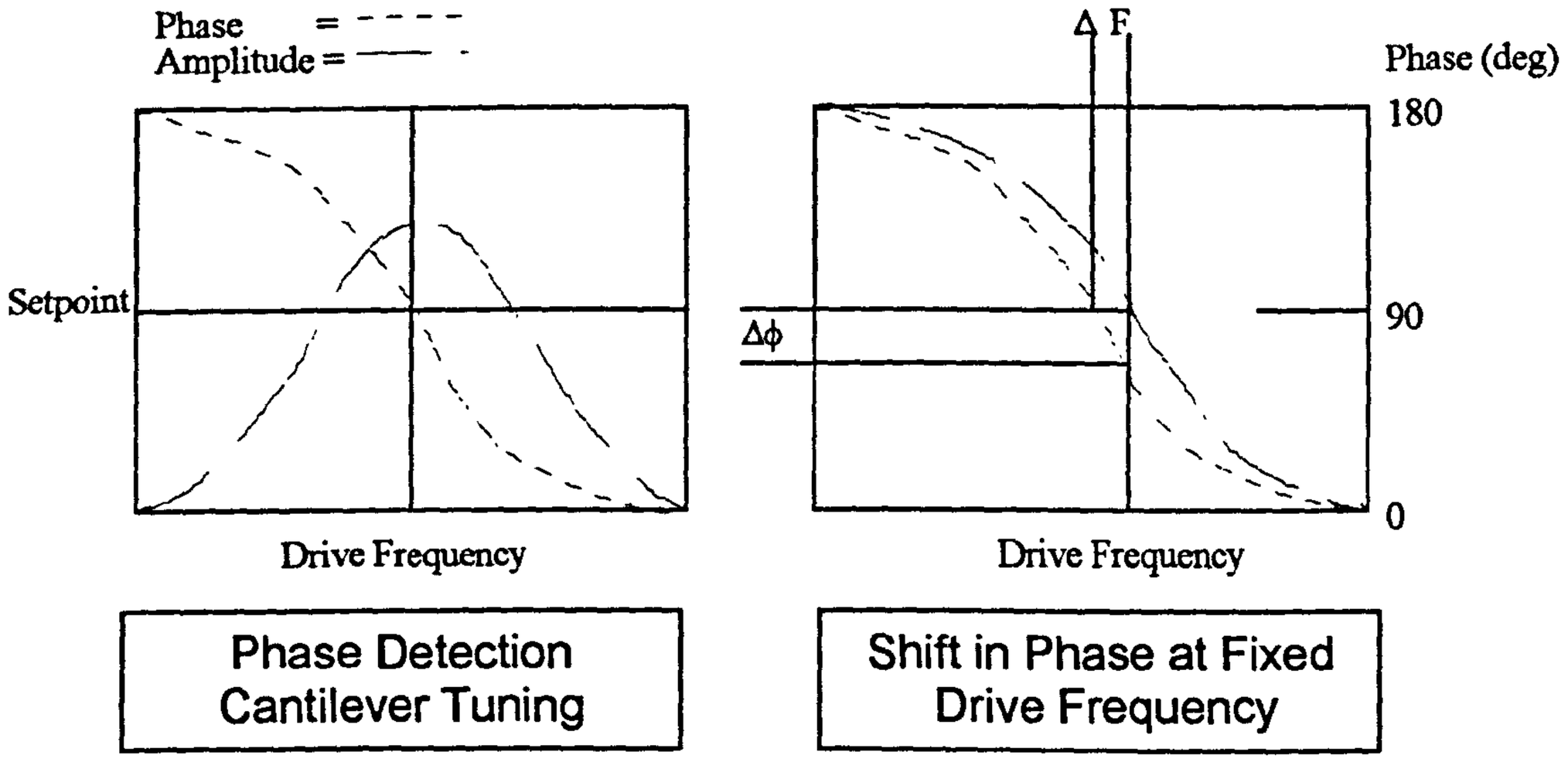

Figure 4.13 Showing cantilever tuning and shift in phase due to EFG.

The phase is set to cross the centre line (90 degrees), gradients in the electrostatic force cause a shift in frequency ΔF, which give rise to the

detected shift in phase $\Delta\phi$. Reductions in phase shift give rise to reductions in contrast whilst an increase in phase shift results in an increase in contrast.

(b) Surface Potential Imaging

In this mode the microscope adjusts the voltage on the tip until the minimum electric force is experienced by the tip. At this point the potential of the tip and sample are the same. In this way the microscope can build up an image of the surface based on the potential variations across the surface. Since the maximum voltage that can be applied to the tip is +/- 12V the technique is effectively limited to this voltage range. The makers recommend sample surface voltages of less than 10V and ideally a voltage range of +/- 5V.

4.2.3. Artifacts

In the use of these instruments, the experimenter must be aware of the ability of the machine to provide false images in certain circumstances. It is usual to refer to these false images as artifacts. There are some recognised situations that can produce these effects and also some recognised tests, which can be carried out to either confirm images as real or as an artifact.

The following are some situations where artifacts are known to be a problem (also see Appendix B):-

- Tip Imaging
- Noise or Incorrect Feedback Artifacts
- Cantilever Backlash
- Image Processing

(a) Tip Imaging

The tip used for the probe must be matched to the type of sample surface expected and also the type of forces that it is wished to image. If this is not done then depending on circumstances tip imaging can occur. When this happens the image displayed can in fact be the image of the tip, this is most likely to happen when the sample has features that are sharper than the tip.

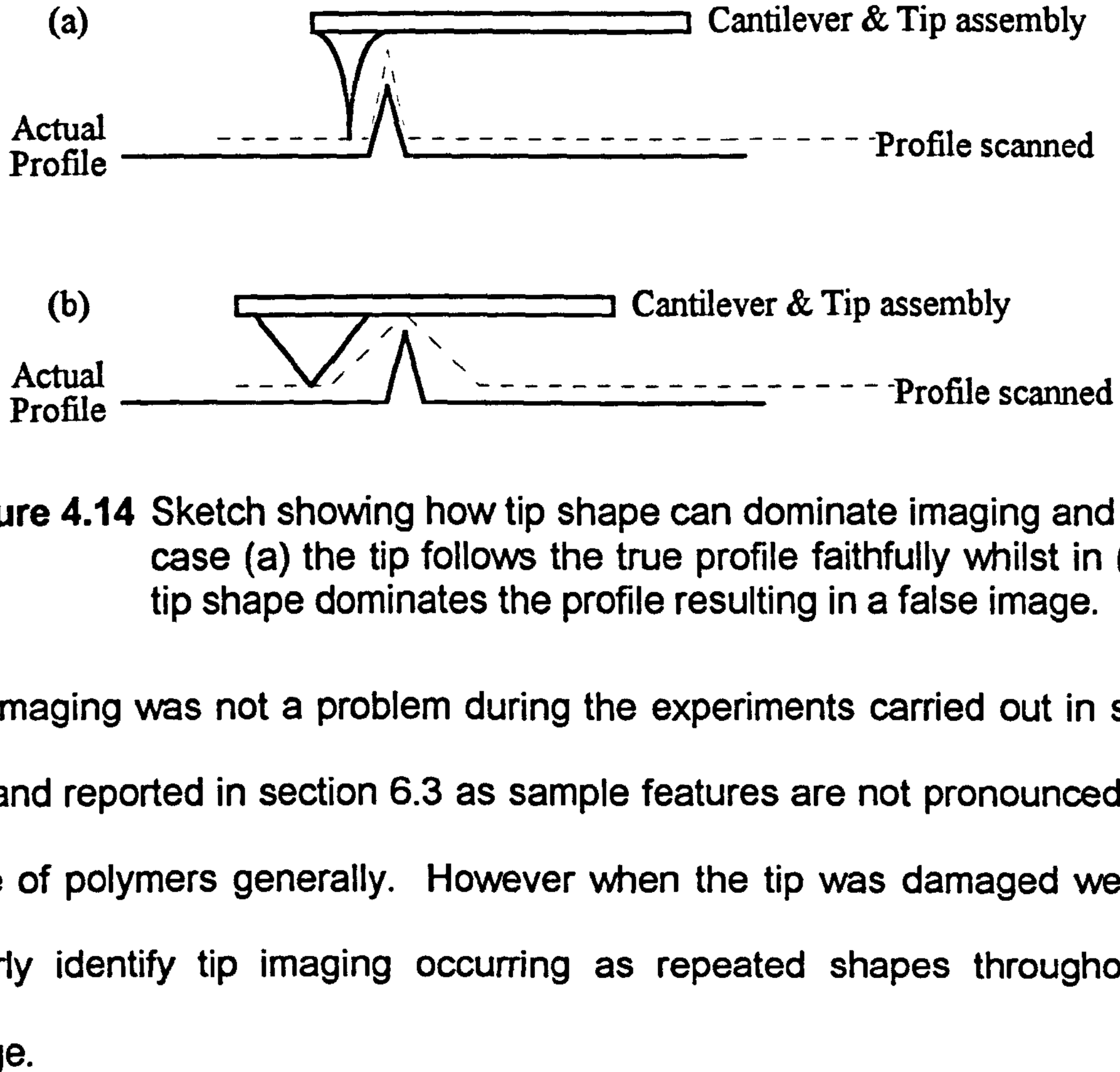

Figure 4.14 Sketch showing how tip shape can dominate imaging and that in case (a) the tip follows the true profile faithfully whilst in (b) the tip shape dominates the profile resulting in a false image.

Tip imaging was not a problem during the experiments carried out in section 5.4 and reported in section 6.3 as sample features are not pronounced in the case of polymers generally. However when the tip was damaged we could clearly identify tip imaging occurring as repeated shapes throughout the image.

(b) Noise or Incorrect Feedback

The feedback control must be optimised for the correct image to be obtained and is crucial to obtain the best performance from the instrument. Unfortunately in the real world when the feedback gains have been optimised for sensitivity at one part of the scan they may be too high in another part of the scanned area due to differences in topography. One of the effects that can result from this is "ghosting", this manifests itself as bright areas on the uphill side of sharp features and dark areas on the downhill side. This effect was experienced several times during the data collection phase of these experiments.

(c) Cantilever Backlash

As the probe assembly is scanned back and forth the cantilever can flex at the beginning and end of each scan line as the probe changes direction. This results in the appearance of artifacts at the edges of the scan. This effect was also experienced during these experiments.

(d) Image Processing

Image processing plays an extremely important part of the experimental procedure in SPM techniques. It can correct for curvature of the piezoelectric scanning table, remove scan lines, filter out interference from other equipment and enhance images by the use of different colour tables. Image processing can however lead to false images if used indiscriminately. In order to avoid these problems the very minimum use was made of image processing during these experiments. In addition where image processing was used any comparative images were treated in a similar fashion.

In order to ensure that details were the result of true imaging and not the result of artifacts as described above, the following tests were carried out to confirm apparent features.

- Scans were repeated to ensure that details stayed the same.
- Scan directions were changed to ensure that image details moved as expected.
- Scan sizes were changed to ensure that details scaled correctly.

- Samples were rotated to ensure that details repositioned themselves as expected.

- Repeated scans at different scan speeds to see if details changed, (feedback problems).

These tests were carried out as and when required. Where image details are still the subject of some doubt, this has been indicated in the text.

(e) Topographical Breakthrough in EFG Mode.

As the probe is retracted towards the lift height for EFG imaging when there is a relatively strong electrostatic charge present on the surface of the sample then the cantilever can be dragged closer to the surface than the desired lift height. This can result in topological breakthrough in the EFM image whereby the image becomes a normal height image rather than an EFG image. In extreme cases this can happen over the whole surface of the sample. This was avoided by carrying out the following procedures.

- The samples were washed with Isoproponol to neutralize surface charges.

- The tip was retracted further than the desired lift height and then returned to the lift height. This breaks any initial attraction between surface and tip.

- Any close correlation's between surface features and EFG image features were closely scrutinised and repeated scans and additional samples were examined to confirm the findings.

5. Experimental

5.1. Introduction

As already discussed, the boundary between the inner semi-con core covering and the bulk insulator is one of the key regions in determining the long term performance of high tension cables. At the same time it is by definition extremely difficult to examine this region without introducing morphological, rheological and chemical changes by the very act of sample preparation (Zharkov (1974)). The main techniques used in this work, Raman Spectroscopy, FTIR and SPM, are primarily surface examination techniques. As the semi-con/insulator boundary area is an interior region of the cable produced during a continuous extrusion process it is a major problem to be able to both reproduce meaningful experimental conditions and have this surface available for examination without inducing spurious results.

The initial approach chosen was to simulate the interface region; firstly by using a point – plane system but looking at the interface between the plane electrode and the sample rather than at the pin – sample interface. Secondly a parallel electrode arrangement was used with one of the electrodes being a semi-conducting polyethylene material similar to that used in the manufacture of high voltage cables. Actual cable samples were then examined, and the results correlated so as to draw meaningful conclusions. During the development of the experimental techniques used some additional equipment was constructed. Details of this are reported in Appendix D.

5.2. Sample Preparation

The three types of experiments carried out required different sample preparation techniques due to either the type of sample or the experimental techniques. The three main techniques are discussed in the following paragraphs.

5.2.1. Pin-Plane Experiments

In this series of experiments the basic sample configuration consisted of a point-plane arrangement as shown in Figure 5.1.

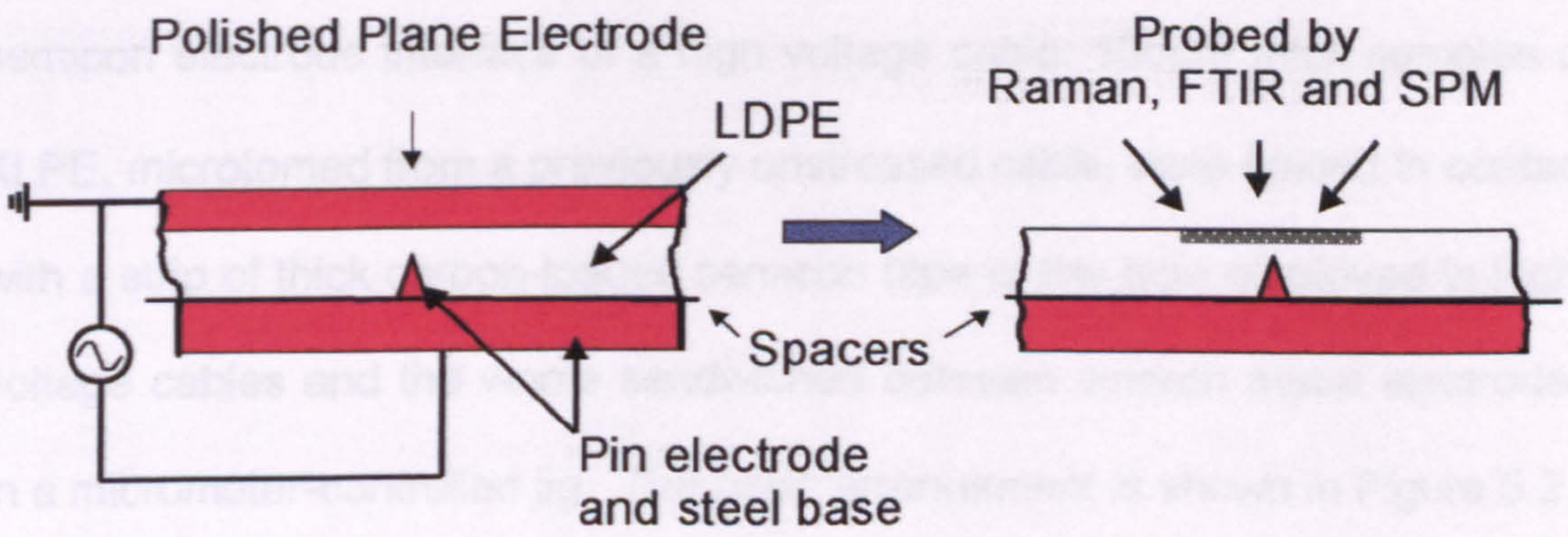

Figure 5.1 Point plane electrode arrangement showing removable plane electrode, sample, spacers, steel point electrode and steel base. The grey region defines the area examined.

The point electrode consisted of a steel needle of tip radius 50μm permanently mounted on a planar stainless steel circular stub and projecting 3mm above it. A sample of LDPE, 3mm thick, warmed until it became

translucent so that it was relatively soft and undue mechanical stresses would not be set up in it, was then carefully pressed on to the stub. The gap between the needle tip and the surface of the sample was controlled by the use of a set of 10μm thick LDPE spacers inserted between the sample and the base electrode. A polished circular planar electrode was then pressed on to the sample surface using a specially constructed jig and micrometer. Alternating voltages, accurate to ±1.5%, were applied between the electrodes for known times with the plane electrode grounded.

5.2.2. Simulated Semicon-XLPE Interface Experiments

The second apparatus was designed to simulate the conditions at the semicon electrode interface of a high voltage cable. 100μm thick samples of XLPE, microtomed from a previously unstressed cable, were placed in contact with a strip of thick carbon-loaded semicon tape of the type employed in high-voltage cables and the whole sandwiched between smooth metal electrodes in a micrometer-controlled jig. The basic arrangement is shown in Figure 5.2.

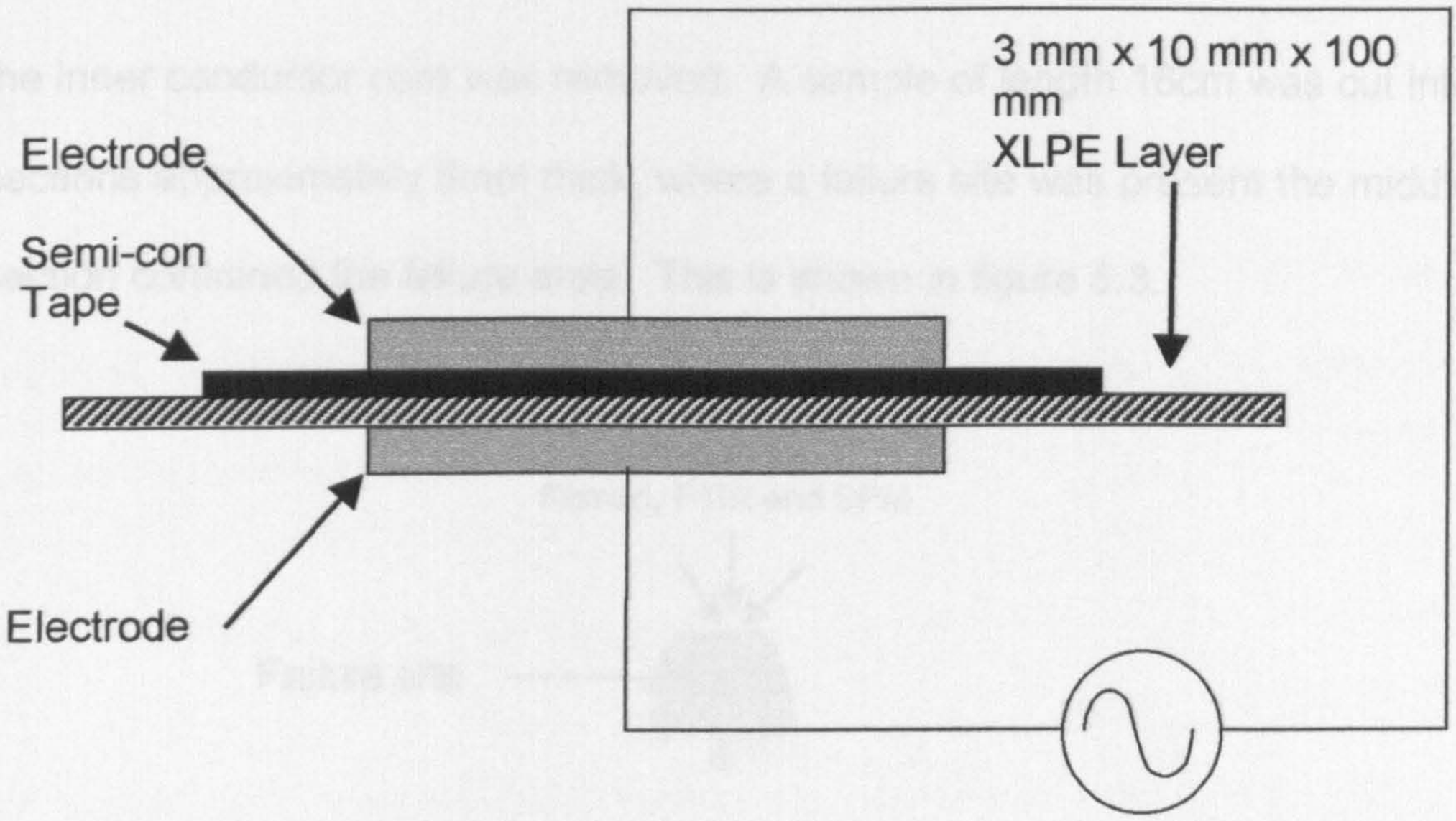

Figure 5.2 Outline sketch showing electrode arrangement used to simulate the conditions existing at the semi-con / insulator interface in power cables, the sample size was 3mm x 10mm.

The semicon layer being quite soft made intimate contact with the XLPE sample; this ensured that the interface presented was a reasonable approximation of that found in a typical high voltage cable.

Alternating voltages were applied to the bottom electrode whilst the top electrode, which was in contact with the semi-con tape was earthed. After electrically stressing the XLPE sample, the semicon tape could be readily removed and the XLPE surface scanned with the spectrometer.

5.2.3. High Voltage Cable Samples

For these experiments actual cable samples were used, these were manufactured by BICCGeneral and subjected to an increasing ramp voltage to the point of failure. The cable samples were then finally prepared for examination on site by firstly cutting the cable down a centreline to leave two lengths of semi-circular cable. All outer coverings were then stripped off and

the inner conductor core was removed. A sample of length 16cm was cut into sections approximately 5mm thick, where a failure site was present the middle section contained the failure area. This is shown in figure 5.3.

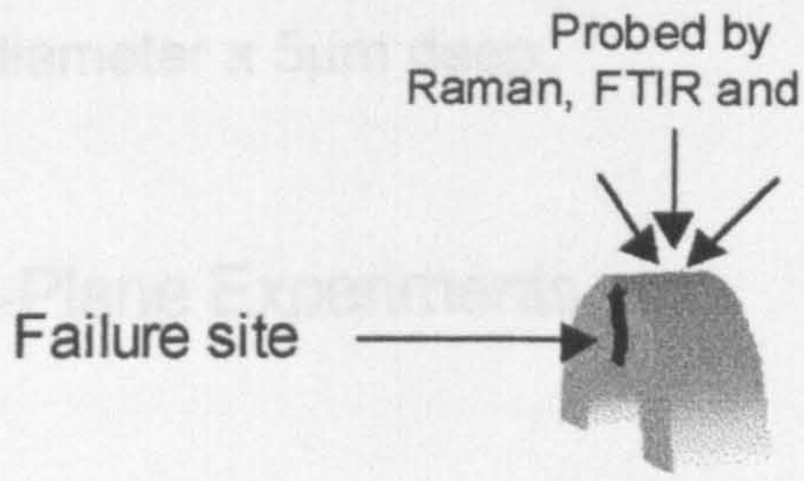

Figure 5.3 Outline sketch showing the cable samples, ready for examination each section is 5mm thick.

This approach was taken so that: -

- The outer surface was available for analysis; this area is essentially comparable to the area examined in both the previous experimental sections i.e. 5.2.1 and 5.2.2.
- The inner bulk insulation was also available to be probed at various depths.

5.3. Raman Spectroscopy

The Raman spectrometer, a Renishaw Ramanscope 1000 with a HeNe laser, motorised stage and 50X objective, had a maximum resolution in confocal mode of 2 μm diameter x 5μm deep.

5.3.1. Pin-Plane Experiments

After subjecting the pin-plane samples to an electric field (see § 5.2.1) for a chosen time, the planar electrode was carefully removed and the sample transferred to the confocal Raman spectrometer. The spectrometer beam was focussed onto (or in some cases below) the sample surface and a spectrum obtained.

Experiments to determine the development of the spectrum at a chosen spot on the sample surface as a function of stressing time required repeated transfer of the sample between the voltage source and the spectrometer. On returning a sample to the spectrometer, it was possible to locate the same chosen spot in the polymer accurately, using the tip of the needle electrode as a reference point as shown in figure 5.4.

Tip of electrode visible through the optical microscope attached to the Spectrometer.

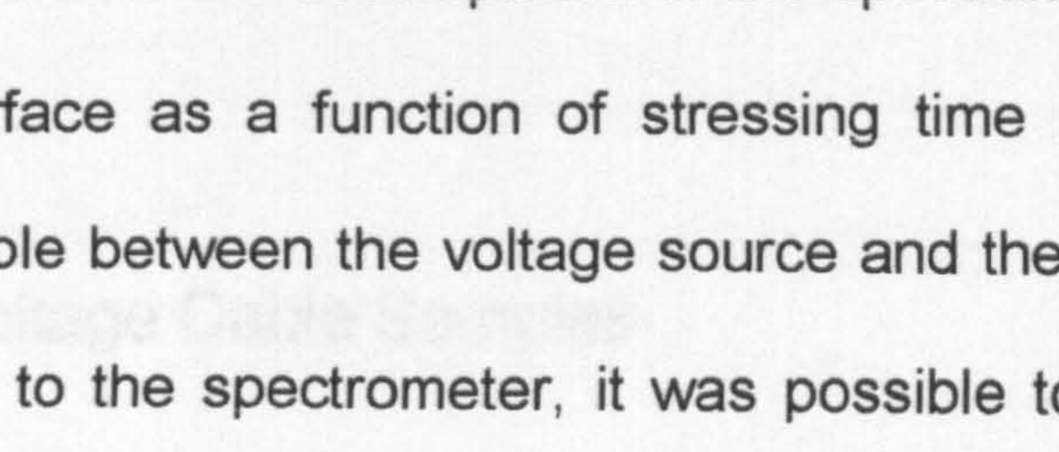

Figure 5.4 Side view of sample after plane electrode has been removed.

5.3.2. Simulated Semicon-XLPE Interface Experiments

In the case of the XLPE/semicon experiments (see section 5.2.2), the macroscopically uniform field precluded an obvious preferred site for activity although microscopic inhomogeneities in the semicon electrode layer would lead to localized field enhancement. In view of this the Raman objective was scanned across the XLPE surface along a line corresponding originally to the centre-line of the semicon electrode; the choice of the centre line was made to avoid any results being due to discharges from the electrode edges. The top and bottom electrodes were in close contact to exclude atmospheric effects – in addition the semicon layer was quite soft and readily moulded itself to the underlying LDPE surface. All of the experiments were conducted in air and the semicon layer extended beyond both top and bottom electrodes in order to further minimize any effects due to razzing around the edge of the sample.

5.3.3. High Voltage Cable Samples

These samples that were supplied by BICCGeneral had already been electrically stressed. Following sample preparation as outlined in section 5.2.3 the collection of Raman spectra was reasonably straightforward.

Having been sectioned as shown in figure 5.3 the cable samples presented several opportunities to examine the spectrum of the bulk insulation at various depths as the inner semicon core covering was approached. This is shown in cross section in figure 5.5.

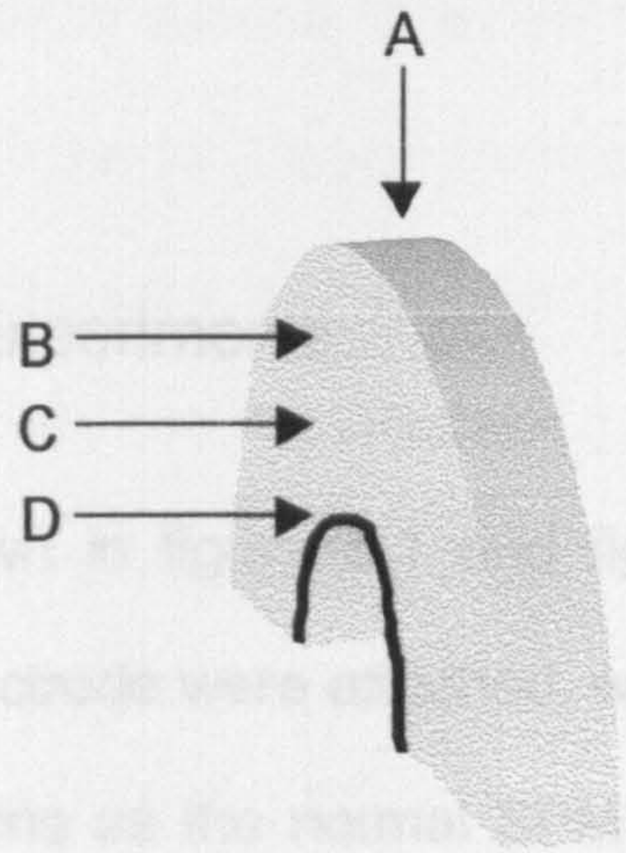

Figure 5.5 Section of the cable showing how spectra could be obtained at the surface, A, as well as at various depths, B, C and D approaching the inner semicon core covering.

5.4. SPM Studies

5.4.1. Pin-Plane Experiments

As the steel stub (shown in figure 5.1 and figure 5.4), to which both the sample and the point electrode were attached, was designed to be exactly the same size and dimensions as the normal SPM steel sample mounting plate transferring the sample to the SPM was extremely simple. Once again the location of the high stress area could be reliably located by observing the needle electrode through the optical microscope attached to the SPM. (Figure 5.4)

Data was captured in three of the operating modes available namely, Topographical, Phase Imaging and Electric Force Gradient. It was found that Phase imaging gave the best representation of the surface of the sample, Topographical imaging was used as confirmation of features whilst Electric Force Gradient images provided information on the presence of surface layer charges. A significant amount of work was carried out to investigate Phase imaging and this is presented in Appendix B.

5.4.2. Simulated Semicon-XLPE Interface Experiments

The sample stub for the SPM is 15mm in diameter, so it was possible to remove the excess material from around the active sample region (3 x 10 mm) and then fix the sample to the stub. This avoided having to cut the sample at all and ensured that the whole sample was available for investigation.

In order to make the sample surface available for both Raman Spectroscopy and Scanning Probe Microscopy the sample was first fixed to a piece of virgin LDPE which was then attached to the SPM stub. This was necessary to avoid any fluorescence effects in the Raman spectrum arising from the spectrometer "seeing" the stainless steel stub.

5.4.3. High Voltage Cable Samples

Sectioning the sample was unavoidable in this instance, however as these experiments were designed to look for confirmation of the results obtained in section 5.4.1 and 5.4.2 in a real cable sample this was not seen as a problem. The samples were sectioned to enable the required area to fit within the 15 mm diameter sample size imposed by the SPM.

5.5. FTIR

The FTIR equipment included a diamond ATR device as already outlined in section 4.1.4. This enabled us to use two different approaches to the examination of our samples. It was possible using the ATR to examine the sample spectroscopically by placing the sample on top of the ATR device whilst still mounted; however this proved very difficult to do in practice and gave a less than ideal spectrum. Therefore all FTIR work was carried out by removing the sample from the fixed electrode/base arrangement and treating it as any other FTIR sample. This meant that the samples were sectioned to enable a high quality spectrum to be obtained. Once this was carried out the sample could no longer be returned to the electrical field for further stressing.

6. Results

The motivation behind this thesis was to investigate possible structural changes induced in LDPE and XLPE by high alternating electrical fields as discussed in section 3.3.

It is important to appreciate that the changes in the material being investigated may occur long before the material breaks down and indeed long before any gross physical changes such as micro void creation, partial discharge or electrical tree growth.

The surface investigation techniques available and used here have already been discussed in chapter 4 whilst the experimental techniques were described in chapter 5.

The results presented were found to be repeatable over a number of samples of XLPE and LDPE. The individual results given here were chosen in order to be representative of the overall findings of the author during these experiments.

6.1. Raman Spectroscopy

6.1.1. Pin Plane Experiments

A series of typical Raman spectra, obtained at the surface of a sample of LDPE above the point electrode at A, are shown in Figure 6.01.

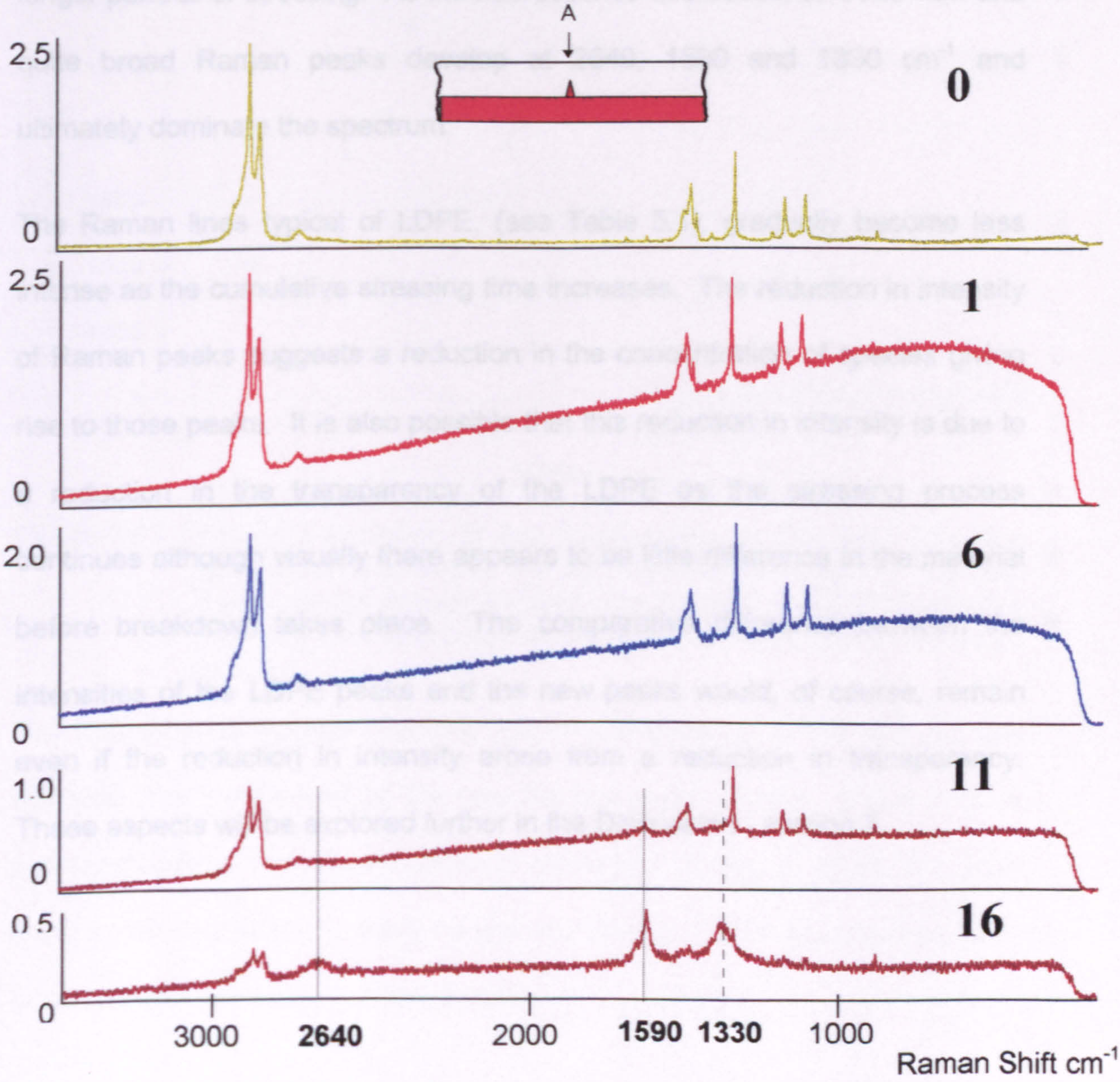

Figure 6.01. Series of Raman spectra for LDPE showing the way the spectrum develops with time whilst under an electrical field. The bold figures on the right indicate the time in minutes for which the sample was subjected to the field, which in this instance was about 6×10^7 Vm^{-1}.

At zero time, before the application of a field, the spectrum is that normally expected for LDPE and there is an absence of laser-induced fluorescence as indicated by the flat background. After 1 minute of stressing however, with a RMS field at the polymer surface of approximately 6 x 10^7 Vm^{-1}, a large fluorescence background has developed but this decays dramatically after longer periods of stressing. As the fluorescence decreases, so three new and quite broad Raman peaks develop at 2640, 1590 and 1330 cm^{-1} and ultimately dominate the spectrum.

The Raman lines typical of LDPE, (see Table 5.1), gradually become less intense as the cumulative stressing time increases. The reduction in intensity of Raman peaks suggests a reduction in the concentration of species giving rise to those peaks. It is also possible that this reduction in intensity is due to a reduction in the transparency of the LDPE as the stressing process continues although visually there appears to be little difference in the material before breakdown takes place. The comparative difference between the intensities of the LDPE peaks and the new peaks would, of course, remain even if the reduction in intensity arose from a reduction in transparency. These aspects will be explored further in the Discussion - section 7.

6.1.1.1. Field-Induced Fluorescence Intensity as a Function of Time

Concentrating on the fluorescence background in figure 6.01, the growth and subsequent decay of the fluorescence was plotted by selecting a particular Raman shift, in this case 614 cm^{-1}, and recording the intensity (counts). A typical result is shown in Figure 6.02.

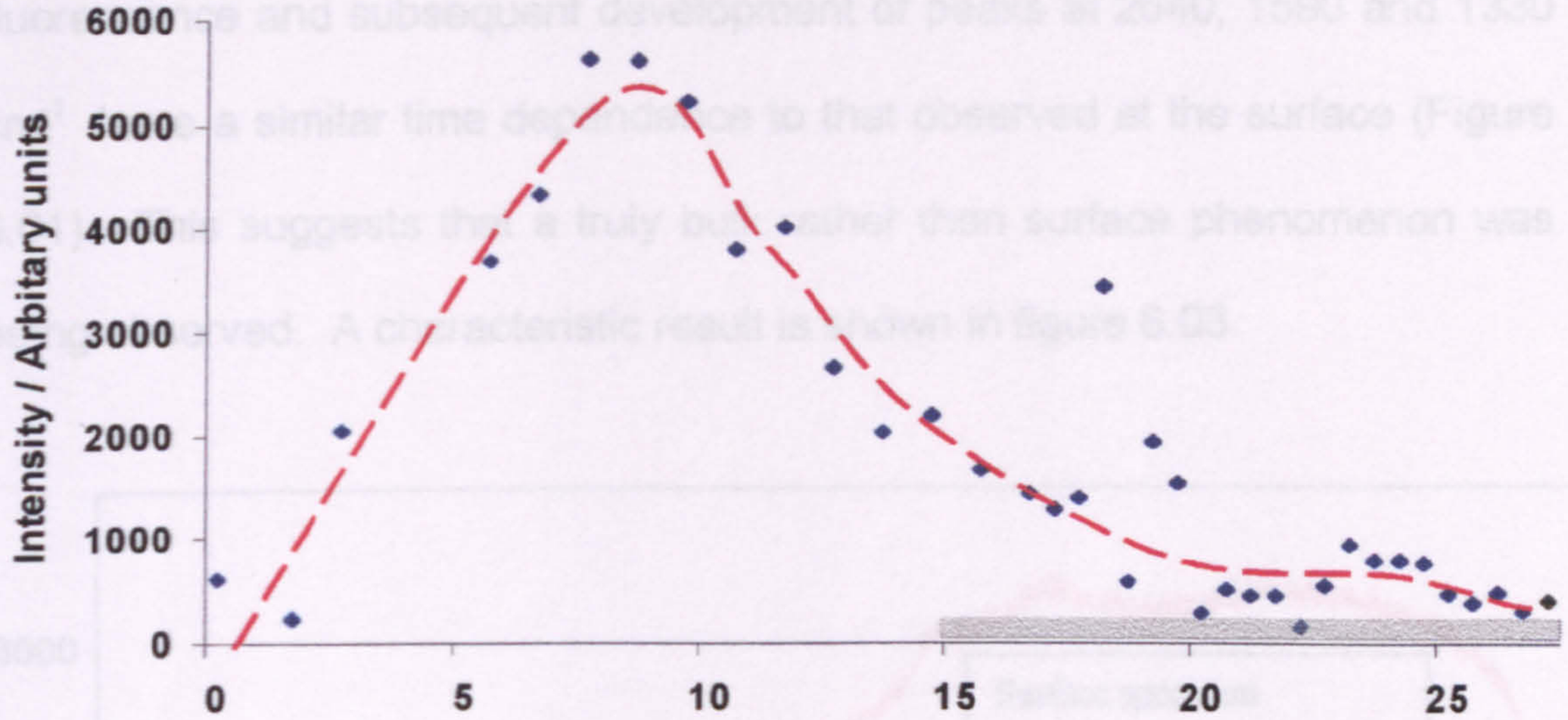

Figure 6.02. The time evolution of the fluorescence at 614 cm^{-1} following application of a field at the surface of 6 x 10^7 Vm^{-1}. The new Raman peaks appear (indicated by the grey band) at 15 minutes stressing time and begin to dominate the spectrum at about 20 minutes.

The fluorescence increases quickly following application of the field but has decayed to a low level when the new Raman peaks appear. Figure 6.02 is representative of the results obtained although the time at which the peak occurs may vary by two to three minutes either way. All of these spectra were collected from the surface of the sample.

It should be noted that in this section and those that follow the actual choice of Raman shift point (i.e. 614 cm^{-1}) chosen is irrelevant and that the same curve

representing the growth and decay of the fluorescence would have been achieved at any particular point on the spectrum.

6.1.1.2. Field-Induced Fluorescence in the Bulk Material

Using the confocal mode it is possible to investigate conditions below the polymer surface down to a depth of 25 μm. It was found that the field-induced fluorescence and subsequent development of peaks at 2640, 1590 and 1330 cm^{-1} have a similar time dependence to that observed at the surface (Figure 6.01). This suggests that a truly bulk rather than surface phenomenon was being observed. A characteristic result is shown in figure 6.03.

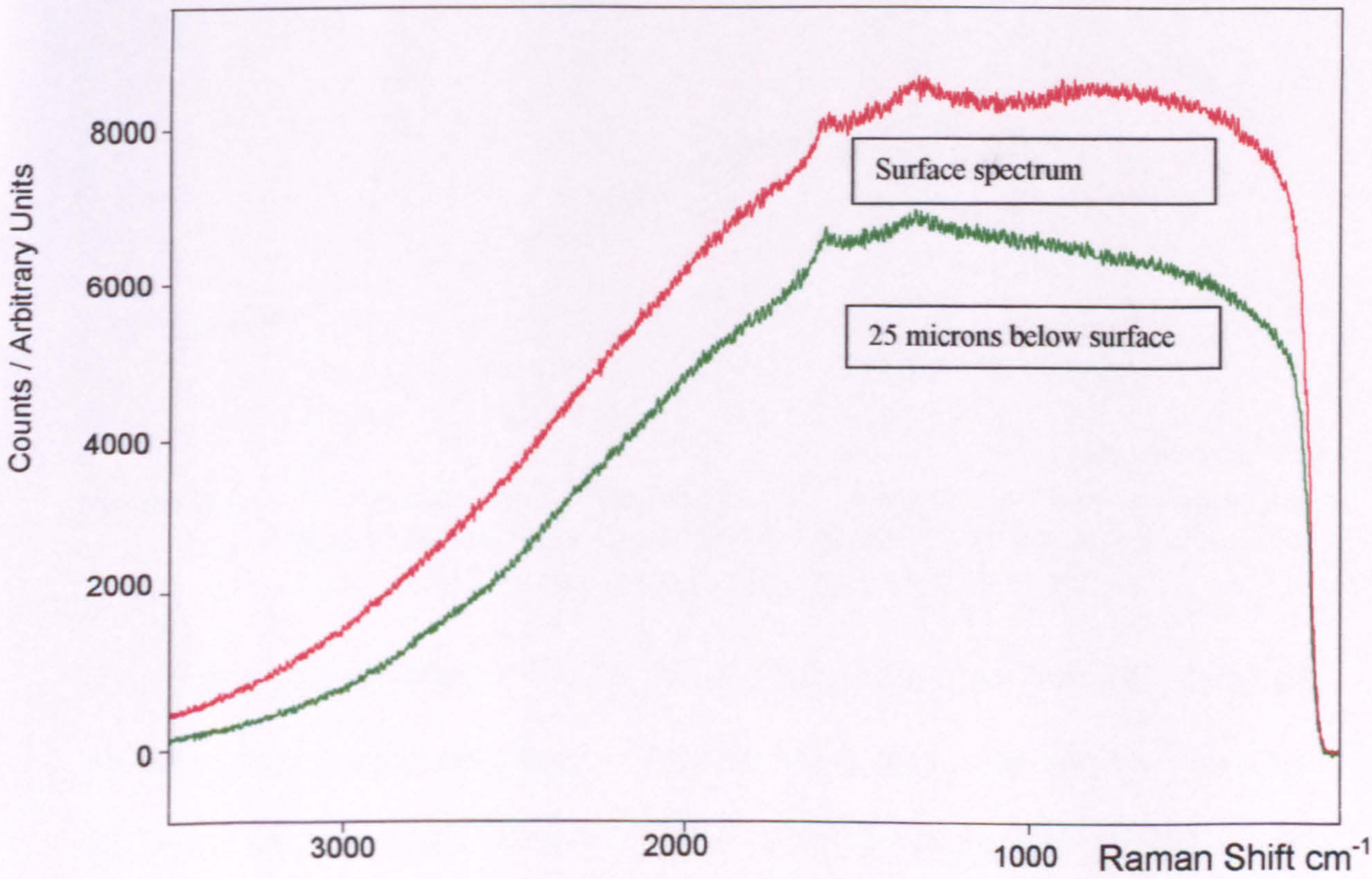

Figure 6.03. The red curve shows the spectrum with the Spectrometer focused on the surface layer of the LDPE, whilst the green curve represents the spectrum obtained with the con-focal Raman focused 25μm below the surface of the LDPE

It can be seen from figure 6.03 that the spectra obtained at the surface and below the surface are essentially the same. Due to the intensity of the fluorescence and the peaks at 1590 and 1330 cm^{-1} the "normal" LDPE peaks are all but invisible. There is a reduction in intensity shown for the spectrum obtained from the bulk; this is to be expected, as the intensity of the Raman Spectrum obtained is dependent on the transparency of the sample.

6.1.1.3. Resistance of Field-Induced Fluorescence to Quenching.

It was found that field–induced fluorescence is very resistant to quenching by the laser light and is thus very different from the residual fluorescence often found in virgin samples of PE. Field-induced fluorescence was still in evidence after the sample had been exposed to laser light continuously for 24 hours whereas residual fluorescence can usually be quenched in a matter of minutes.

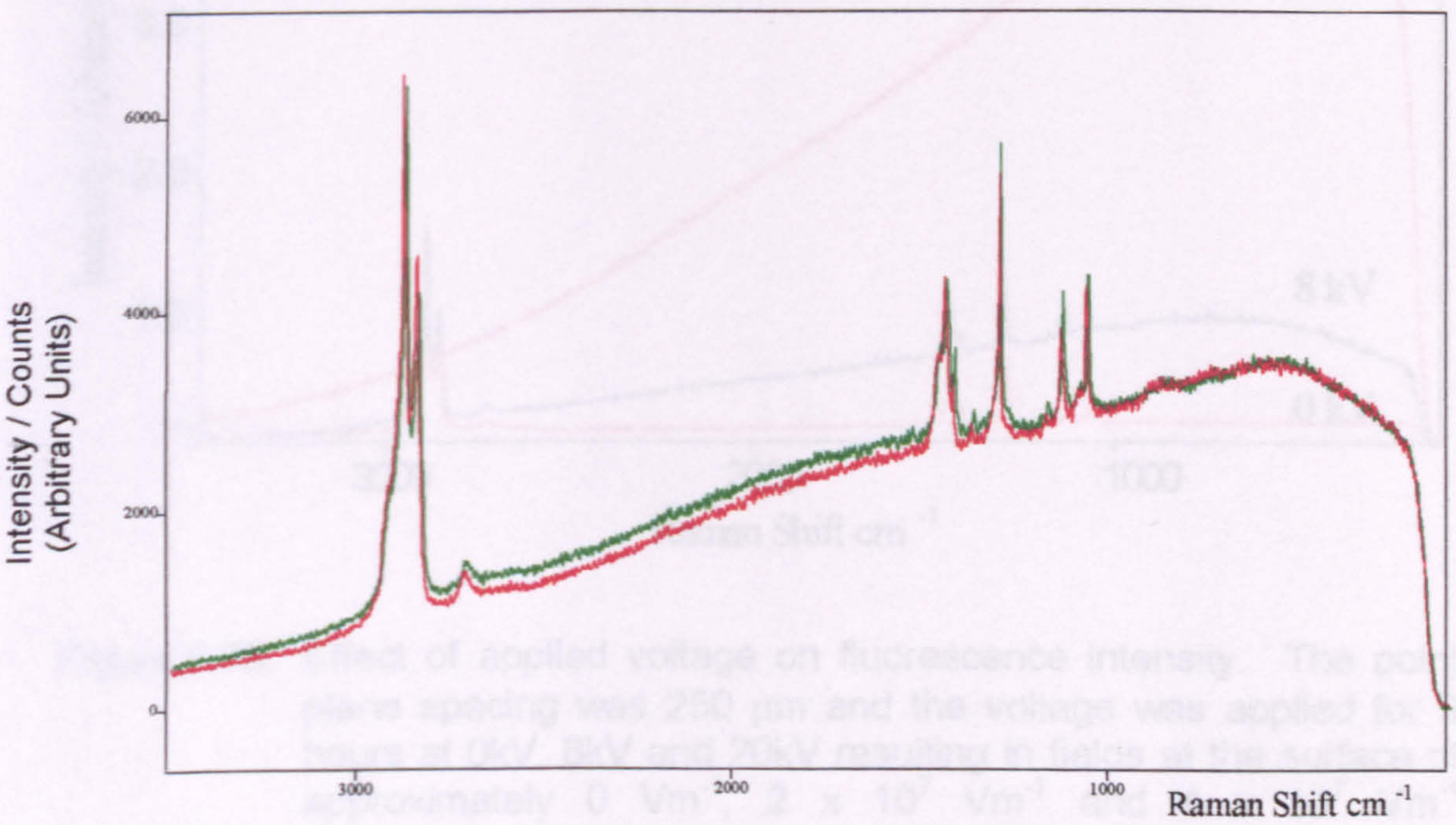

Figure 6.04 A typical result showing the change in the background fluorescence after leaving the sample (LDPE) under the laser light of the Raman spectrometer for twenty-four hours.

The green curve shown Figure 6.04 represents the Raman spectrum immediately following application of an electrical field. The sample was then left in the Raman spectrometer for twenty-four hours with the Raman laser irradiating the sample for the whole time. The sample was not moved at all during this period. A new spectrum was obtained and this is represented by the red curve. As can be seen there is essentially no difference between the two spectra.

6.1.1.4. Field-Induced Fluorescence as a function of Field Strength

The fluorescence intensity was found to increase with the field strength as illustrated in Figure 6.05.

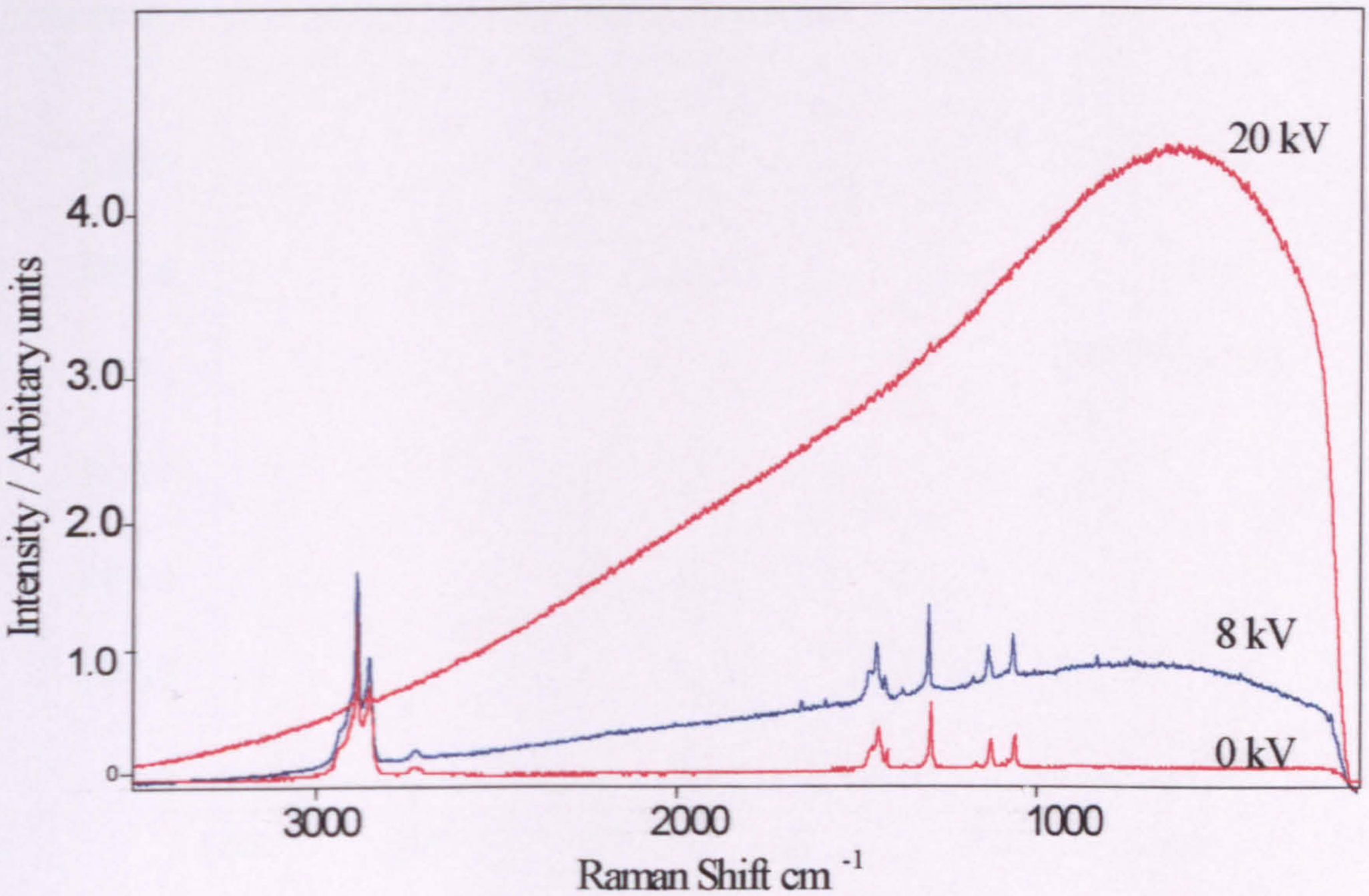

Figure 6.05. Effect of applied voltage on fluorescence intensity. The point plane spacing was 250 μm and the voltage was applied for 3 hours at 0kV, 8kV and 20kV resulting in fields at the surface of approximately 0 Vm^{-1}, 2 x 10^7 Vm^{-1} and 4 x 10^7 Vm^{-1} respectively.

Figure 6.05 shows the spectra obtained at the position of maximum field intensity on the polymer surface directly opposite the pin electrode. The three spectra clearly show the increase in fluorescence as a function of increasing field intensity. The results in figure 6.05 were obtained with a point plane spacing of 250 μm. The same relationship between field strength and fluorescence intensity was obtained by reducing the voltage applied to the pin but maintaining the point plane spacing at 50μm as for the other results

shown previously in this section. This is indicative of the change in fluorescence intensity being the result of the varying electrical field strength.

6.1.1.5. Surface Distribution of Field-Induced Fluorescence

It is possible to scan the spectrometer across the surface away from the point of maximum field at A in order to obtain the surface distribution of fluorescence. A typical result is shown in Figure 6.06.

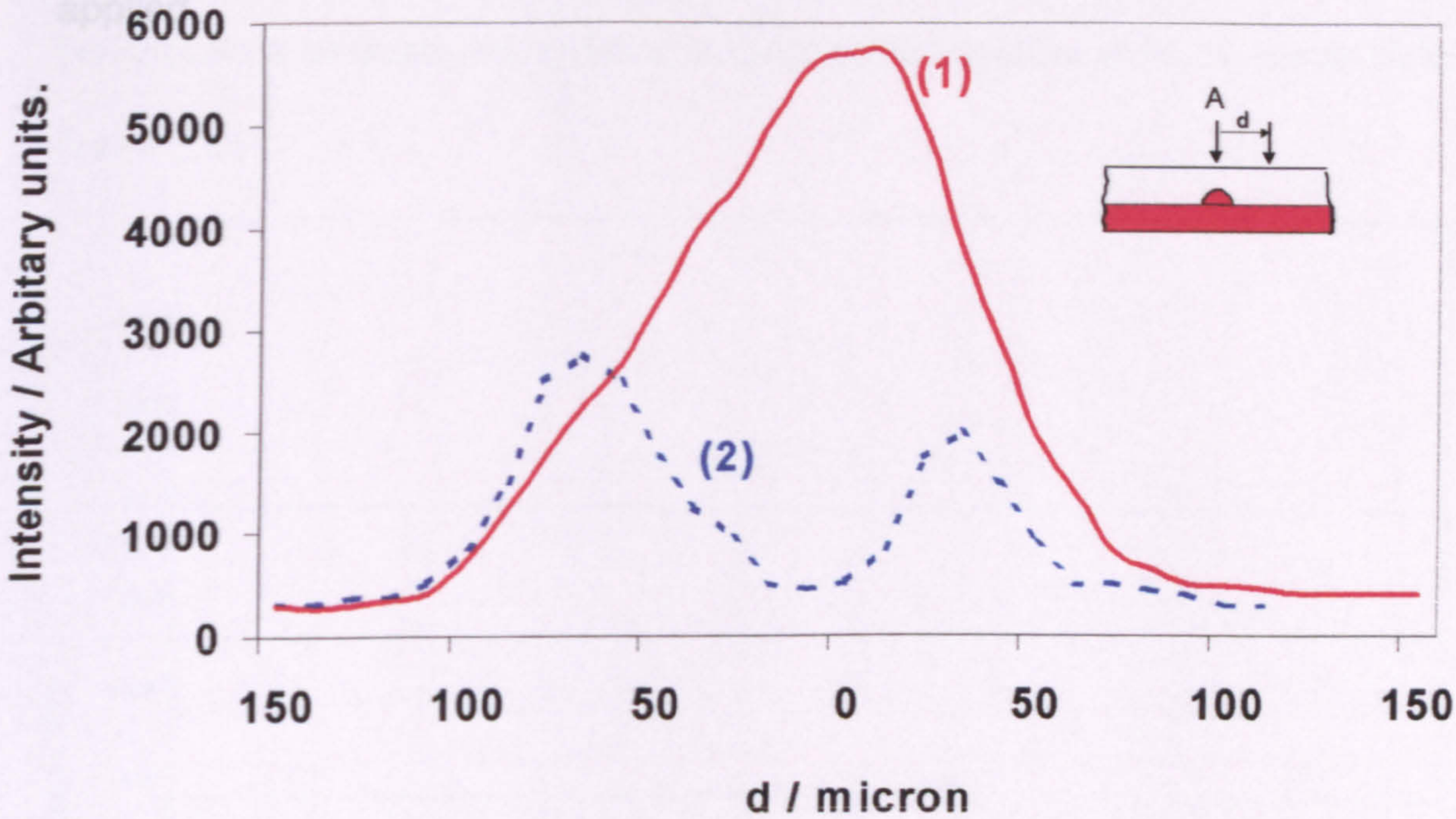

Figure 6.06. Fluorescence at 1741 cm^{-1} as a function of distance, d, across the surface from the point electrode axis at A. (1) The initial distribution. (2) The distribution after 30 minutes in a field of $6x10^7$ Vm^{-1}.

At an early time (1) after voltage application the fluorescence is at a maximum on the axis and falls away symmetrically on either side. Curve (2), obtained after 30 minutes shows that when the fluorescence decays it does so preferentially in the high field central region to give a distribution with a dip in the centre. Although not shown on figure 6.06 this experiment also demonstrated that both the field induced fluorescence and the new peaks at 1590 and 1330 cm^{-1} can coexist in the same sample. In the high field region at A the luminescence has collapsed and the peaks at 1590 and 1330cm^{-1}

have appeared but in the surrounding lower field regions at about 50 μm from the axis the luminescence exists without any evidence for the 1590 and 1330cm^{-1} peaks. This will be discussed further in the discussion (Section 7) but would seem to be consistent with the electrical stress initiating further changes in the structure of the material as a function of both time and field applied.

6.1.1.6. Disordered Longitudinal Acoustic Mode

As discussed in section 4.1.1.3.3 the Disordered Longitudinal Acoustic Mode or DLAM is an indication of the long-range conformational disorder of the polymer chain in the amorphous region. In order to observe the DLAM peaks in our samples it was necessary to remove the electric field induced fluorescence background by fitting a multi-point baseline to each spectrum in figure 6.01.

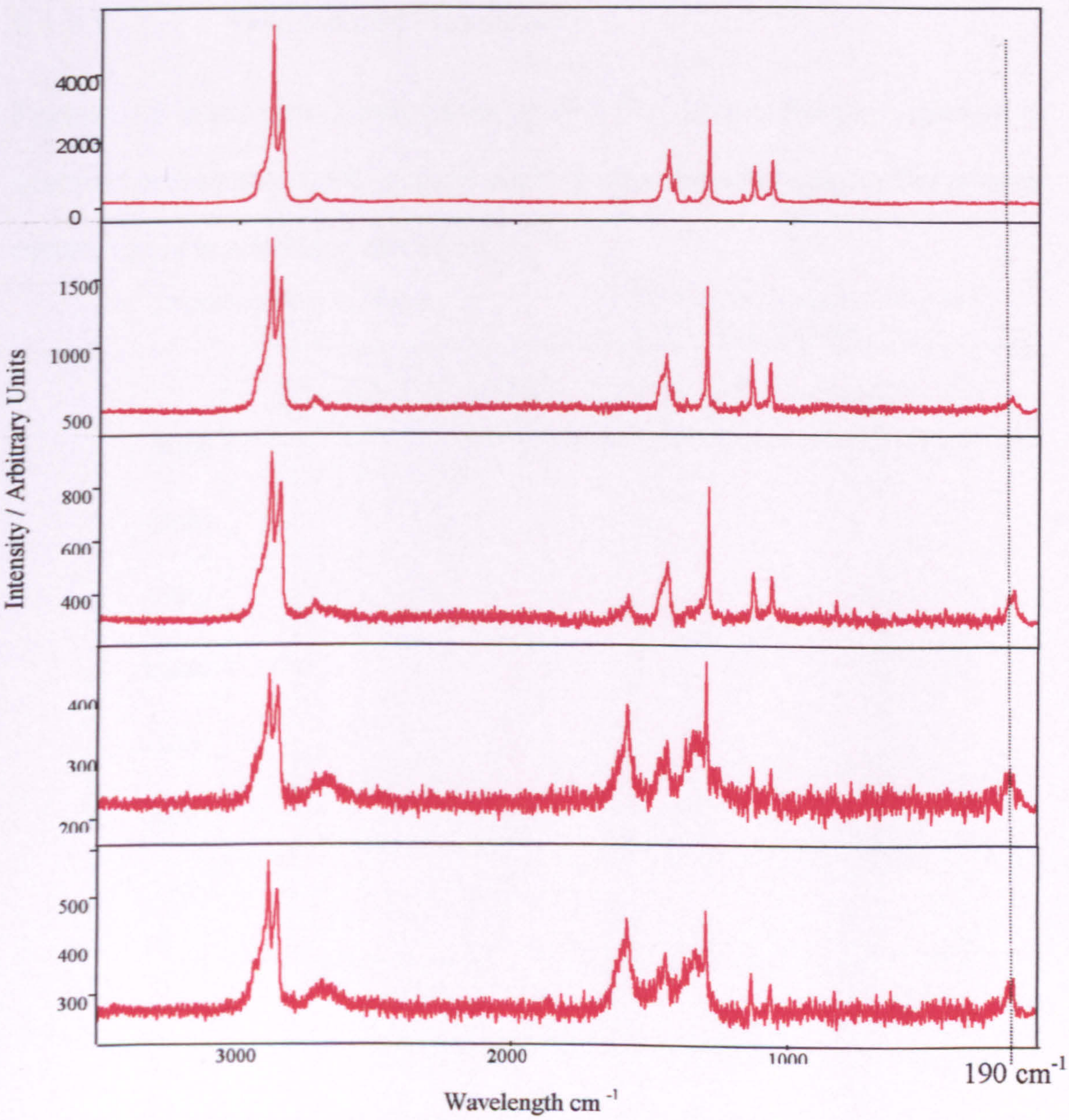

Figure 6.07 Baseline corrected spectra from figure 6.01 showing the development of the DLAM band at 190 cm^{-1}.

As outlined in section 4.1.1.3.3 the DLAM intensity is related to the long-range conformational disorder in the polyethylene. These results would therefore support the view of increasing conformational disorder in the polymer chains with increasing time under an electrical field. These results will be discussed further and integrated with those from previous and following sections in chapter 7.

6.1.2. Simulated Semicon-XLPE Interface Experiments

In the case of the XLPE/semicon experiments, the macroscopically uniform field precluded an obvious preferred site for activity although microscopic inhomogeneities in the semicon electrode layer would lead to localized field enhancement. The experimental sample arrangement has already been described in section 5.2.2.

6.1.2.1. Field Induced Fluorescence

Figure 6.08 shows the fluorescence at 767 cm^{-1} as the Raman objective is scanned across the XLPE surface along a line corresponding to the original centre-line of the semicon electrode.

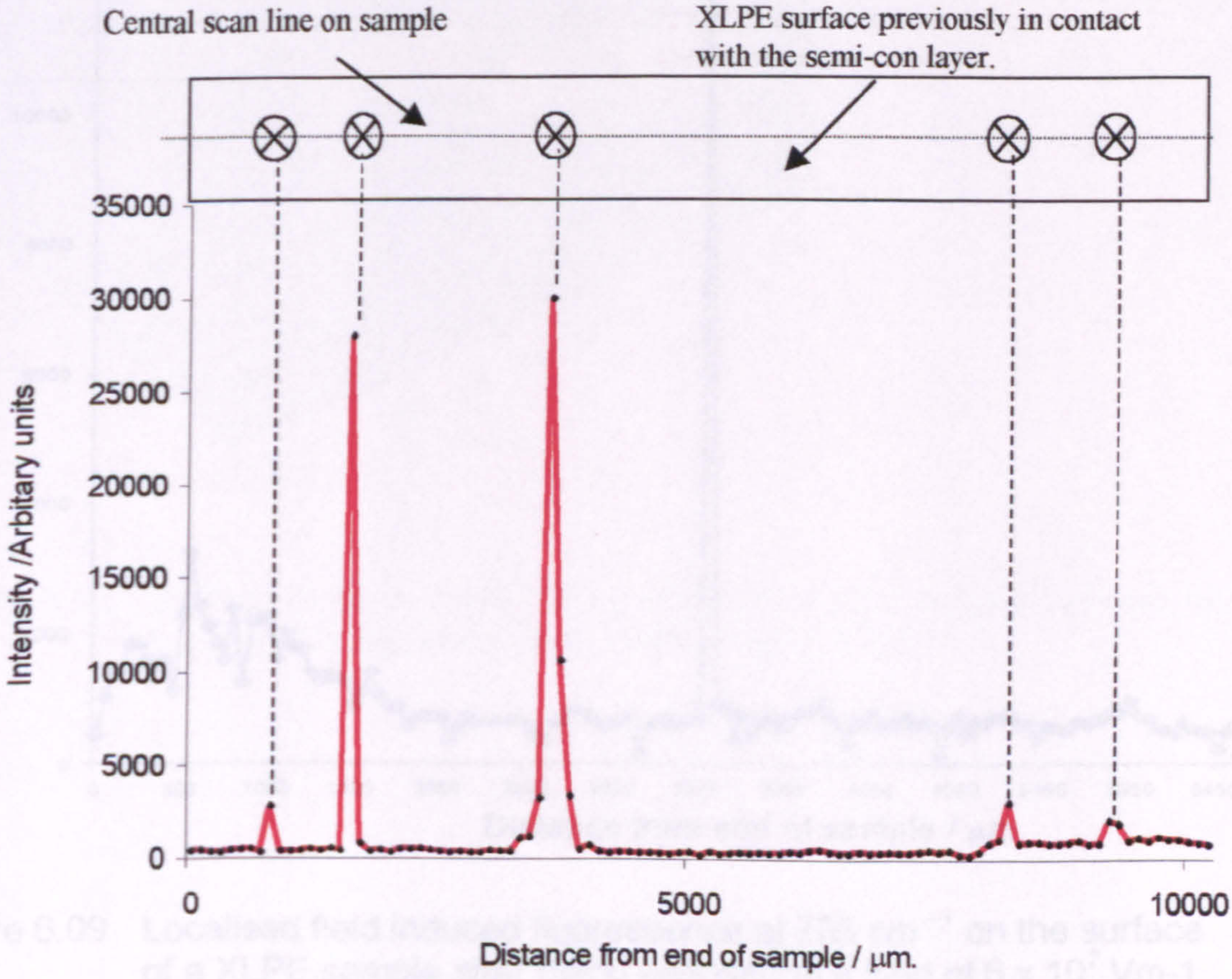

Figure 6.08 Field induced fluorescence at a Raman shift of 767 cm^{-1} on the surface of a XLPE sample exposed to a field of 6 x 10^7 Vm^{-1} in contact with a semicon electrode for a time of 6 hours.

Typically, several highly localised areas of fluorescence were found. For the sample shown in Figure 6.08 there are two major sites of activity, with one extending over about 300 μm or so. All the activity was sited in macroscopically uniform field regions well away from the edges of the semicon electrode.

Figure 6.09 was obtained in exactly the same way as Figure 6.08 but at a different Raman shift.

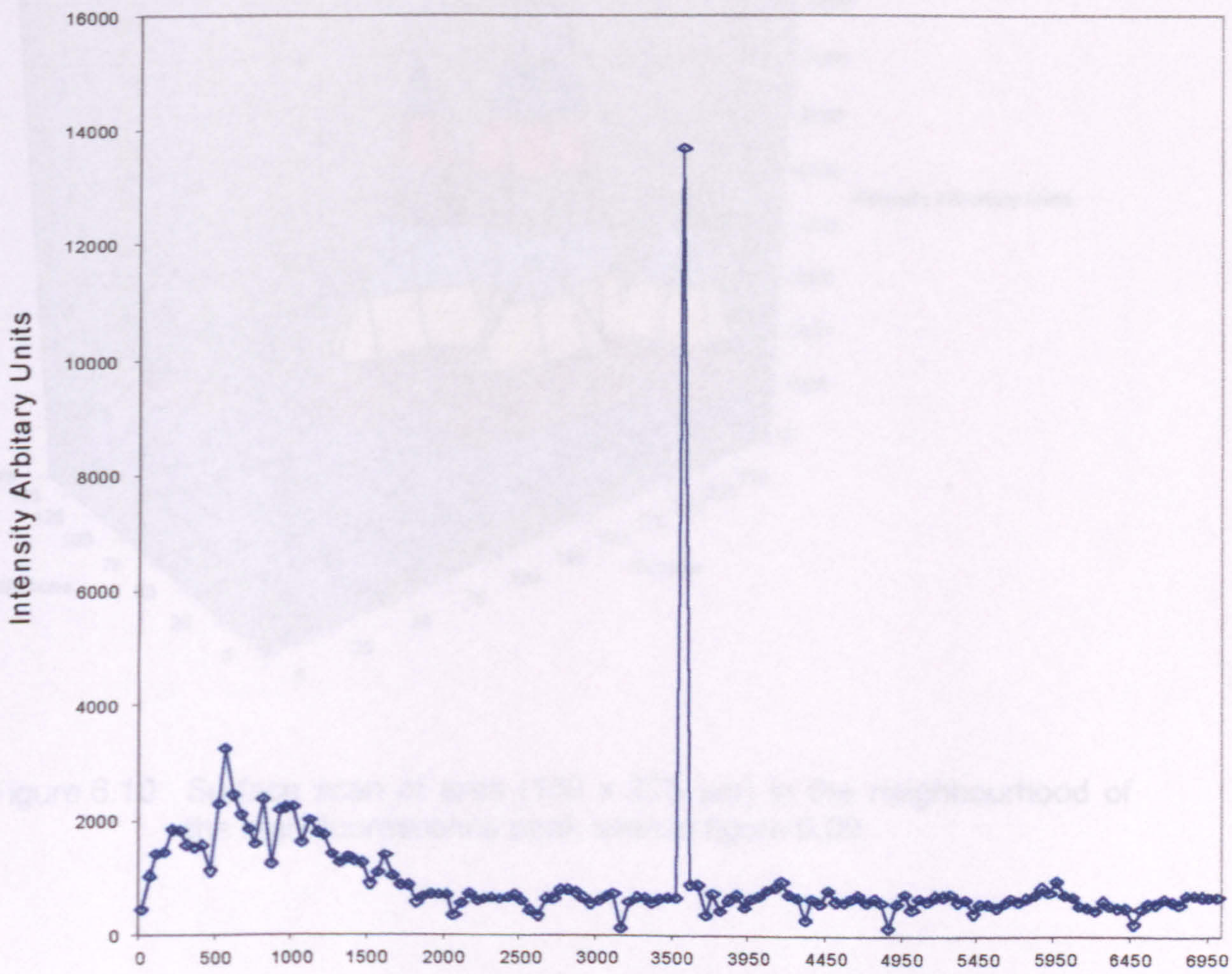

Figure 6.09 Localised field induced fluorescence at 705 cm^{-1} on the surface of a XLPE sample after being exposed to a field of 6×10^7 Vm-1 in contact with a semicon electrode for a time of 1 hour.

6.1.2.2. Surface Distribution of Fluorescence

The surface area surrounding the high fluorescence peak in figure 6.09 was mapped by performing a two dimensional scan of the area. The area investigated was 150 microns by 275 microns. The fluorescence profile over this region is presented in figure 6.10; unfortunately due to the finite number of data points the resolution is not very good.

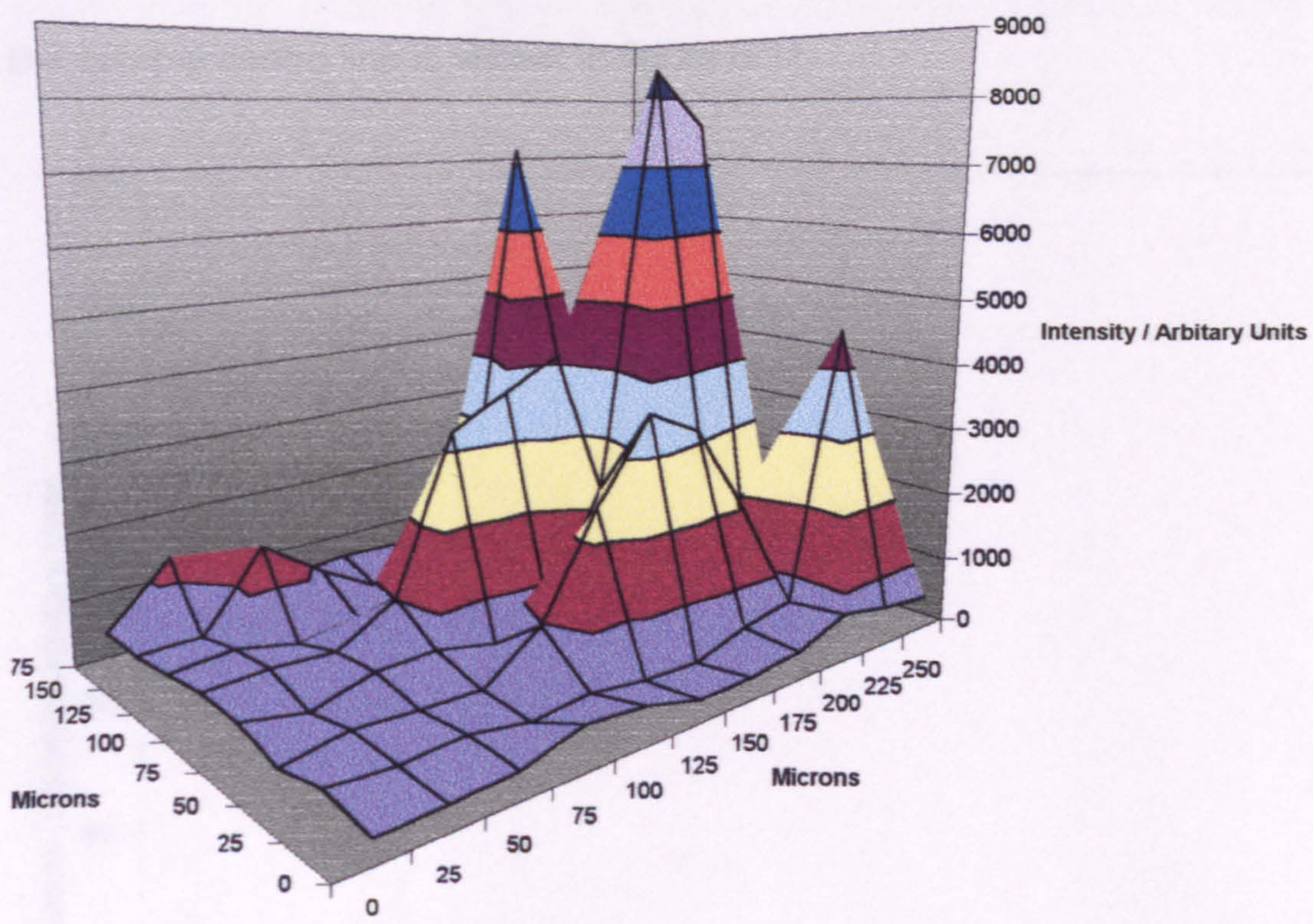

Figure 6.10 Surface scan of area (150 x 275 μm) in the neighbourhood of the high fluorescence peak seen in figure 6.09.

6.1.2.3. Zero Field Fluorescence

To investigate the possibility that the fluorescence peaks were the result of the experimental arrangement, rather than field induced, several virgin samples were placed in the experimental jig and left for a period of twenty-four hours without an electrical field applied. A series of Raman spectra were then obtained along the centre line of the sample in exactly the same as for the samples used in figures 6.08 and 6.09. A typical fluorescence profile across the sample centre line is shown in figure 6.11.

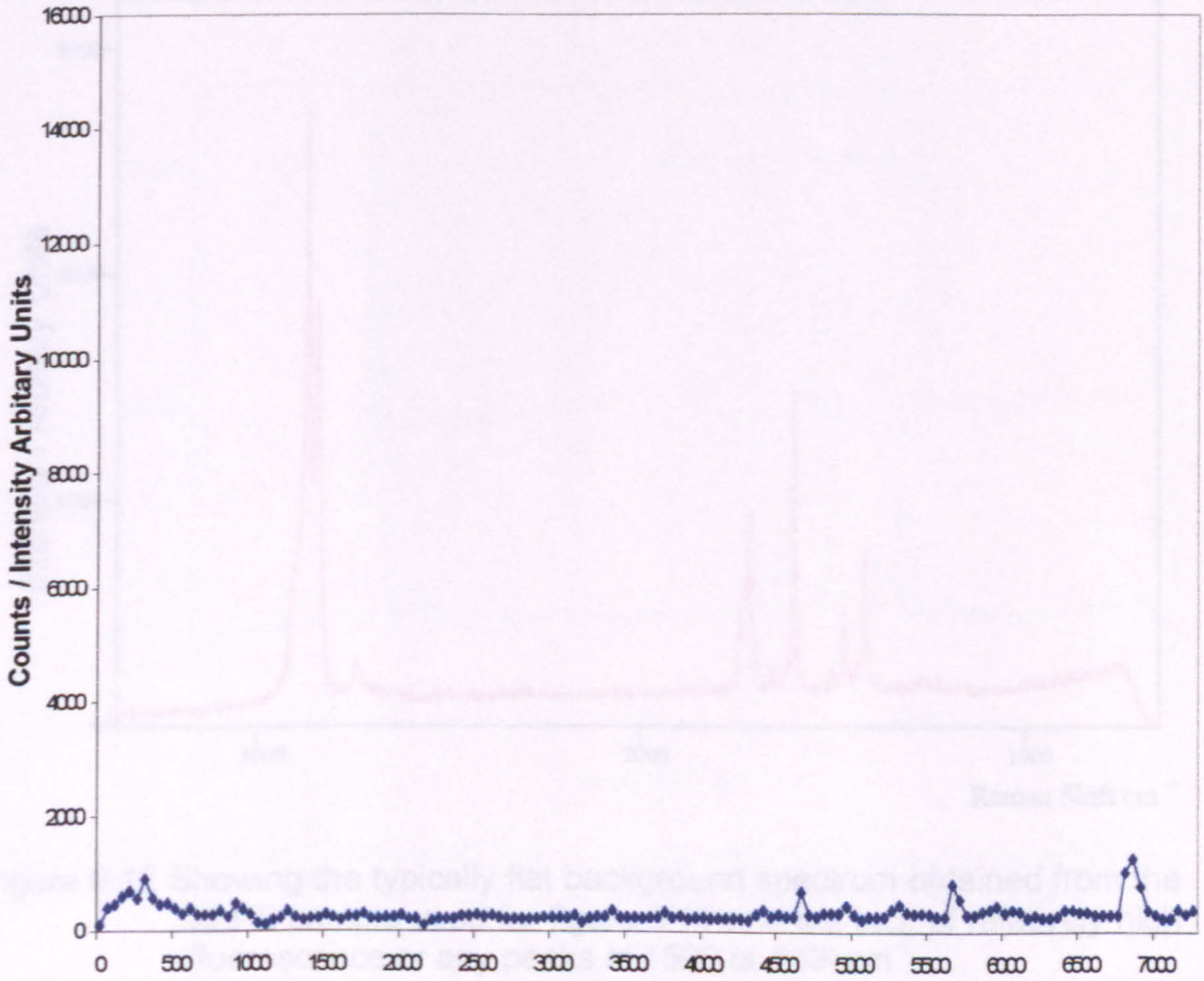

Figure 6.11 Fluorescence profile across the surface of a virgin XLPE sample in the same experimental arrangement as figure 6.08 and 6.09 but not exposed to an electrical field.

Figure 6.11 shows an essentially flat fluorescence profile. Any individual areas showing an increase in fluorescence over 1000 counts were found by optical microscopy to be the result of dust contamination on the surface of the XLPE. This fluorescence is characterised by its much lower intensity and also because it is possible to remove it by quenching. The same maximum Y axis scale has been used in both figure 6.09 and 6.11 to allow a direct visual comparison to be made. Individual spectra from this series displayed a typical XLPE spectrum showing little in the way of fluorescence and no indication of peaks at 1590 or 1330 cm^{-1}, as shown in figure 6.12.

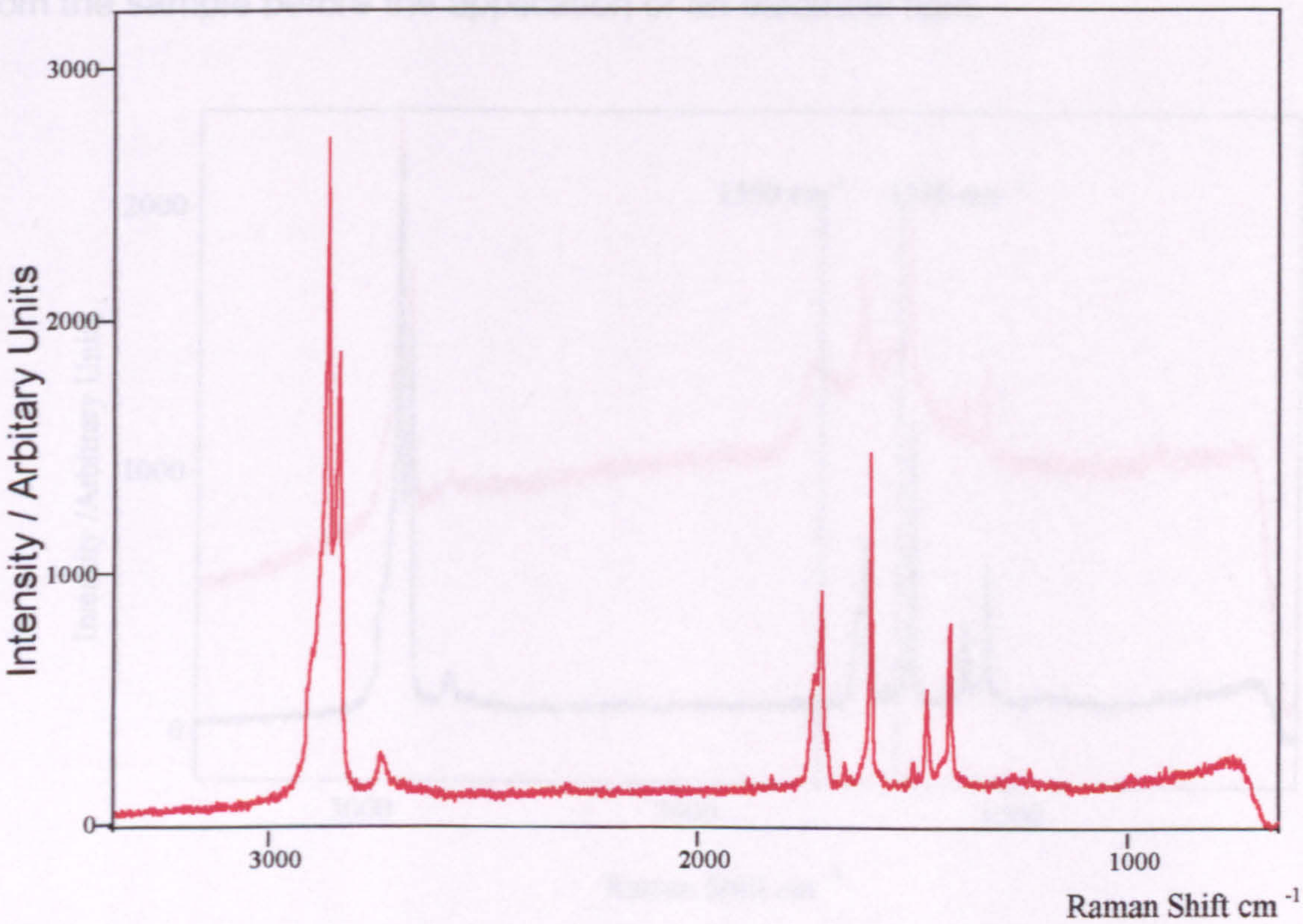

Figure 6.12 Showing the typically flat background spectrum obtained from the XLPE sample used for figure 6.11 and the lack of relatively high fluorescence or any peaks at 1590 or 1330cm^{-1}.

These results confirm that the high seen in figure 6.08 and 6.09 are due to the application of the electrical field across the sample.

6.1.2.4. Spectral Development Over Time

The spectral development as a function of time under an electrical field was also investigated. It was found that as the time under the field increased the number of the individual fluorescence peaks also increased compared to the numbers seen in figures 6.08, 6.09 and 6.10. In addition the development of the two new peaks at 1590 and 1330 cm^{-1} was observed; the red curve in Figure 6.13 is a full spectrum scan which shows a typical result obtained after applying the field for nine hours. This is compared to the black curve obtained from the sample before the application of an electrical field.

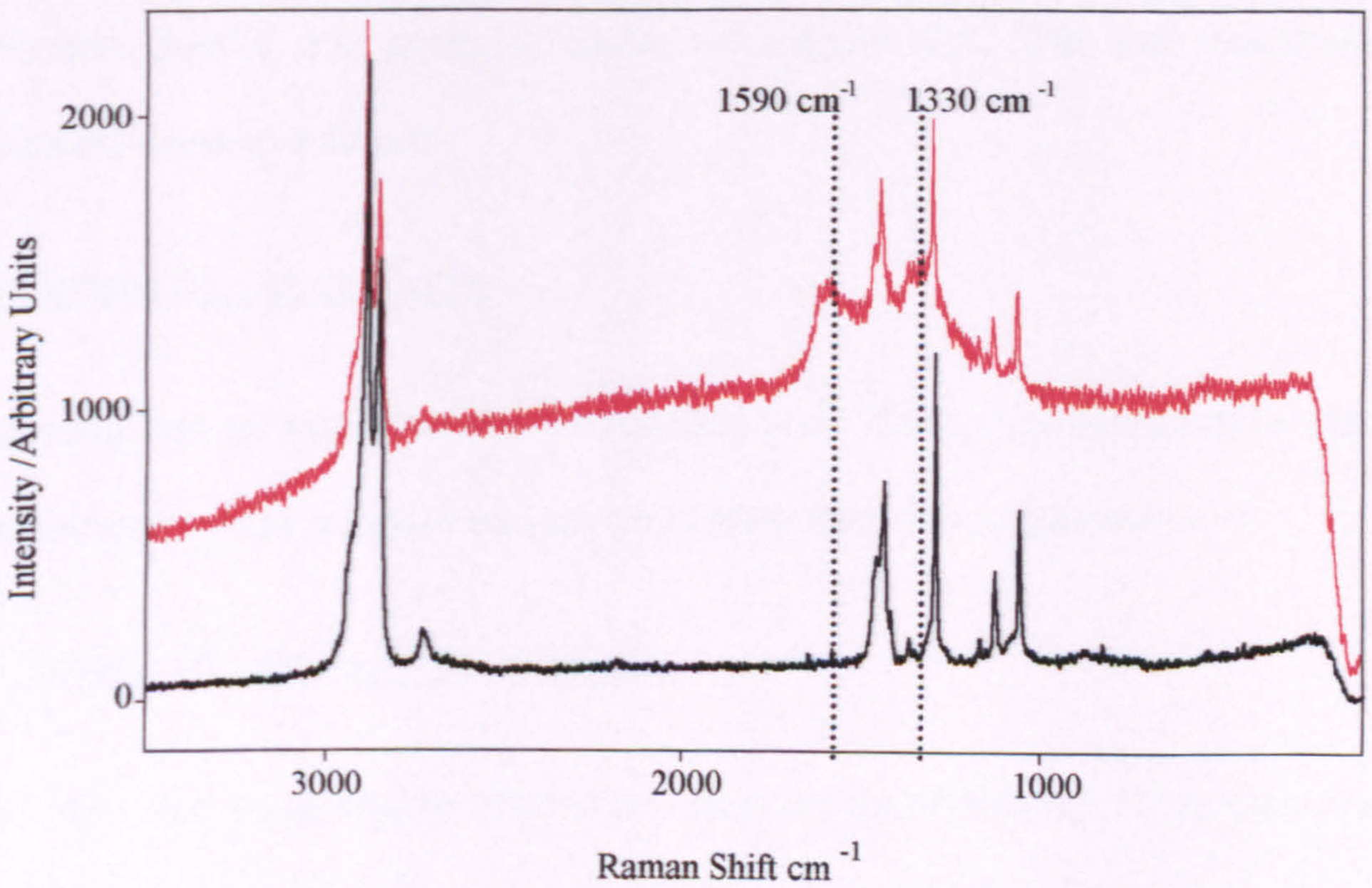

Figure 6.13 Spectrum obtained from a XLPE sample placed in an electrical field of $6x10^7$ Vm^{-1} for 9 hours (red curve). As well as increased background fluorescence, the two new peaks at 1590 and 1330cm^{-1} are in evidence. The black curve shows an initial spectrum before application of an electrical field

It should be remembered that in this situation we are dealing with a plane - plane electrode system (section 5.2.2) and that the electrical field strength will be far lower at the XLPE – Semicon boundary than at the XLPE - stainless

steel boundary examined in the pin - plane experiments – section 6.1.1. This is the reason why the length of time under the field is nine hours before the appearance of the peaks at 1590 and 1330 cm^{-1}. For a pin – plane system (figure 6.01) the fluorescence has already increased to a maximum and begun to die away before the spectrum in figure 6.13 was obtained.

6.1.3. Cable Experiments

All of the investigations into cable samples involved cables manufactured, prepared and tested by BICC Cables, Wrexham, UK. The experimental conditions and procedures used to subject the sample to a high electrical field were very different from those used in obtaining the results in sections 6.1.1 and 6.1.2. They were in fact those used in the testing of actual cable samples before bulk manufacturing commences and prior to delivery to the customer so that certification can take place. The four different cable samples investigated were all from the same original stock core, the general construction details are given in section 2, figure 2.1. The four samples investigated were as follows:-

Cable Sample 01 - Virgin Cable

This sample was straight from the production line. Testing or preparation was not carried out by the supplier except for cutting from the production run.

Cable Sample 02 - Delivery Tested Cable

This sample was subjected to normal pre-delivery cable testing. This involves placing the cable under stress conditions based on the IEC 502 standard for polymeric cables. No failure sites were present in this sample.

Cable Sample 03 - Cable Tested to Failure at Termination

This sample was subjected to ramp testing until failure took place – in this sample the failure occurred at a termination site.

Cable Sample 04 - Cable Tested to Failure Mid-Cable.

This sample was subjected to ramp testing until failure took place – in this sample the failure occurred in mid-cable.

6.1.3.1. Cable Sample 01 - Virgin Cable

These samples yielded a typical Raman Spectrum of XLPE with very little evidence of fluorescence and no evidence of the new peaks at 1590 and 1330 cm^{-1}. Spectra were obtained from several different sites along the length of the sample in order to obviate any contamination or inhomogenities influencing the results. A typical result is presented in figure 6.14.

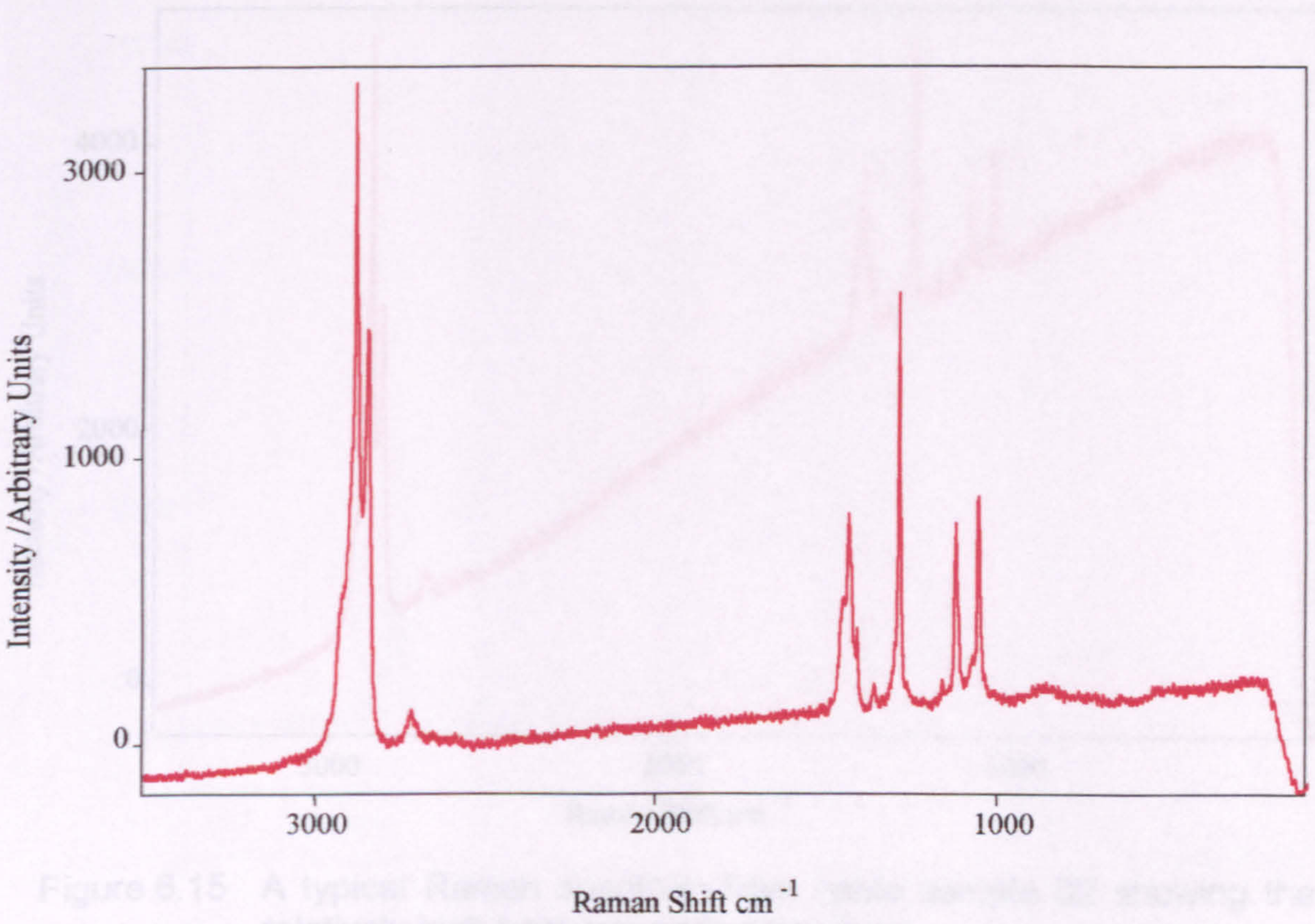

Figure 6.14 A typical spectrum from cable sample 01. Very little background fluorescence is shown and no evidence of the peaks at 1590 and 1330cm^{-1}. This spectrum is very similar to figure 6.12 also obtained from a sample (XLPE) that has not been exposed to an electrical field of any sort.

6.1.3.2. Cable Sample 02 - Ramp Tested Cable

This cable having been subjected to pre-delivery testing by the manufacturers was expected to show some signs of fluorescence but no indications of the new peaks at 1590 or 1330 cm^{-1}. Samples were prepared and Raman spectra obtained in exactly the same way as for cable sample 01. A typical spectrum is presented in figure 6.15.

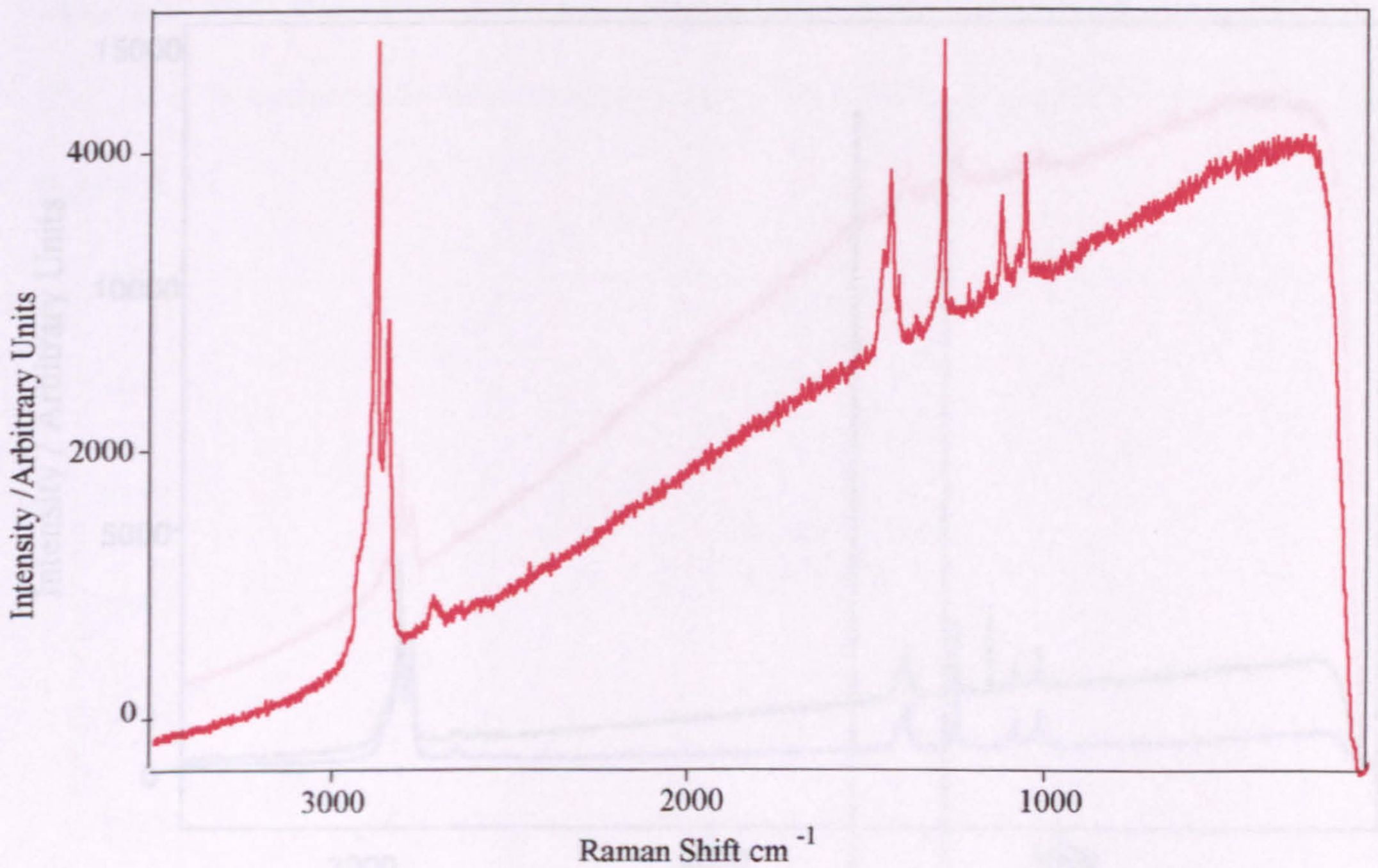

Figure 6.15 A typical Raman spectrum from cable sample 02 showing the relatively high background fluorescence.

A comparison between figure 6.14 and 6.15 shows the much higher background fluorescence in cable sample 02. All the spectra obtained from samples of this cable were very similar to those presented here. No evidence for the new peaks at 1590 and 1330 cm^{-1} was found in any of the spectra obtained from either sample 01 or sample 02.

6.1.3.3. Cable Sample 03 - Cable Tested to Failure at Termination

This cable had been subjected to ramp testing by the manufacturers until failure occurred, in this case at a termination site. It was expected that the Raman spectra would show a mixture of high background fluorescence and also closer to the failure site the new peaks at 1590 or 1330 cm^{-1}. Samples were prepared and Raman spectra obtained in exactly the same way as for Sample 01 and Sample 02. A typical spectrum is presented in figure 6.16.

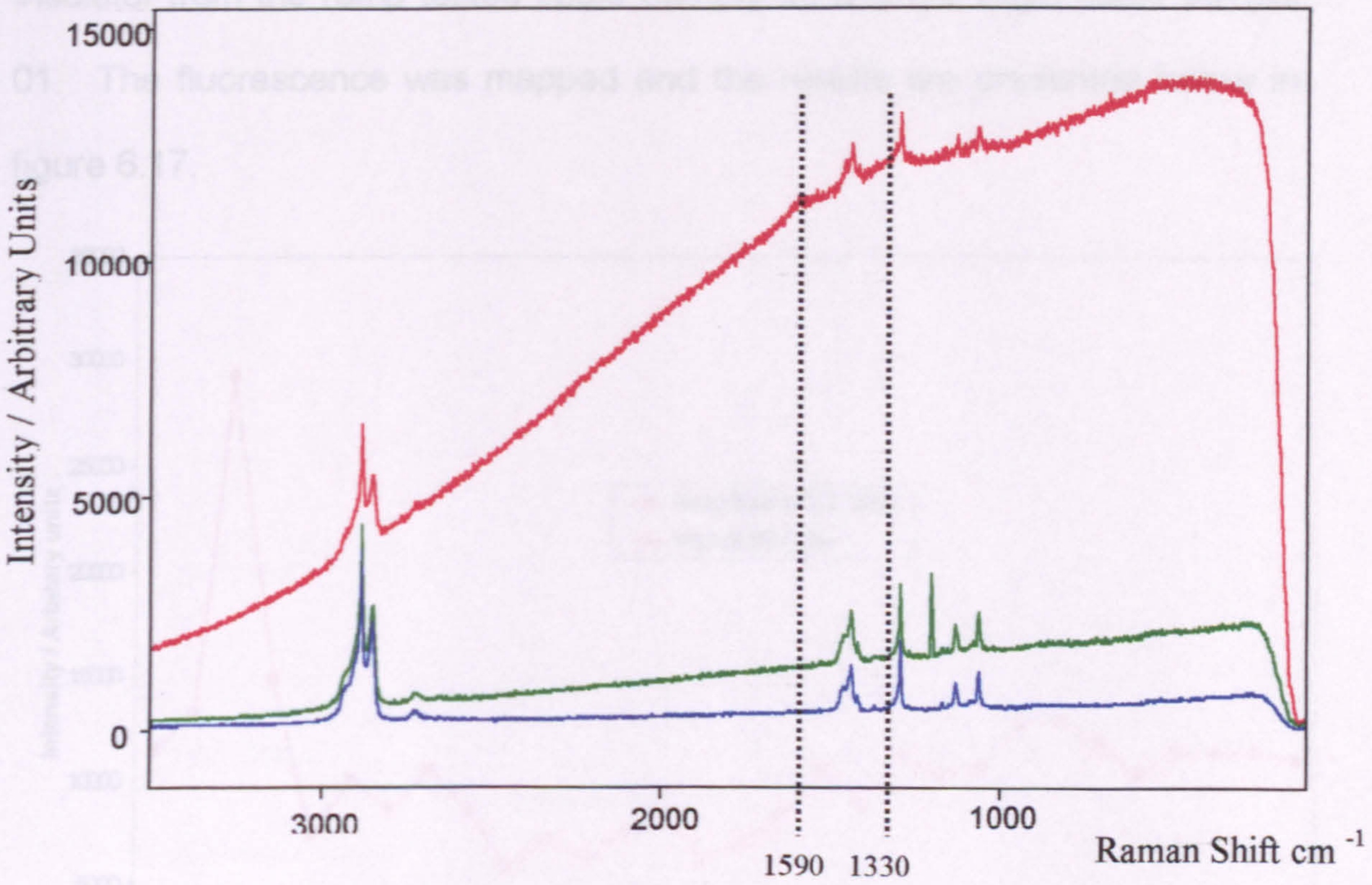

Figure 6.16 The red curve is a typical Raman spectrum from Sample 03 from the vicinity of the failure site. Showing the very high background fluorescence and also the appearance of the two new weak peaks at 1590 and 1330 cm^{-1}. The green curve is a typical spectrum from sample 02 whilst the blue curve represents a typical spectrum from sample 01.

The spectra (red curve figure 6.16) obtained from near the failure site displayed high levels of relative fluorescence as expected and in addition several of the spectra also displayed the weak peaks at 1590 and 1330 cm^{-1}. The peaks at 1590 and 1330 cm-1 seen in the red spectrum in figure 6.16

become much clearer when examined using the multi-point baseline technique used for figure 6.07. This is in distinct contrast to the Raman spectra from both Sample 01 and Sample 02 (blue and green curve respectively) neither of these samples showed any sign of peak development at 1590 and 1330 cm^{-1}.

A sequence of spectra was obtained across the outer surface of the XLPE insulator from the ramp tested cable Sample 03 and the virgin cable sample 01. The fluorescence was mapped and the results are presented below in figure 6.17.

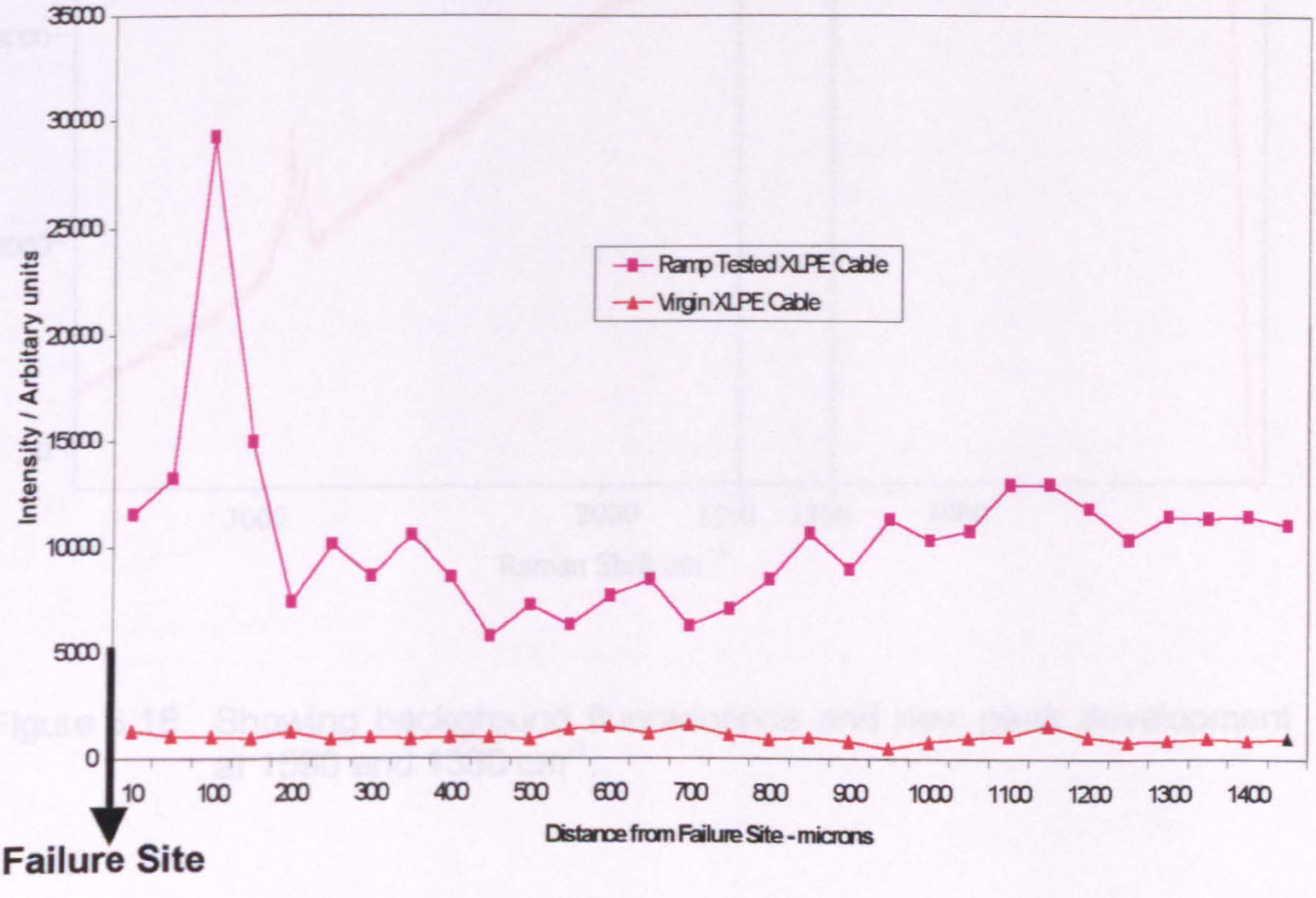

Figure 6.17 Fluorescence mapped at 710 cm^{-1} on both Sample 01, the virgin cable, and Sample 03, the cable tested to failure in a ramp test.

The virgin cable sample 01 displays a consistently low background fluorescence level across the whole of the XLPE surface scanned. The ramp tested cable sample 03, meanwhile, displayed a much greater variance in

level from one scan to the next. It should be noted that close to the failure site the fluorescence level was relatively low and new peak development was observed – as the distance from the failure site increased the fluorescence peaked and then reduced again. These results are consistent with the pin-plane results shown in figure 6.06 curve (2). Signs of new peak development were observed at other sites on the cable surface coincident with lower levels of fluorescence one such example is shown in figure 6.18.

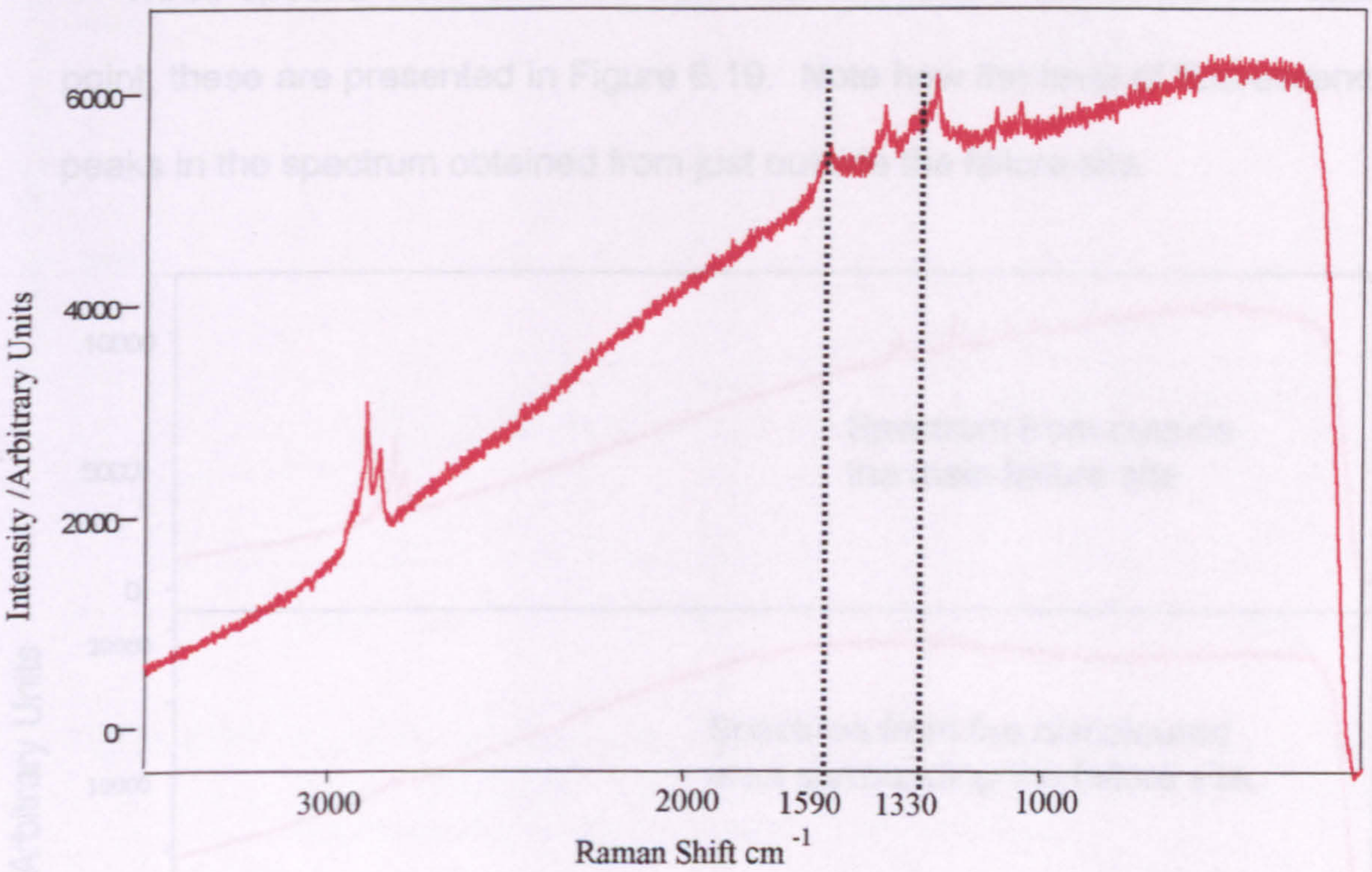

Figure 6.18 Showing background fluorescence and new peak development at 1590 and 1330 cm^{-1}.

6.1.3.4. Cable Sample 04 - Cable Tested to Failure Mid-cable.

This cable, having been subjected to ramp testing by the manufacturers until failure occurred in mid-cable, was also expected to show high background fluorescence and the appearance of the new peaks at 1590 or 1330 cm^{-1}. The general scans of the cable surface showed the expected spectral features of high background fluorescence and peak development at 1590 and 1330cm^{-1}. Three spectra were obtained from near the failure site at the mid-cable point; these are presented in Figure 6.19. Note how the level of fluorescence peaks in the spectrum obtained from just outside the failure site.

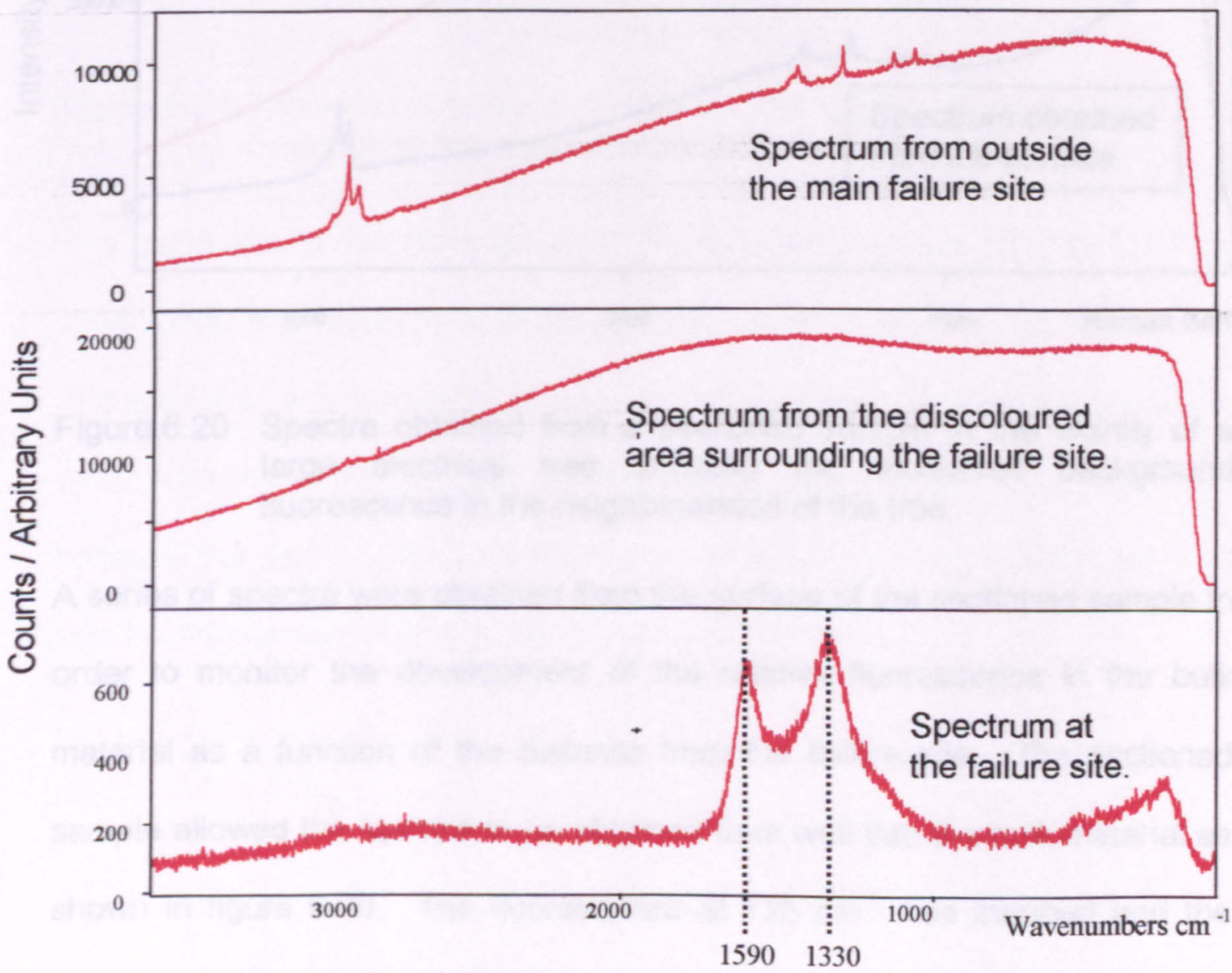

Figure 6.19 Three spectra obtained from the outer surface of the cable insulation in the region of the failure site. Showing the increased fluorescence and subsequent peak development at 1590 and 1330 cm^{-1} at the failure site.

The cable was then sectioned as shown in Figure 6.5 and a spectra obtained from the surface and from 150 μm into the surface in the area of a large electrical tree as shown in Figure 6.20.

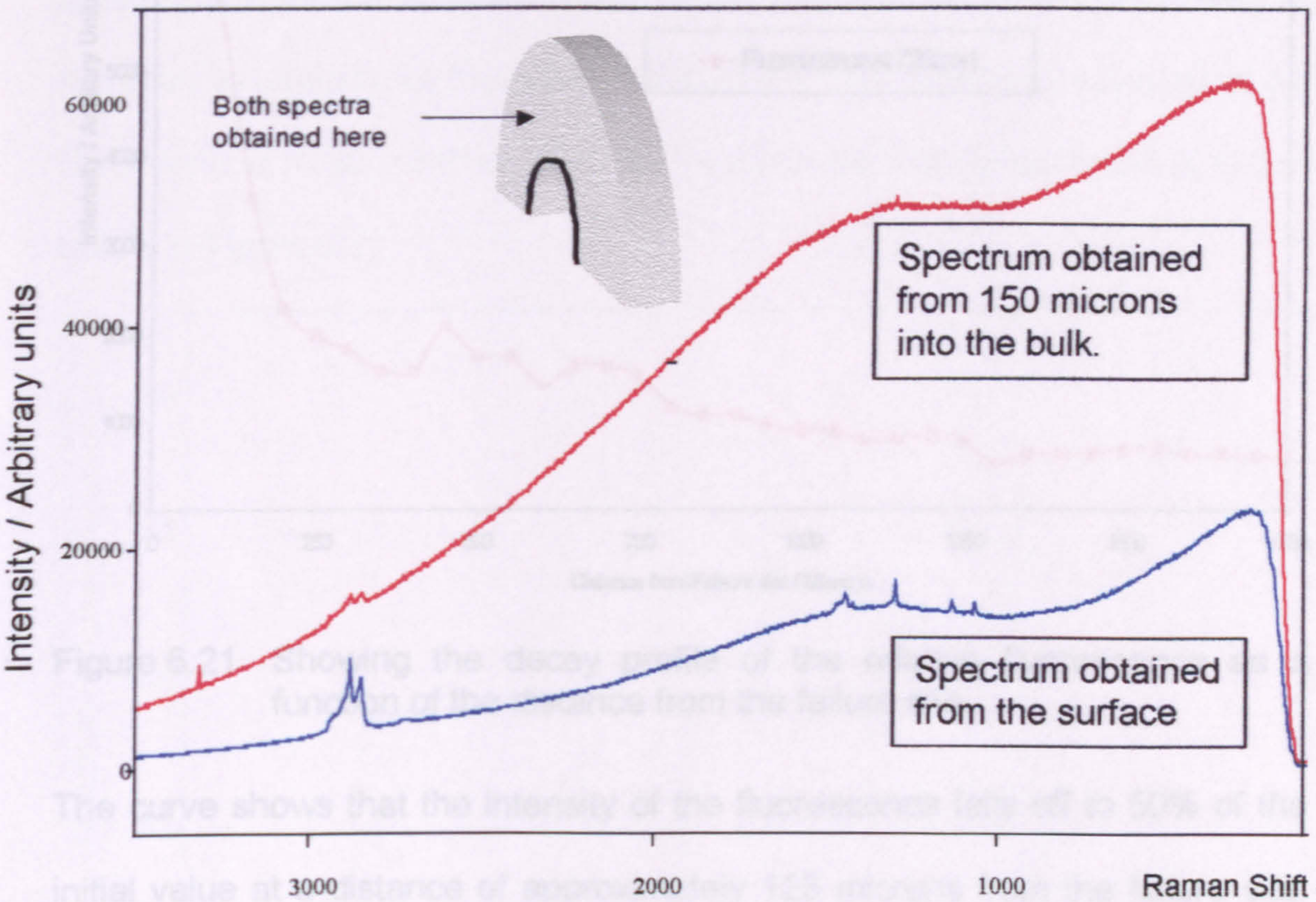

Figure 6.20 Spectra obtained from a sectioned sample in the vicinity of a large electrical tree showing the increased background fluorescence in the neighbourhood of the tree.

A series of spectra were obtained from the surface of the sectioned sample in order to monitor the development of the relative fluorescence in the bulk material as a function of the distance from the failure site. The sectioned sample allowed the spectra to be obtained from well into the bulk material as shown in figure 6.20. The fluorescence at 725 cm^{-1} was mapped and the results are shown in figure 6.21.

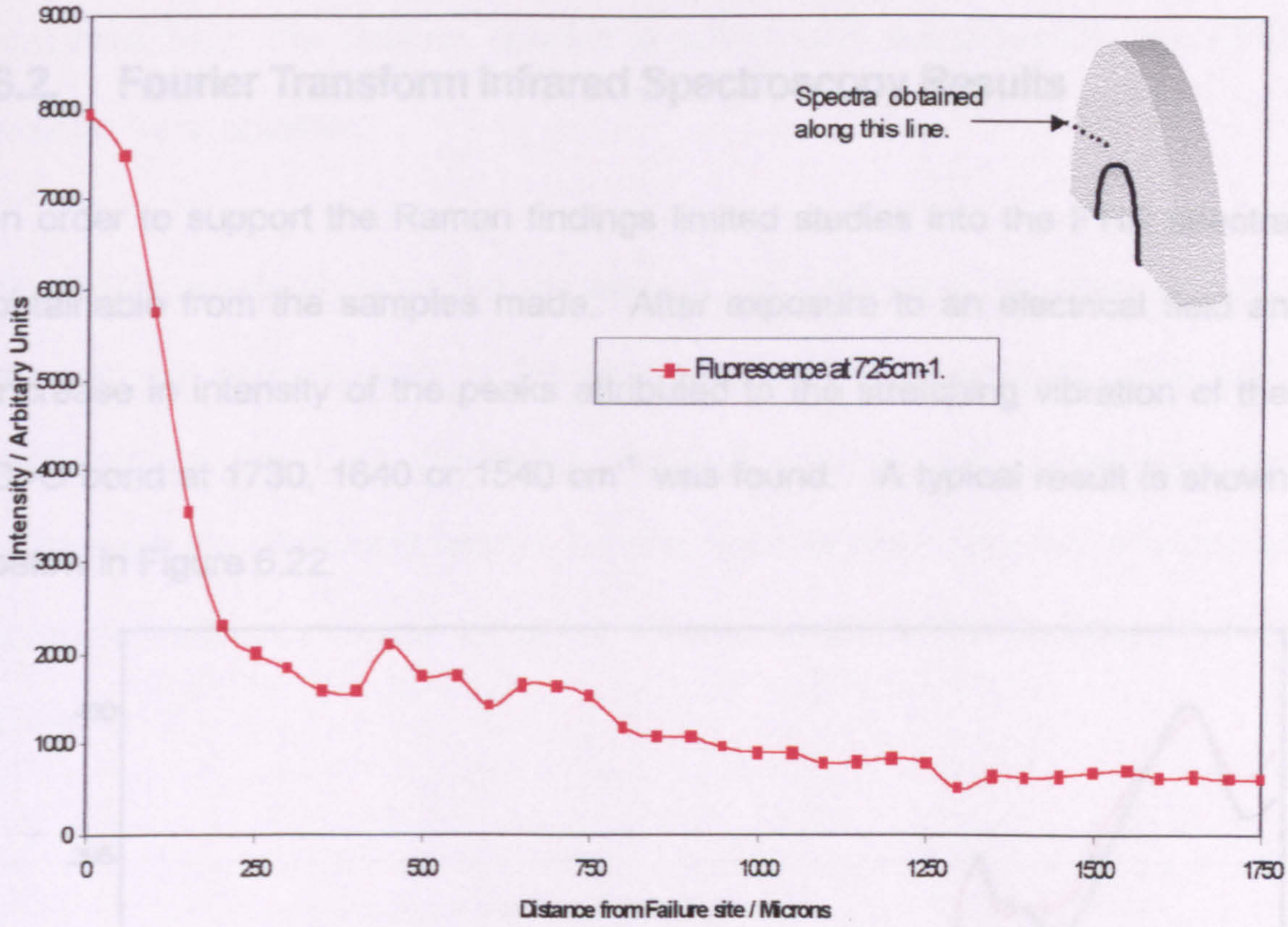

Figure 6.21 Showing the decay profile of the relative fluorescence as a function of the distance from the failure site.

The curve shows that the intensity of the fluorescence falls off to 50% of the initial value at a distance of approximately 125 microns from the failure site. The extent of the fluorescence extends out to ~250 microns as opposed to ~100 microns in the pin-plane experiments, figure 6.06. This could be because this sample had suffered a catastrophic breakdown whilst figure 6.06 was from a sample which had not actually broken down.

6.2. Fourier Transform Infrared Spectroscopy Results

In order to support the Raman findings limited studies into the FTIR spectra obtainable from the samples made. After exposure to an electrical field an increase in intensity of the peaks attributed to the stretching vibration of the C=O bond at 1730, 1640 or 1540 cm^{-1} was found. A typical result is shown below in Figure 6.22.

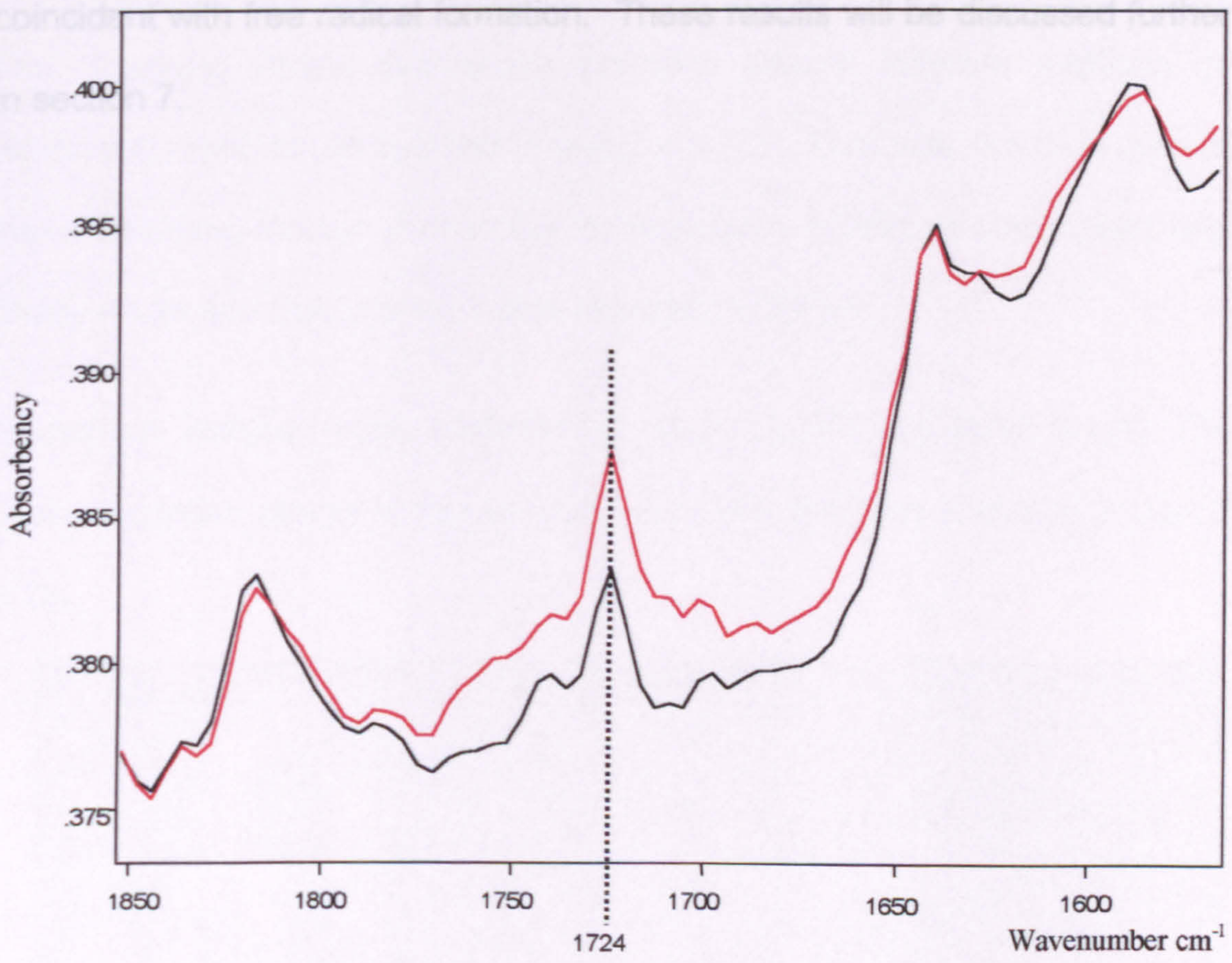

Figure 6.22 Typical FTIR spectra of LDPE after being exposed to an electrical field of 6 x $10^7 Vm^{-1}$; the black trace shows the spectrum obtained from the bulk material far from the area of high field application whilst the red trace shows the spectrum obtained from the sample close to the area of high field application.

These spectra were obtained from the same pin – plane samples used for the results presented in section 6.1.1. The samples were exposed to the

electrical field, the Raman spectra acquired and subsequently the FTIR spectra were obtained.

The FTIR results showing the increase in the C=O peak, together with the appearance and increase in intensity of the Raman peak at 1590 cm^{-1} attributed to the C=C stretching vibration, support the proposition that changes in the vibrational spectra are the result of chain scission following or coincident with free radical formation. These results will be discussed further in section 7.

6.3. Scanning Probe Microscopy Findings

In addition to the Vibrational Spectroscopy work reported in section 6.1 and 6.2 the surface structure of the samples was investigated using scanning probe microscopy. It was expected that changes would be observed in the surface morphology of the polymer at the micrometre and possibly the nanometre scale.

The Scanning Probe Microscope provides several different methods of examining samples as outlined in section 4.2.2. Use was made of two of these operating modes; Atomic Force Microscopy (AFM), in both height and phase mode and Electrostatic Force Microscopy (EFM).

Numerous images were captured of virgin LDPE surfaces during the characterisation phase of this project. A typical example is shown in figure 6.23.

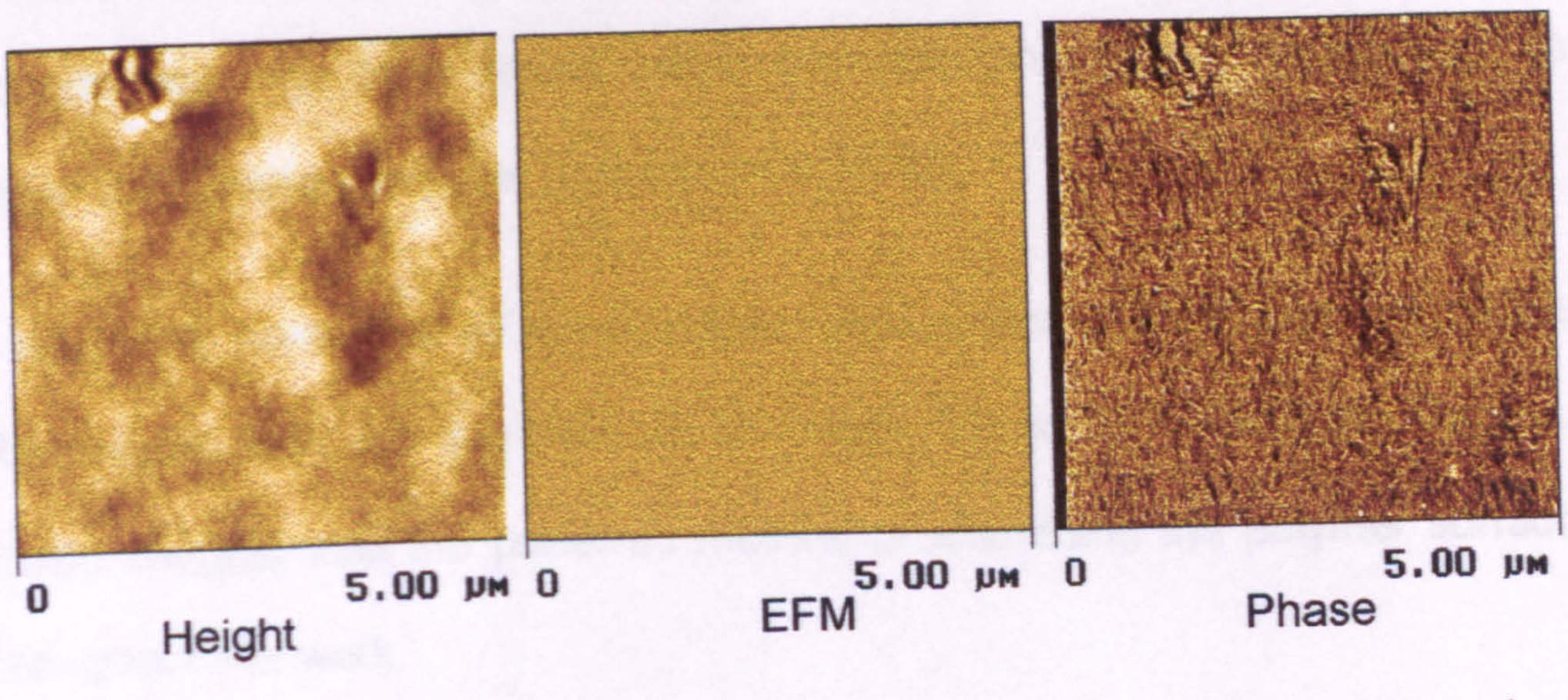

Figure 6.23 shows the three main image collection techniques used during this project namely Height mode, Electrostatic Force Mode (EFM) and Phase imaging.

The height image shows the typical structure of the LDPE at this scan size, i.e. 5 µm x 5 µm. There is a lack of detail although some features can be

seen and some smaller features are apparent although edge definition is missing.

The Electrostatic force image shows a complete lack of detail which is to be expected as this particular sample had been washed with isoproponal before examination; this procedure ensures that any surface charges are neutralised. Therefore the long-range electrostatic forces, which EFM is designed to detect, would be largely absent and a featureless image is to be expected.

The phase image, on the other hand, shows a good level of detail at the 5 μm scan size and was found to reveal detail regularly at scan sizes down to 1 μm. The features apparent in this image are due to the lamellar structure of the polyethylene; this was confirmed by comparison with other published work showing the same structure. (Digital Instruments Application Note – AFM Part 8; Vansco et al, 1996) The ability to image the lamellar structure was of crucial importance as crack propagation during electrical stressing of polyethylene has been found, using transmission electron microscopy, to follow the lamella structure. (Hozumi et al 1988)

It should be noted that all three images were obtained simultaneously by the Microscope, they are therefore all of exactly the same area of the sample. Phase imaging was the preferred method of examining the polymer surface throughout this work.

6.3.1. Surface Morphology

In early experiments to investigate the effect of high electrical on the surface morphology of LDPE, 200 V ac was applied to the tip of the scanning probe microscope whilst it was in contact with the polymer. The lower surface of the polymer was fixed to an earthed stainless steel stub. As the tip has a radius of approximately 10 nanometres this voltage was sufficient to produce an extremely high field at the surface of the polymer. Using as a very rough guide the simple equation,

$$E_f = (V/R) \qquad \textbf{6.01}$$

where E_f is the electrical field, V is the applied voltage and R is the radius of the tip the field can be calculated. A potential of 200 volts therefore gives a field of 2×10^{10} Vm^{-1} at the tip. The following image shows the effect on the surface of the polymer of a field of this magnitude.

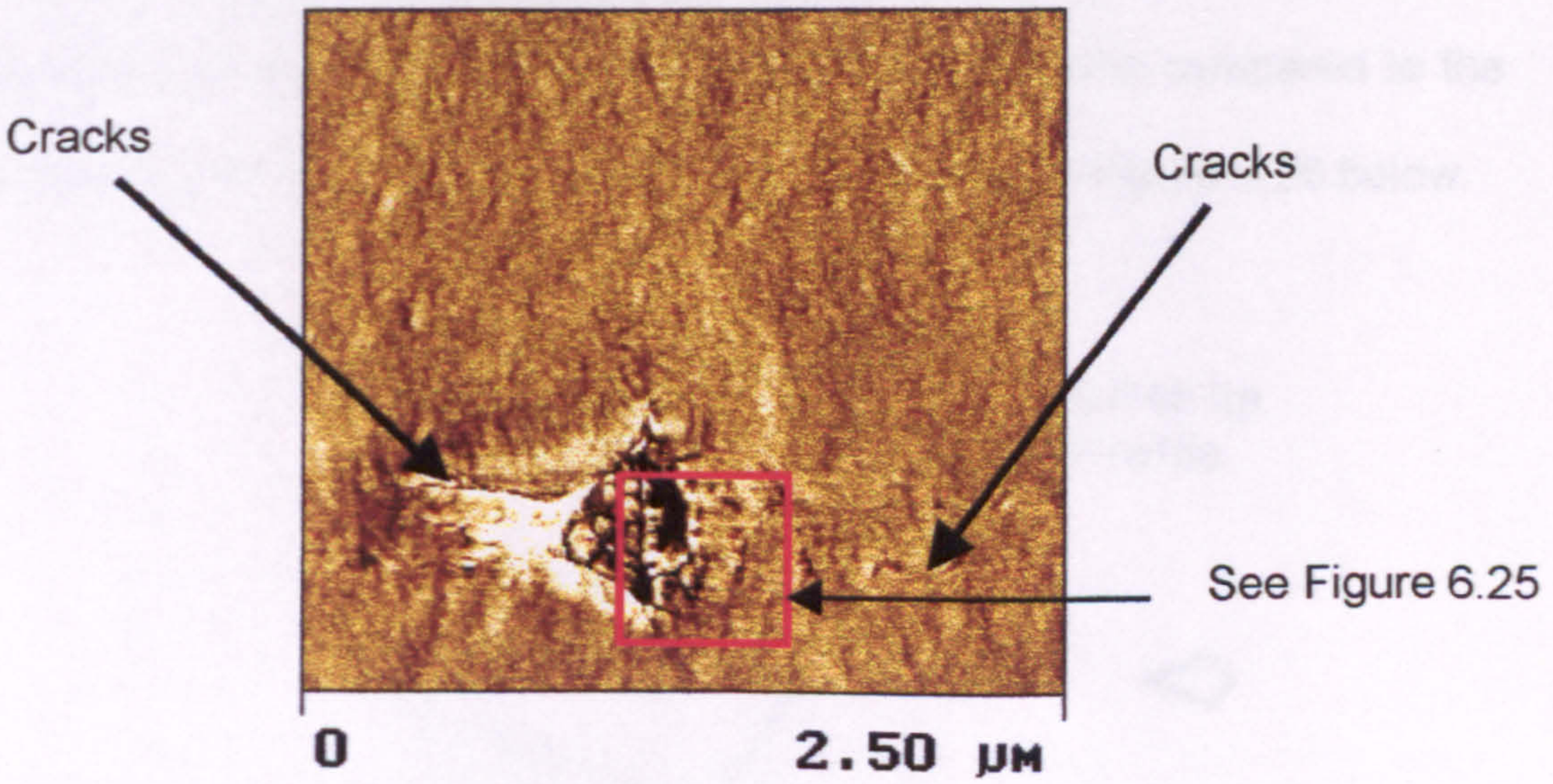

Figure 6.24 Showing the effect of a field of 2×10^{10} Vm^{-1} at the SPM tip whilst it is held stationary in contact with the surface of the polymer.

In Figure 6.24 cracks can be observed following the orientation of the lamella, Figure 6.25 shows these cracks in detail.

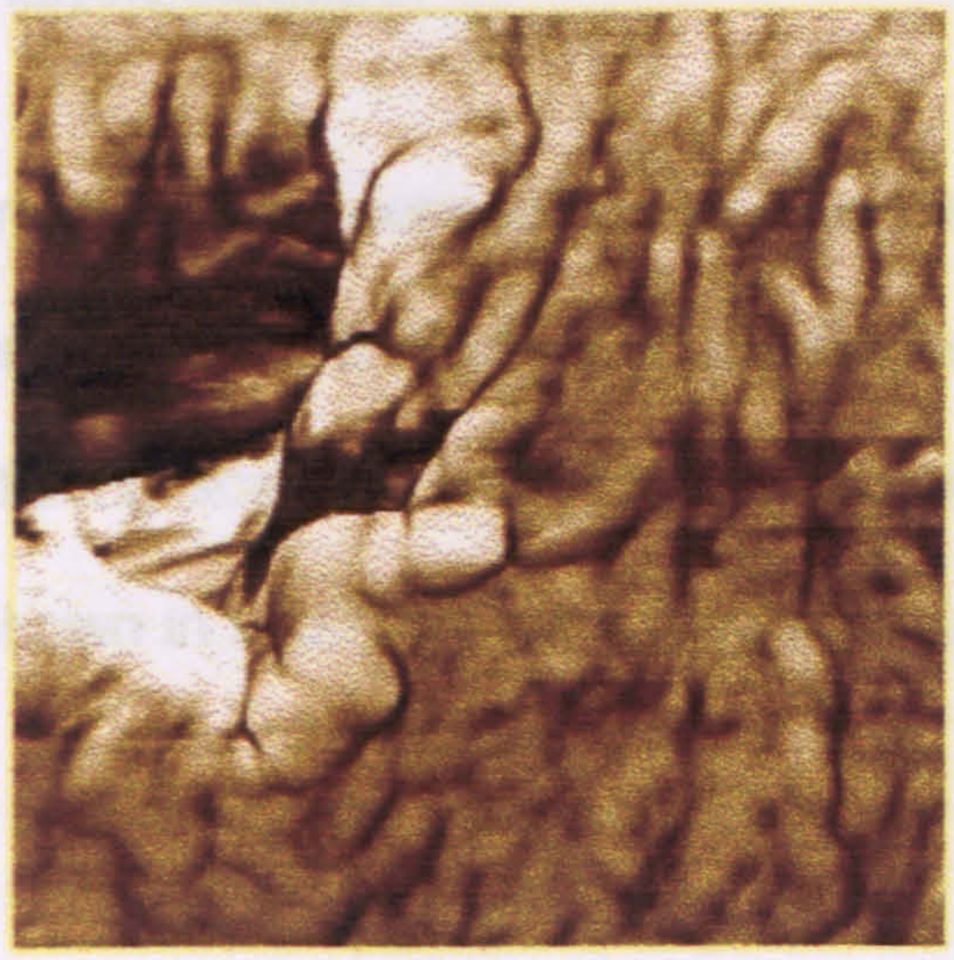

Figure 6.25 A 500 nm by 500nm scan of the region indicated in Figure 6.24 showing the cracks tending to follow the lamella rather than cutting across the lamella structure.

Additionally in the central region of the damaged area the lamella structure has been severely modified. It should be noted that the damaged area, whilst it follows the outline profile of the SPM tip itself, is in fact much larger. The outline profile of the damaged area shown in Figure 6.24 is compared to the profile of the SPM tip at the expected depth of insertion in Figure 6.26 below.

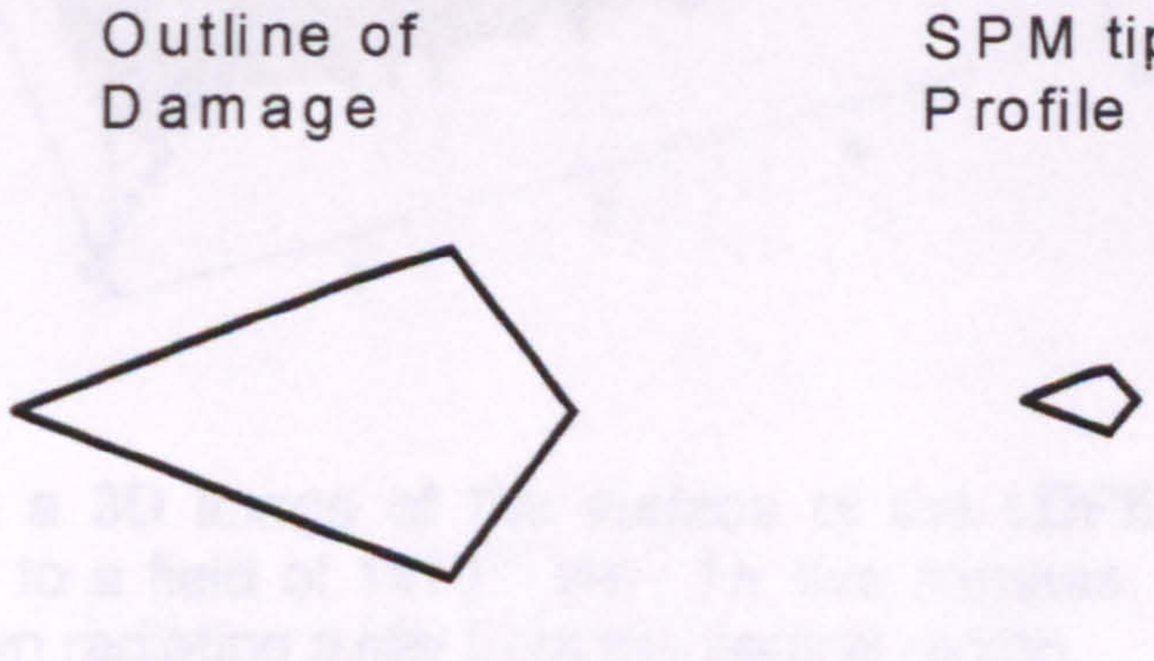

Figure 6.26 The comparative sizes of the damaged area and the tip at the expected depth of insertion into the polymer. The ratio is 5:1 in the linear dimension.

The overall dimensions of the tip were calculated from the manufacturers data sheets whilst the size and depth of insertion were obtained from the Microscope image analysis software.

It was found in general that the cracks observed were radially orientated from the central area where the highest field would have been encountered. This was determined by taking scans at random positions around the high field region. The image shown in figure 6.27 is one of a series of images showing this phenomenon.

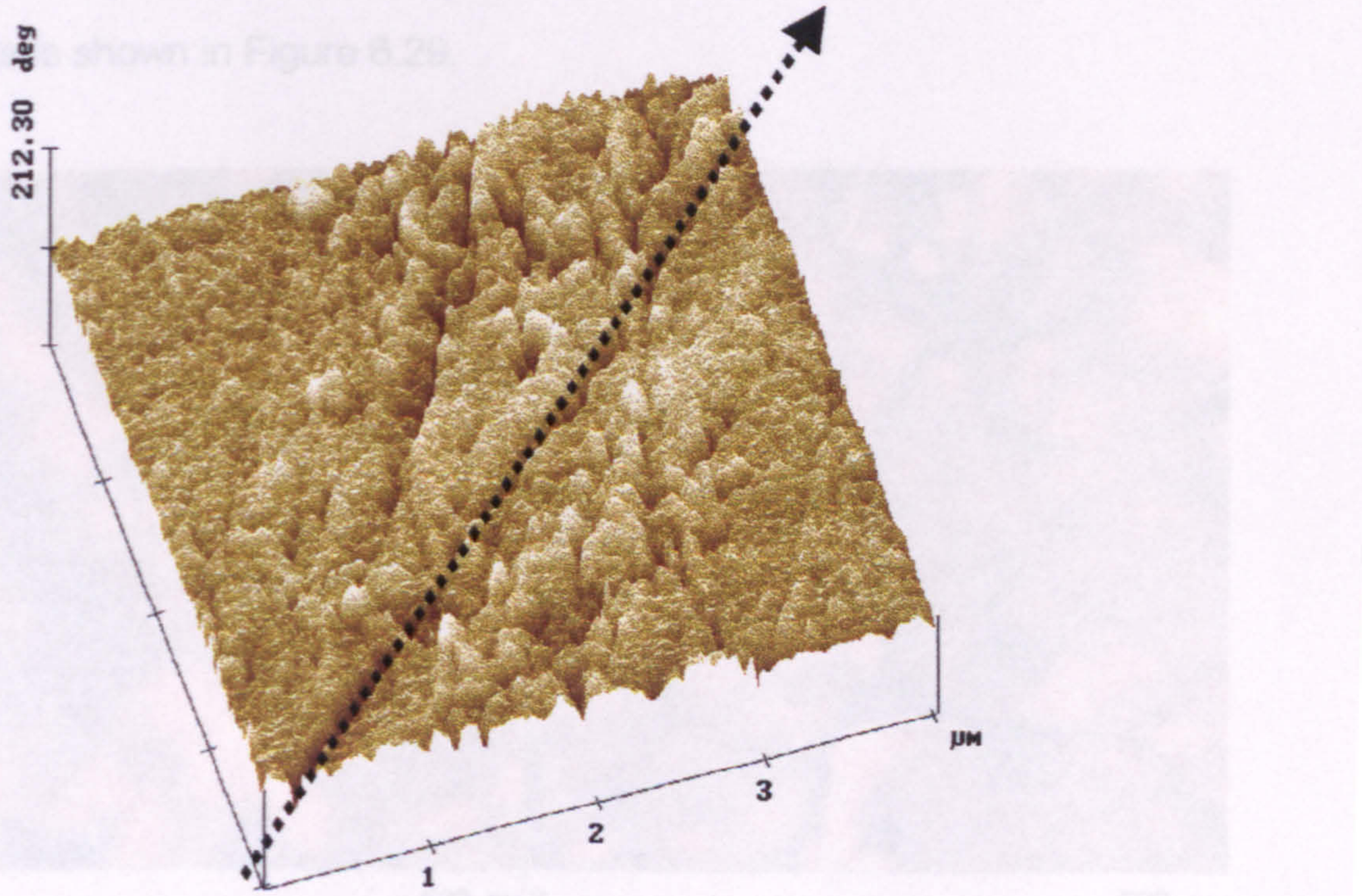

Figure 6.27 Showing a 3D image of the surface of the LDPE after being exposed to a field of $1x10^{12}$ Vm^{-1} for five minutes. The cracks are shown radiating away from the central region.

It was expected that a disruption of the lamella structure similar to that shown in Figure 6.27 would be found in samples from the Raman experiments

described in section 5. It is worth remembering that the experimental arrangement in these experiments was as shown below in figure 6.28.

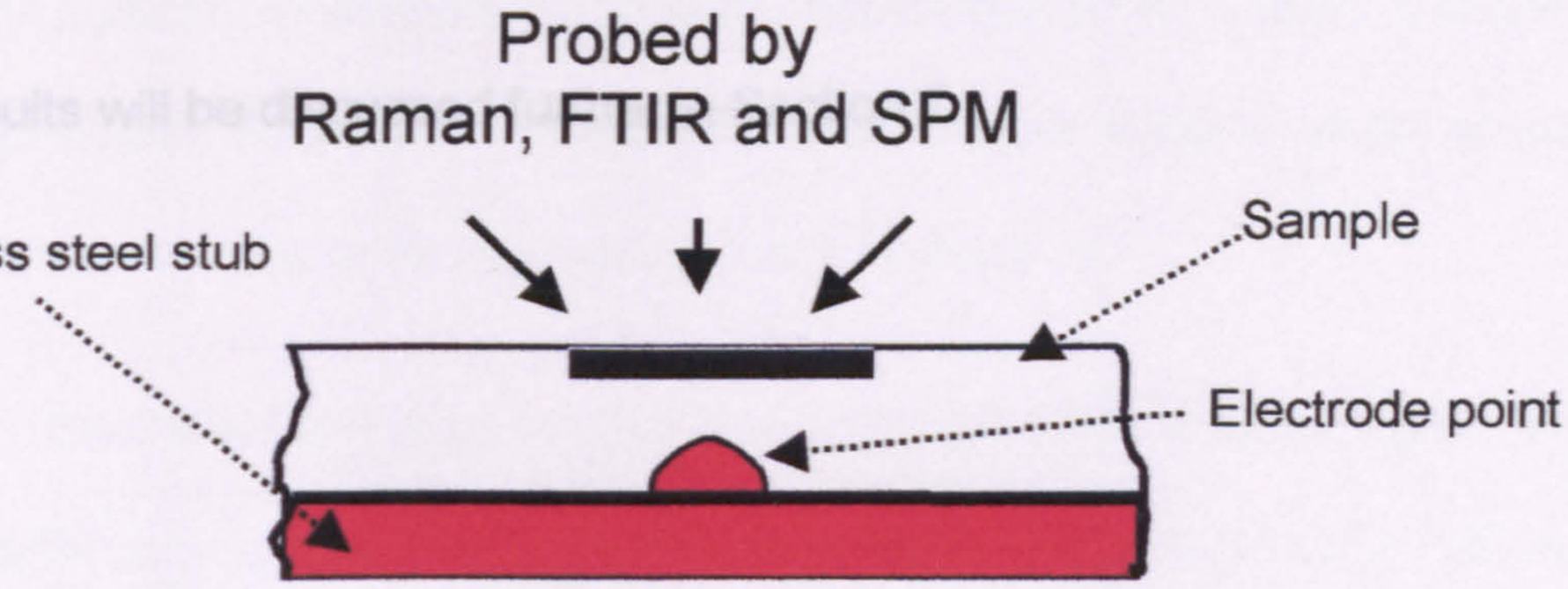

Figure 6.28 Showing the sample arrangement and the area, indicated in grey, being probed by the SPM.

The samples were exposed to the field for the required length of time and then transferred to the SPM immediately. A typical scan of a sample from these experiments is shown in Figure 6.29.

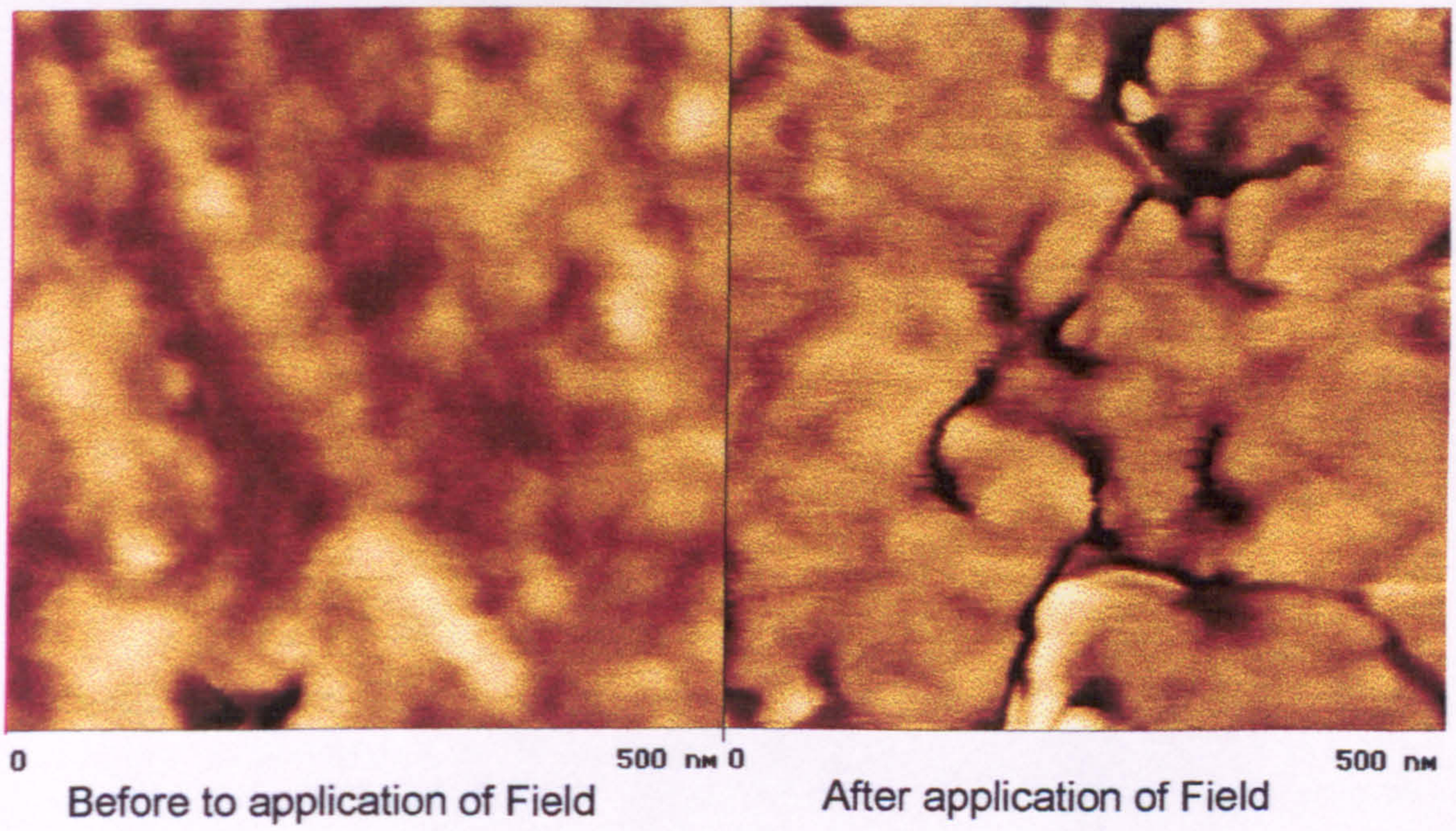

Figure 6.29 Showing the effect of the application of a field of 6×10^7 Vm^{-1} for 16 minutes at the surface of the polymer. Prior to the application of the field the surface shows no sign of the cracking. After application of the field however the surface reveals a crazed structure at numerous places.

This type of surface disruption was found in numerous places arranged radially round the high field region.

These results will be discussed further in Section 7.

6.3.2. Field Induced Electrostatic charges

As already outlined in section 4.2.2 and section 6.3 EFM detects the long range electrostatic force due to charges either in the surface layer or just below the surface layer of the sample under investigation.

As in 6.3.1 the initial work was carried out using the SPM probe to apply the potential difference across the polymer; the sample preparation was outlined in section 5.4.1.

The EFG image, figure 6.30, was obtained simultaneously with that presented in figure 6.24 and is typical of those obtained in that series of experiments.

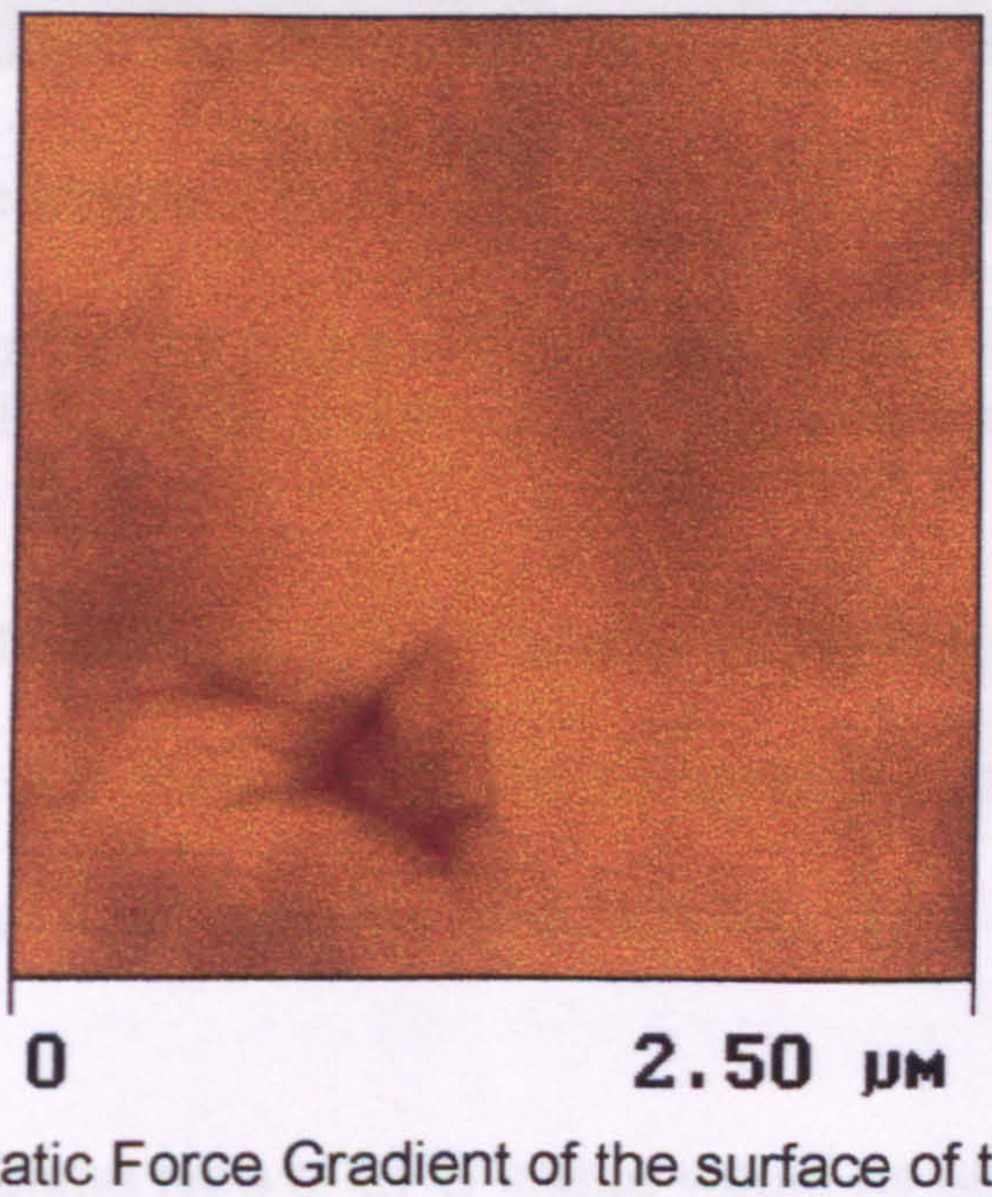

Figure 6.30 Electrostatic Force Gradient of the surface of the LDPE following application of an electric field of 2×10^{10} Vm^{-1} with the microscope probe. The dark area represents a high charge density in that area of the sample.

It must be remembered that the probe was 100nm above the surface of the sample when this image was captured. The image shows that in the area of the surface damage shown in figure 6.24 a clear contrast difference

corresponding to the outline of the damage can be seen. A comparison between the two images, figure 6.31, also shows that the EFG image shows contrast differences directly corresponding to the cracks seen in the Phase image in figure 6.24. This indicates that trapped charge is present in the damaged region of the surface.

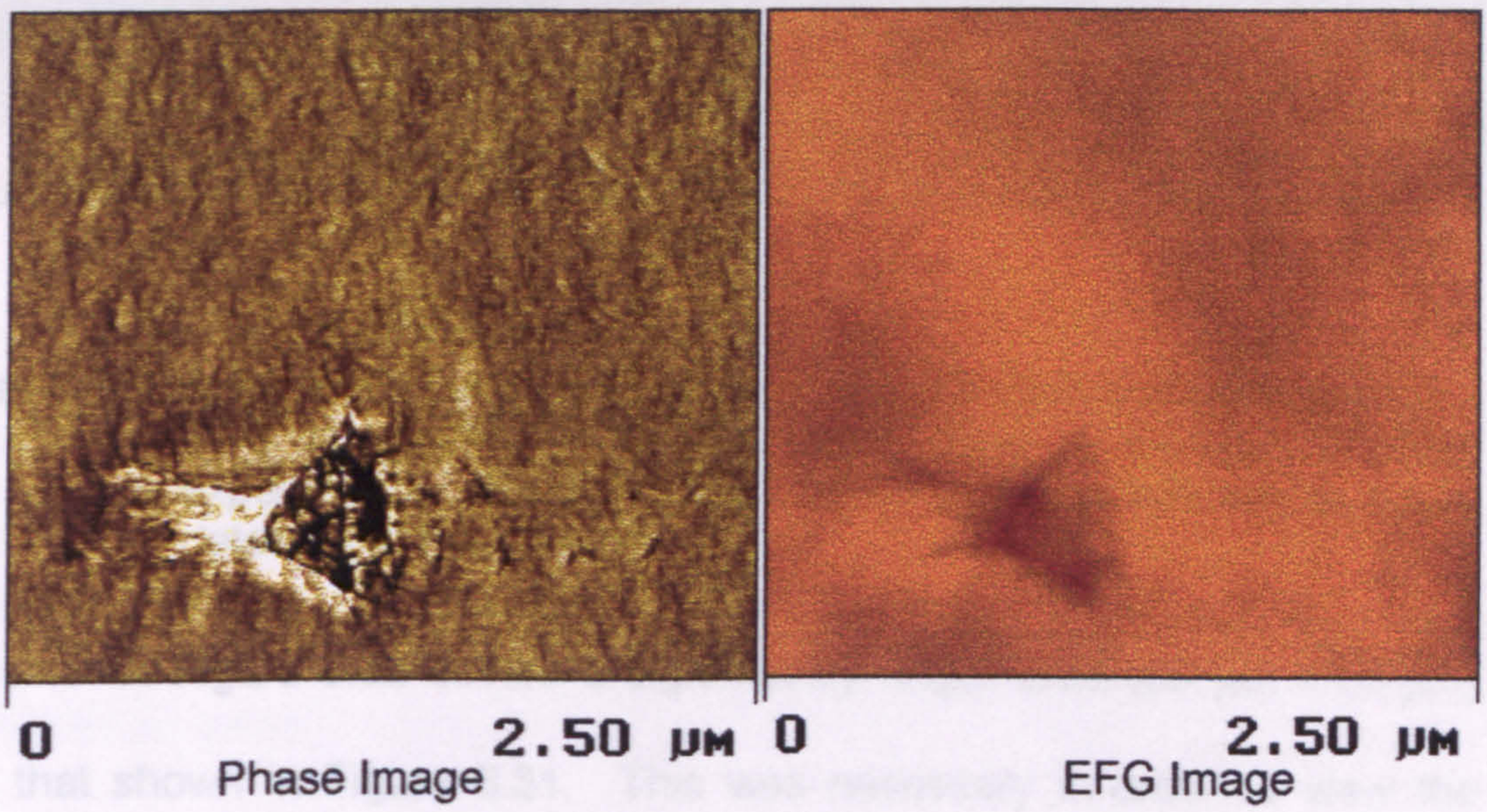

Figure 6.31 Showing the correspondence between the contrast differences in the EFG image and the actual physical features in the phase image.

It is interesting to note that the EFG image is not a duplicate of the Phase image; it accentuates the deeper cracks in the severely damaged region and also as they spread out away from the main damage area.

It was hoped that the same type of EFG image would be seen in the pin-plane samples described in Section 5.2.1. Although the physical damage was not as severe as that seen in figure 6.24, a clear contrast difference could be seen in the samples examined as shown in Figure 6.32.

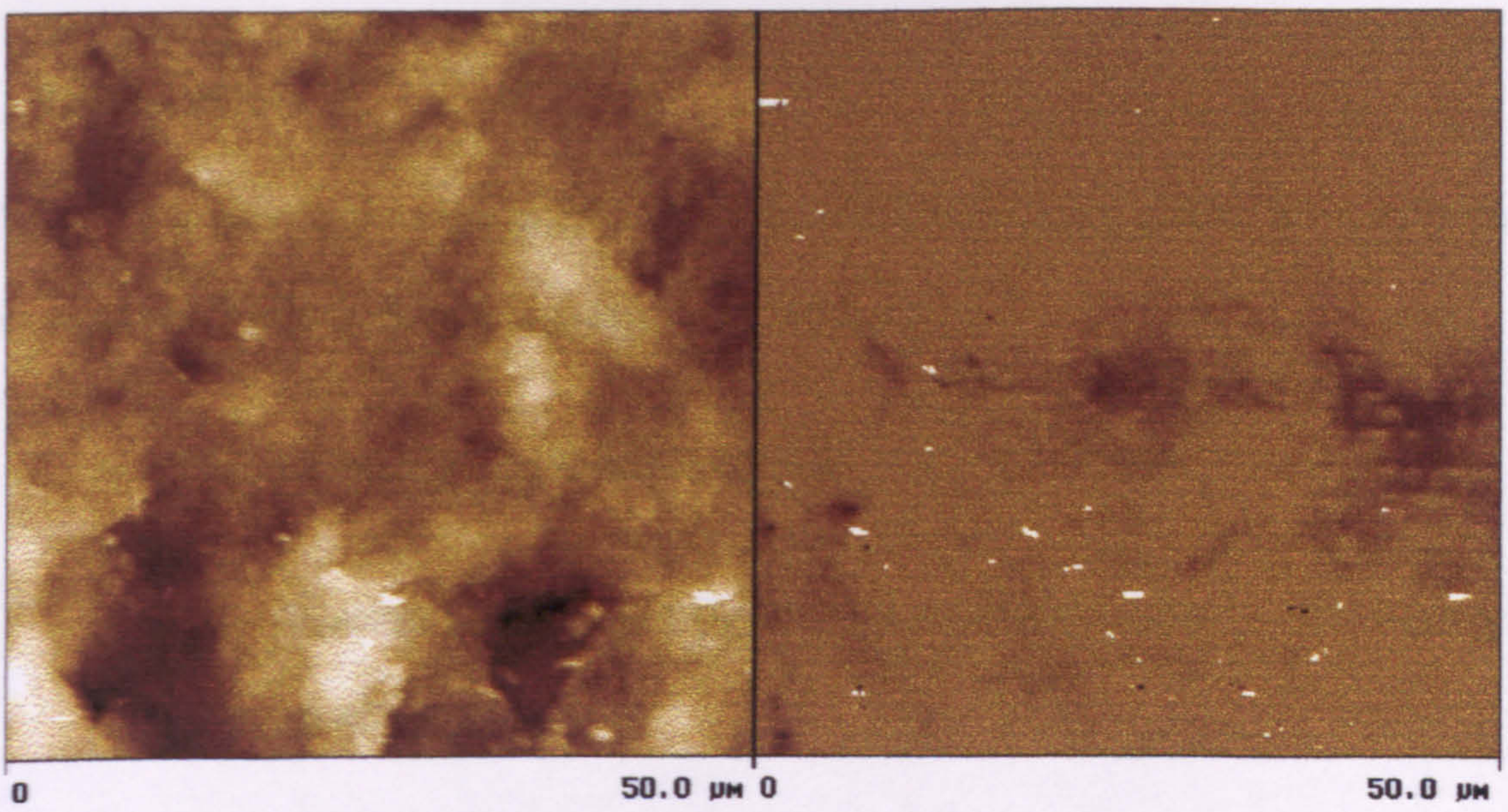

Figure 6.32 A 50 micron scan showing the height image and corresponding EFG image for a XLPE sample used in the pin – plane experiments. The EFG image shows electrostatic forces being detected at the surface.

The scan in Figure 6.32 covers a significantly larger area (50 µm x 50 µm) than that shown in Figure 6.31. This was necessary in order to view the contrast differences remembering that this was obtained from the surface opposite the pin – see figure 6.28 and figure 5.1. The electrode in this area was the removable polished plane electrode and therefore extended over the whole sample area. This resulted in much larger areas of charge deposition concentrated in the high field region opposite the pin electrode. Phase imaging becomes less useful when the image being captured exceeds 10 x 10 µm and therefore height imaging was used for the comparison. In spite of this there are clear signs of electrostatic forces being detected by the SPM either from on the surface of the sample or more likely from just below the surface of the sample. This will be discussed further in Section 7.

7. Discussion

The results reported in Section 6 raised several interesting points in relation to the ageing of bulk polymer insulation as follows:-

- Electric field induced fluorescence,
- The development of two peaks not normally seen in the Raman spectra of polyethylene,
- An increase in the DLAM peak intensity.
- Physical changes to the lamella structure.

Each of these findings will be discussed and possible explanations advanced for the results seen.

7.1. Electric Field Induced Fluorescence.

The discovery of field induced fluorescence was unexpected and a significant amount of time was spent in the early stages trying to eliminate this effect from the results being obtained. However, it quickly became obvious that the fluorescence being observed was very different from that seen in a typical Raman spectrum of commercial grade LDPE.

The residual fluorescence seen in many virgin polyethylene samples can be removed by quenching the sample using an intense light source. The ability of the field induced fluorescence to withstand this quenching process, Figure 6.04, gives rise to the question – does field induced fluorescence have a

different origin from that which gives rise to the "normal" fluorescence seen in low density polyethylene. It is useful at this point to summarize the fluorescence results obtained.

- The intensity increases rapidly to a peak and then decays as a function of time of application of the electrical stress. (Figure 6.02).

- The fluorescence is a bulk rather than a surface phenomenon. (Figures 6.03, 6.21).

- It is highly resistant to quenching by an incident light source. (Figure 6.04).

- The intensity is a function of the electrical stress applied. (Figures 6.05, 6.06).

Field induced fluorescence shows a marked difference in behaviour from fluorescence in virgin LDPE samples. In virgin polyethylene samples the intensity is at a maximum when the sample is first placed under the laser light source and then decreases rapidly (logarithmically) over a few minutes until the intensity is negligible. In field induced fluorescence the intensity starts at a negligible level and then increases in line with exposure time to the electrical field. The intensity reaches a maximum and then begins to decrease as a function of time under the electrical field. If the sample is not re-exposed to the electric field then the fluorescence remains at the level of intensity already reached irrespective of time spent under the laser light source.

The behaviour of the field-induced fluorescence is thus very different from that of the residual fluorescence. However to identify the molecular species giving rise to fluorescence in any given situation is quite difficult. It is however reasonable to assume that if the species giving rise to the two types of fluorescence were the same then the Raman Shift of the fluorescence profiles would also be the same. In addition if they originate from the same species then the absolute wavelength of the fluorescent light would be independent of the wavelength of the light source. (Guilbault ed 1990) In order to investigate this the intensity of the fluorescence profile was plotted against wavelength using a green diode and a red Helium-neon laser source with virgin and aged samples. (Figure 7.01).

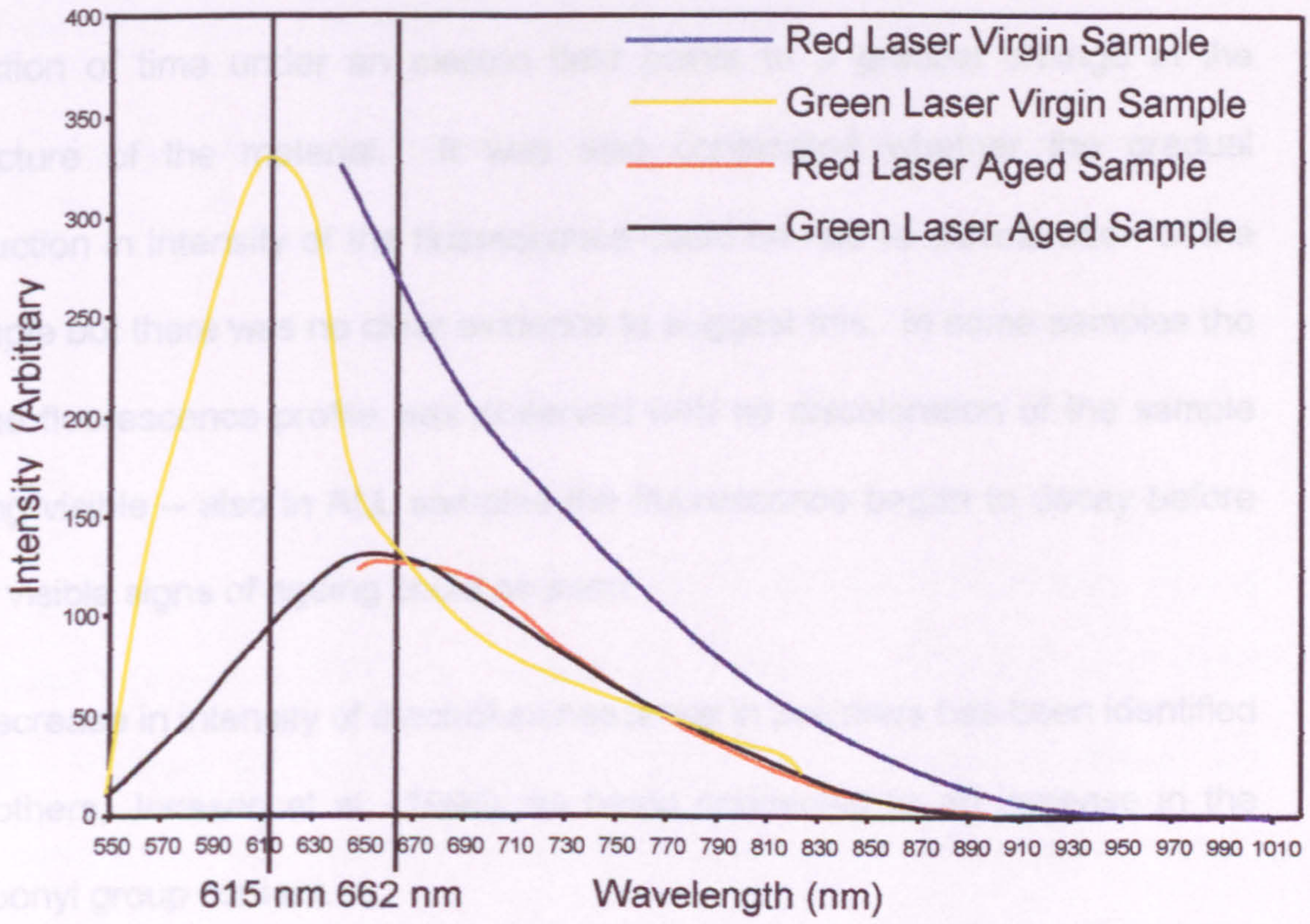

Figure 7.01 A comparison of the fluorescence profile for aged and unaged LDPE illuminated with both the green diode laser and the red helium neon laser. The peak wavelength for aged and unaged are indicated.

Figure 7.01 shows that there is indeed a significant difference between the wavelength profile of the fluorescence light detected from a virgin sample and when the sample has been aged in an electrical field. In addition the wavelength of the fluorescent light from the aged sample is the same, whether the incident light is red or green i.e. the wavelength of the fluorescent light from the sample is independent of the incident light wavelength. There is a difference in the intensity of the light from the two virgin samples, which is the result of the initial fluorescence being partially quenched by the red laser before the green laser was used. The fluorescence observed in the virgin and aged samples can therefore reasonably be attributed to different species.

The decrease in intensity of the observed fluorescence from the sample as a function of time under an electric field points to a gradual change in the structure of the material. It was also considered whether the gradual reduction in intensity of the fluorescence could be due to discoloration of the sample but there was no clear evidence to suggest this. In some samples the same fluorescence profile was observed with no discoloration of the sample being visible – also in ALL samples the fluorescence began to decay before any visible signs of ageing could be seen.

A decrease in intensity of electroluminescence in polymers has been identified by others, Jonsson et al. (1996), as being connected to an increase in the carbonyl group content.

These general findings from the pin plane experiments were also found when carrying out the plane – plane experiments and subsequently the investigations into actual cable samples supplied by the cable manufacturer.

In the case of the plane – plane experiments the sample configuration was quite different from that of the pin - plane – Figure 5.2. The objective of these experiments was to approach rather more closely the actual conditions occurring at the inner semi – con / insulator interface of electrical cables. Figure 6.08 and 6.09 showed typical results with several sites displaying highly localised fluorescence. Whilst the plane electrode was a uniform polished stainless steel plate the semi-con tape was by definition non-uniform and microscopically there will be highly localized areas giving rise to electrical field enhancement. The surface distribution of the fluorescence around the peak was very similar to that obtained in the pin-plane experiments – Figure 6.06 compared to 6.10 – supporting the assertion that the fluorescence and peak development is the result of the electrical field.

If the changes to the vibrational spectrum of the samples observed are caused by the electrical stress applied to the sample then the actual mechanism giving rise to those changes must be considered. Several researchers (Shimizu, *et al* (1992) and Bamji *et al* (1991) for example) consider that electron injection is one of the prime initiation mechanisms leading to the chain scission and free radical formation necessary for the increase in the C=C 1590 cm^{-1} Raman peak and the 1724 cm^{-1} C=O FTIR peak. However the results presented here make it clear that the effects are observed some distance from the actual electrode; typically the phenomenon could be observe up 100 or 150 microns from the electrode when looking at the surface distribution (Figure 6.06, 6.10 and 6.17). This effect was duplicated in the bulk polymer at distances in the range 250 to 300 microns from the electrodes, Figure 6.03, 6.20 and 6.21. This suggests that electron

injection is not a requirement for the processes leading to the changes in the polymer structure observed and another mechanism provides a path to chain scission and free radical generation not dependent on electron injection. Lewis et al (1996) described the basis for such a model and an outline of their basic concepts was given in Section 3.3.

7.2. Changes in the Vibrational Spectrum.

The possibility that a change in morphology of the bulk insulator occurs resulting in an increase in the carbonyl group content (Section 7.1) is supported by the development of new Raman peaks at 1590 and 1330 cm^{-1} and the reduction in intensity of the normal LDPE peaks.

The appearance of the new Raman peaks is accompanied by the gradual reduction in the intensity of the normal Raman peaks seen in LDPE. (Figure 6.01) In order to investigate this phenomenon the amplitudes of the individual peaks were normalized with respect to the LDPE peak at 1296 cm^{-1}. A typical result is shown in Figure 7.02.

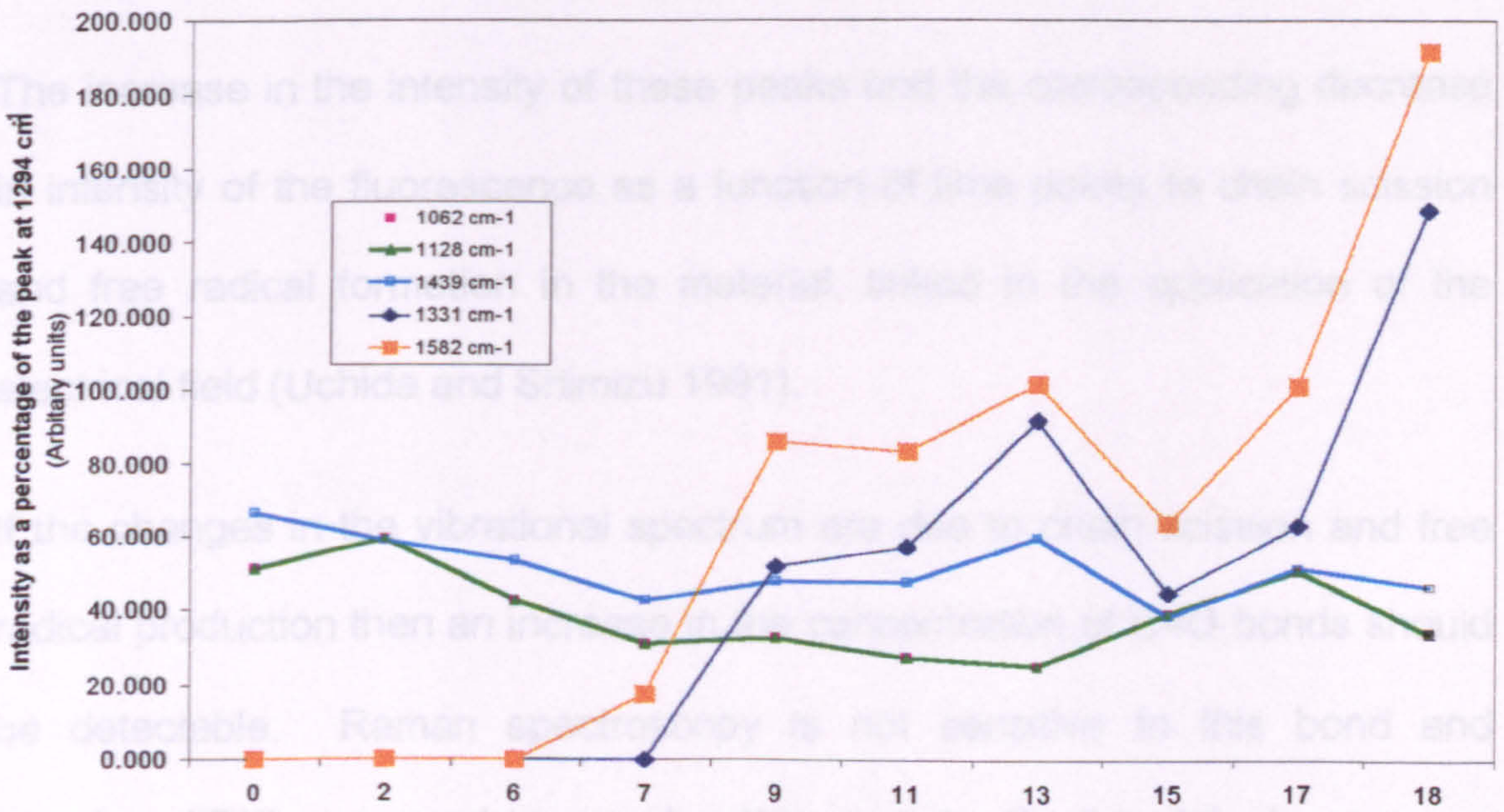

Figure 7.02 A plot of the major peaks in the fingerprint region (section 4.1.1.3.3) normalized to the peak at 1294 cm^{-1}. The curves for the 1128 and 1062 cm^{-1} peaks coincide exactly and only the green curve relating to the peak at 1128 cm^{-1} can be seen.

It is apparent from Figure 7.02 that the relative intensity of the Raman peaks in the fingerprint region change very little even though their intensity is decreasing with time under the electrical field. At the same time the intensity of the two new peaks increases dramatically relative to the peak at 1296 cm^{-1}. The new Raman peak at 1590 cm^{-1}, is indicative of an increase in the presence of the C=C groups. The intensity of this peak reflects the fact that the C=C peak is one of the most intense peaks in the Raman spectrum when present. (Hendra et al. 1991.)

The other new peaks observed in the Raman spectrum (Figure 6.01) namely the peaks at 2640cm^{-1} and 1330 cm^{-1} are attributed to CH_2 deformations and the amorphous phase of the polyethylene respectively. Groenewege *et al* (1965)

The increase in the intensity of these peaks and the corresponding decrease in intensity of the fluorescence as a function of time points to chain scission and free radical formation in the material, linked to the application of the electrical field (Uchida and Shimizu 1991).

If the changes in the vibrational spectrum are due to chain scission and free radical production then an increase in the concentration of C=O bonds should be detectable. Raman spectroscopy is not sensitive to this bond and therefore FTIR was used to examine this aspect. Section 6.2 shows some typical results from these investigations. Figure 6.22 shows an increase in intensity of the FTIR peak at 1724 cm^{-1} which is indicative of C=O stretching vibration. Figure 7.03 shows a difference spectrum derived from Figure 6.22, which confirms the increase in intensity of the peak at 1724 cm^{-1}.

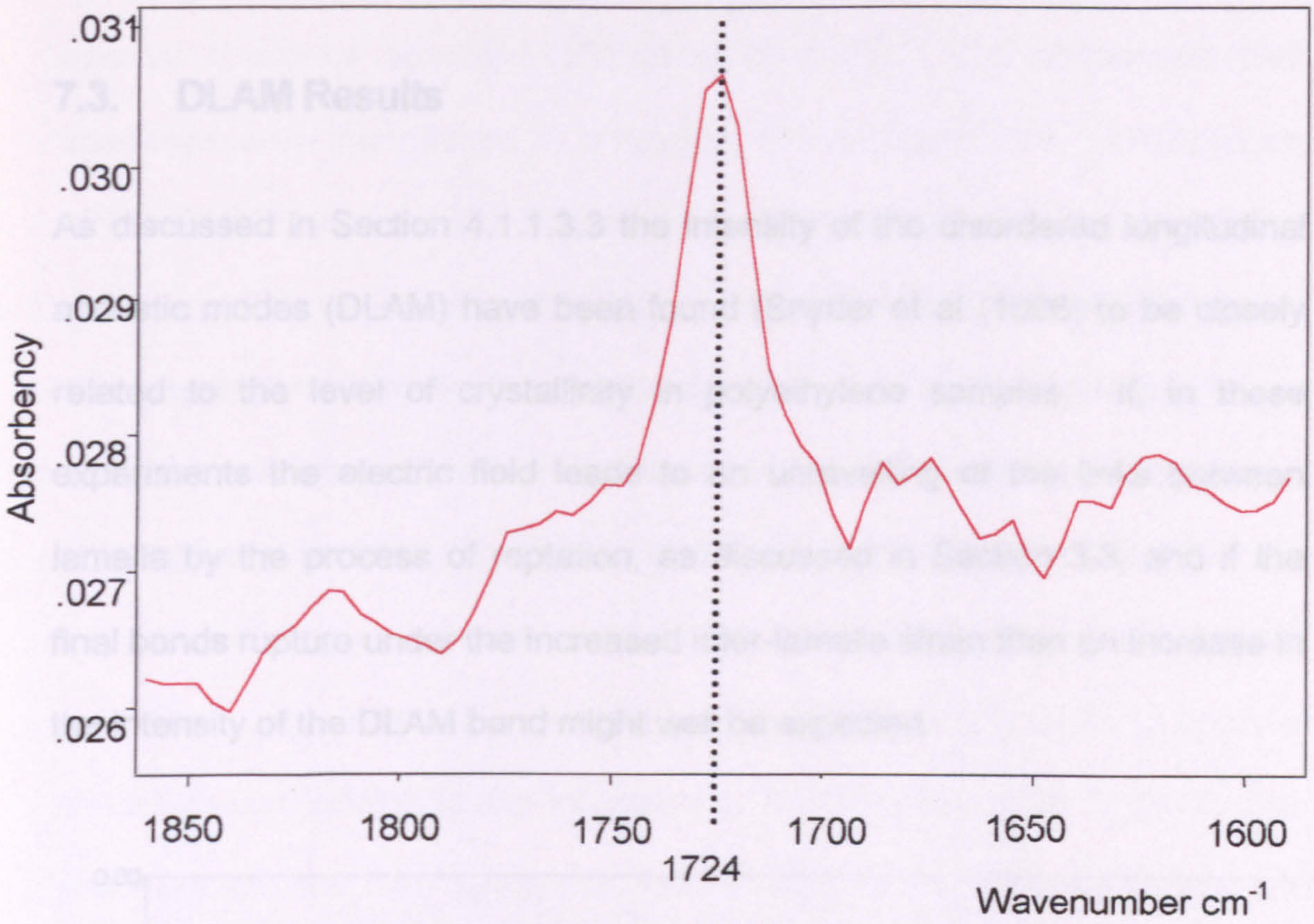

Figure 7.03 A difference spectrum derived from Figure 6.22 showing the increase in the peak at 1724 cm^{-1} attributed to C=O bonds.

This finding confirms and supports the view that the changes in the vibrational spectrum are due to chain scission and free radical production.

7.3. DLAM Results

As discussed in Section 4.1.1.3.3 the intensity of the disordered longitudinal acoustic modes (DLAM) have been found (Snyder et al (1996) to be closely related to the level of crystallinity in polyethylene samples. If, in these experiments the electric field leads to an unravelling of the links between lamella by the process of reptation, as discussed in Section 3.3, and if the final bonds rupture under the increased inter-lamella strain then an increase in the intensity of the DLAM band might well be expected.

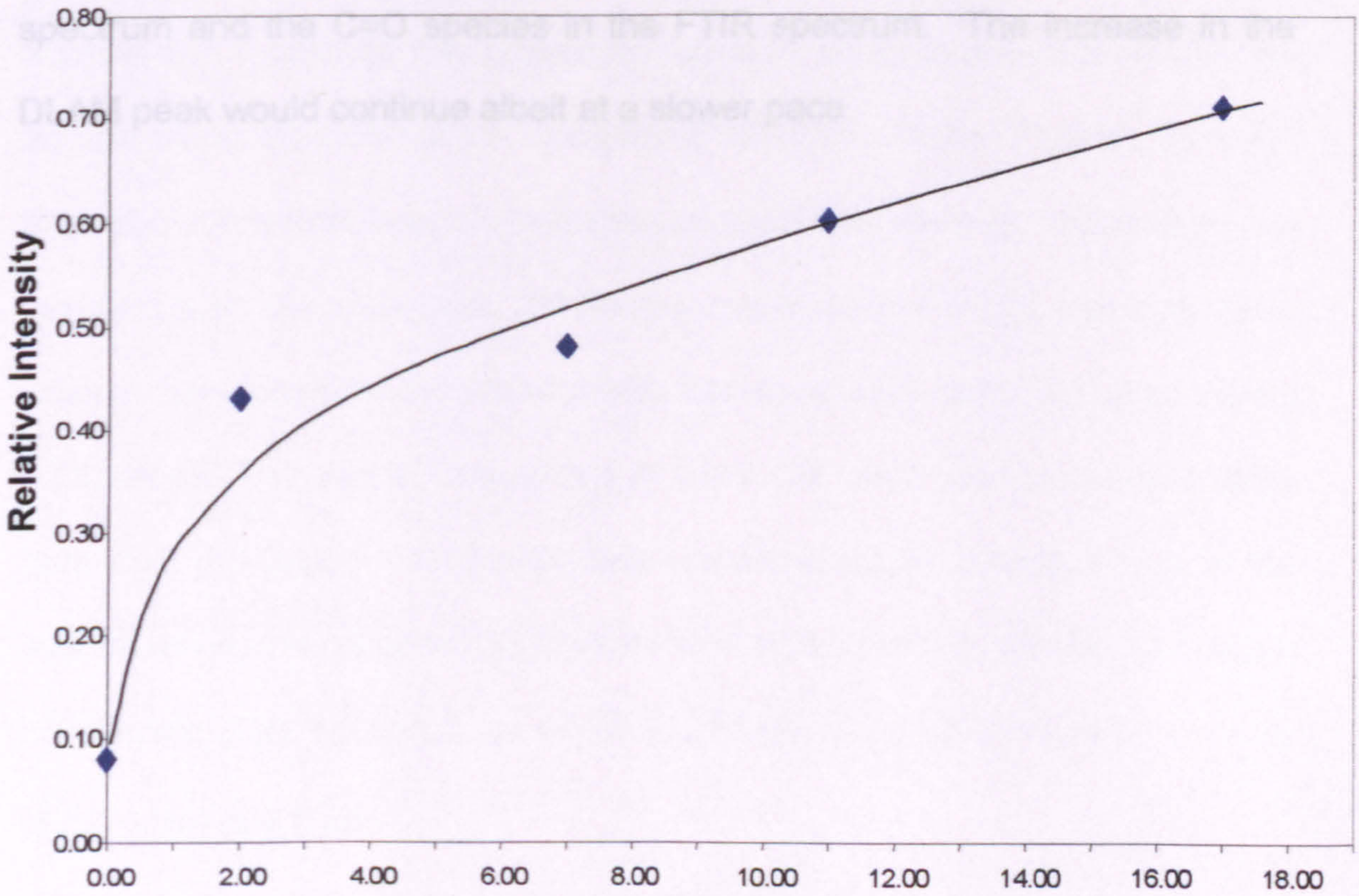

Figure 7.04 Increase in intensity of the DLAM peak at 190cm^{-1} relative to the intense peak at 1296 cm^{-1}.

In order to view the relative increase of the DLAM band the peak intensities were normalized with respect to the intense band at 1295 cm^{-1}, an accepted

internal reference standard. (Strobl et al 1978) The normalised peak intensities were then plotted as a function of time Figure 7.04. The intensity of the DLAM band initially increases rapidly and then the rate of increase reduces. This is consistent with the suggestion that the early structural changes in the material are able to take place rapidly and then less so. It might be that the number of tie molecules able to undergo reptation easily is progressively reduced. The time at which this change occurs coincides with that at which the new peaks at 1590 and 1330 cm^{-1} appear in the Raman spectrum. At this time the remaining tie molecules might begin to undergo chain scission leading to the increases in C=C species seen in the Raman spectrum and the C=O species in the FTIR spectrum. The increase in the DLAM peak would continue albeit at a slower pace.

7.4. SPM Results

The Scanning Probe Microscope was used to investigate the effects of high electrical fields on the surface of LDPE and XLPE. Changes were observed in the surface structure of the polymer well before electrical breakdown could be expected to take place. In addition using the Electrostatic Force Microscope changes in the charge density in the surface layer of the polymer were observed.

7.4.1. Surface Morphology

Section 6.3.1 outlines the procedure used to apply a potential across the sample using the probe of the Scanning Probe Microscope. Figure's 6.24 and 6.25 show a typical image of an area of significant damage induced by the resulting high electrical field. Whilst the overall outline of the damaged area does indeed resemble the probe profile it is larger by a factor of five as Figure 6.26 shows. The overall dimensions of the probe have been calculated using data from the Digital Instruments data sheets; to cause a surface hole of the size observed the probe would have to be inserted into the polymer to a depth of approximately 1.0 to 1.2 μm whilst the measured depth of insertion is only of the order of 0.3 μm.

Concentrating on the actual damage to the polymer surface seen in Figure 6.25 the DI image analysis software was used to find the dimensions of the damaged area as shown in Figure 7.05.

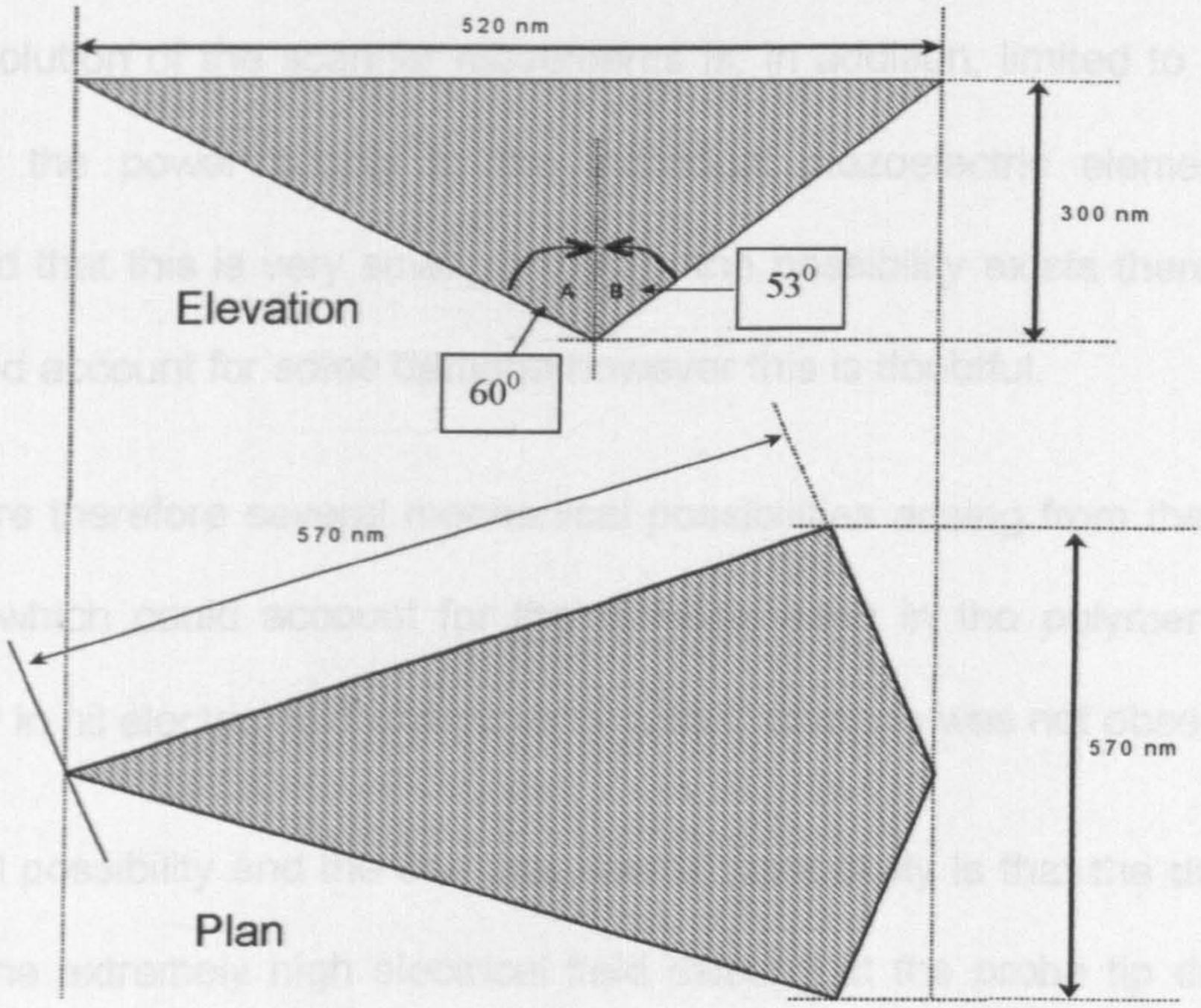

Figure 7.05 Showing the actual size of the damage seen on the polymer surface, Figure 6.25.

Figure 7.05 shows the dimensions and internal angles of the actual damage the comparative angles for the actual probe are A = 26^0 whilst B = 10^0 so it can be seen that whilst the shape resembles the actual probe the dimensions are much larger than the probe size.

The fact that the probe is oscillating and repeatedly tapping the surface (Section 4.2.1) could account for some of the damage, however the sample damage is very much larger than the probe.

In addition the question of the piezo x,y,z scanner stabilisation must be considered. When a change in scan size is requested the response is very quick, however it does not stop immediately and can continue to 'creep' towards the required size for some minutes.

The resolution of the scanner movements is, in addition, limited to the noise level of the power supply to the individual piezoelectric elements, it is expected that this is very small, 1/100nm, the possibility exists therefore that this could account for some damage however this is doubtful.

There are therefore several mechanical possibilities arising from the imaging system which could account for the damage seen in the polymer surface, however in nil electric field experiments similar damage was not observed.

The final possibility and the one that seems most likely is that the damage is due to the extremely high electrical field existing at the probe tip during the charging period. The approximate value of this field can be found by using equation 6.01. Using a nominal figure for the probe tip radius of 10nm and a voltage of 200V, the field at the probe tip would be in the region of 2×10^{10} Vm^{-1}. This field was applied for about ninety minutes.

This is obviously a very high field that would be expected to cause damage to the material surface. In this case it seems that the field has excavated the surface to a depth of ~0.3 μm. This means that the field from the probe would have been extending further into the material, in addition, that the excavated area of the sample would have been in the area of the highest electrical field, at the very end of the probe.

Looking now at the crazing seen most clearly in Figure 6.29 the image analysis software was used to obtain the overall dimensions of the cracks. Figure 7.06 shows a Section analysis on the phase image after application of the electrical field.

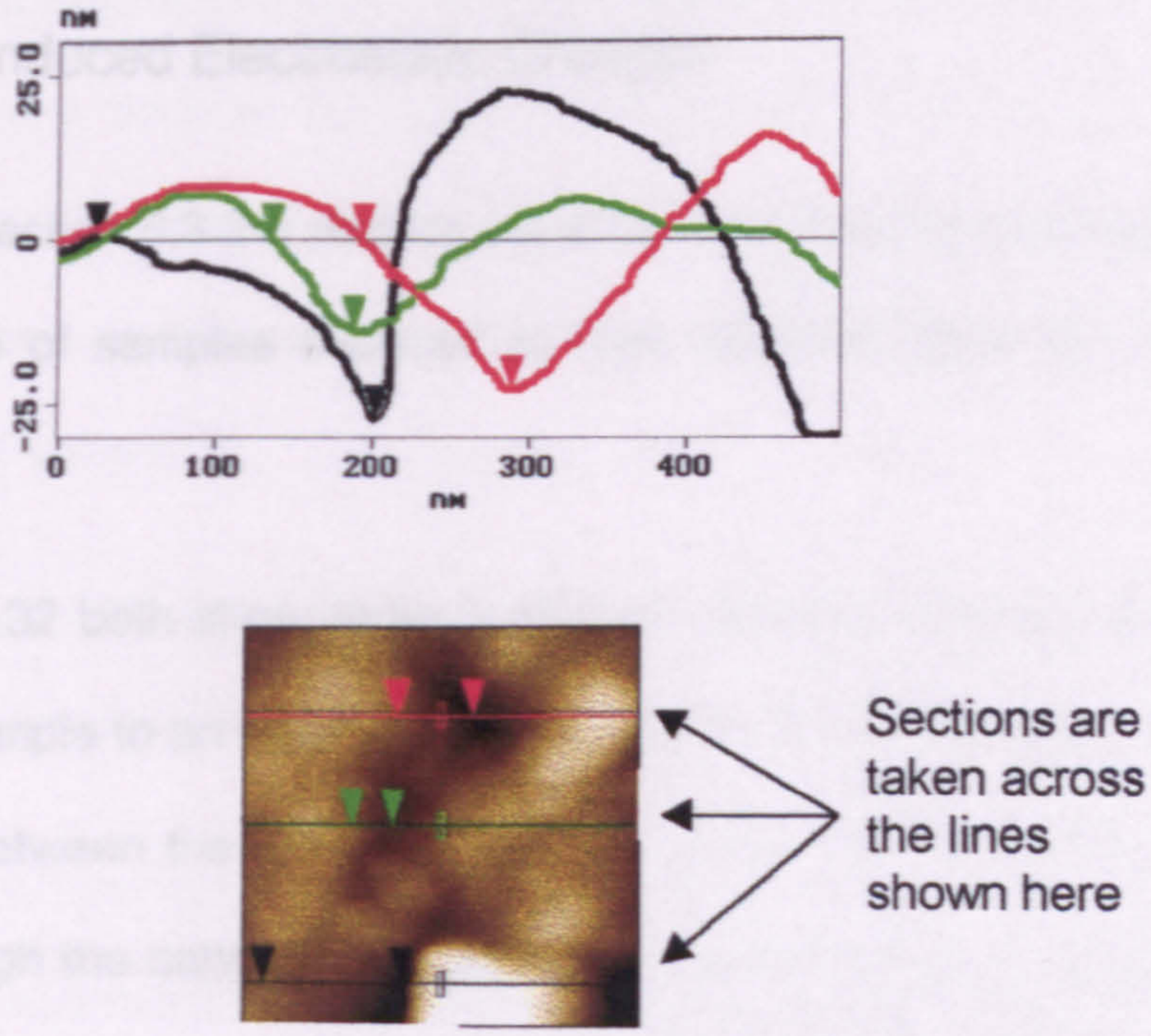

Figure 7.06 A Section Analysis on Figure 6.29 carried out using the proprietary software from Digital Instruments Inc. Showing the depth of the major cracks seen in that image.

The depth of the cracks profiled is red 23nm, green 14nm and black 28nm. As the graph shows they have a sharp profile and are relatively deep on the scale of individual lamella which have been found by others to be ~ 9nm thick; Ania *et al* (1996).

7.4.2. Field Induced Electrostatic Charges

As the shown in Section 6.3.2 a distinct variation in contrast can be observed in the EFM scans of samples exposed to high electrical fields for varying periods of time.

Figure 6.31 and 6.32 both show regions of clear contrast changes following exposure of the sample to an electrical field. Figure 6.31 shows much greater correspondence between the topographical image and the EFG image than Figure 6.32 although the contrast changes by no means result in a duplicate of the topographical image. This is not unexpected since Figure 6.31 was obtained from the immediate area of highest field around the point of contact of the SPM probe whilst Figure 6.32 was obtained from the surface opposite the embedded pin as shown in Figure 6.28. For the sake of clarity a comparison of the area investigated is shown in Figure 7.07.

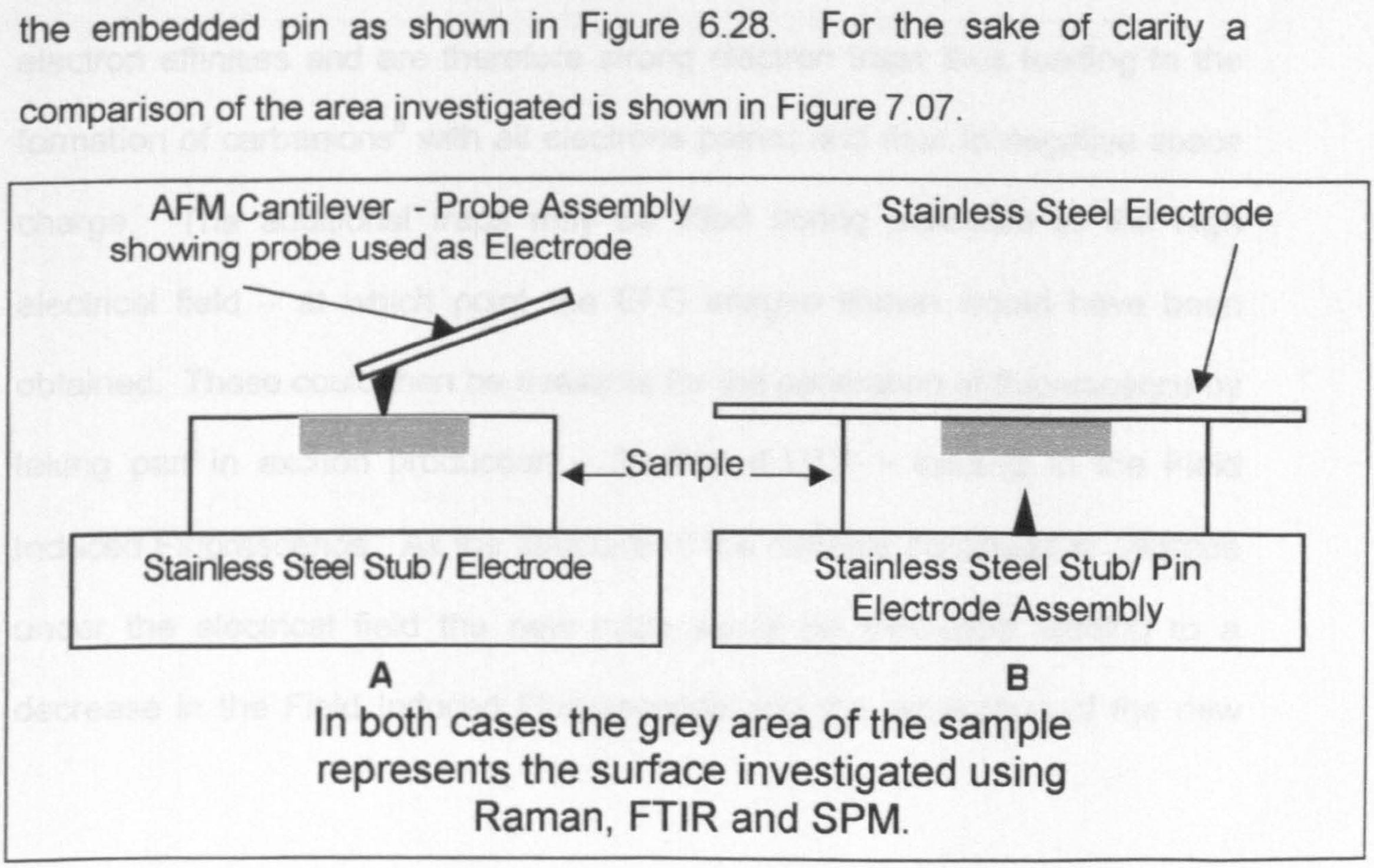

Figure 7.07 Outline sketch comparing the two sample arrangements.

In can be seen from Figure 7.07 that the area examined in A would have been directly under or very close to the highest field region whilst in B the area examined would have been exposed to a more uniform field across the whole sample. This explains the difference in the contrast gradient distribution seen in Figure 6.31 and Figure 6.32.

It should be recalled that the EFG images were obtained from a height of 100nm above the surface of the sample – see Section 4.2.2 and Figure 4.09.

If the electric field is inducing changes in the sample as discussed previously then perhaps the electromechanically induced strain is causing the generation of additional electron traps in the material. These traps may take the form of the free radicals formed following the application of the electric field (Section 3.3). Jansson and Terselius 1979 observed that free radicals can have large electron affinities and are therefore strong electron traps thus leading to the formation of carbanions[8] with all electrons paired and thus to negative space charge. The additional traps may be filled during exposure to the high electrical field – at which point the EFG images shown would have been obtained. These could then be available for the generation of fluorescence by taking part in exciton production – Section 4.1.3.1 – leading to the Field Induced Fluorescence. As the structure of the material continues to degrade under the electrical field the new traps would be destroyed leading to a decrease in the Field Induced Fluorescence and the generation of the new

---

[8] Carbanion – A short lived negatively charged intermediate formed by the removal of a proton from a – C-H bond.

peaks at 1590 and 1330 cm^{-1} as the molecular structure of the polymer is modified.

7.5. Possible Sources of Error

7.5.1. Fluorescence and Changes in the Vibrational Spectra

The question must be asked as to whether the effects seen could be due to other processes within the polymer apart from the electric field. A sharp point or edge above the polymer could lead to local field enhancement and breakdown of the atmosphere – all experiments were carried out in ambient conditions – resulting in oxidation of the surface caused by discharges. It is also possible that the act of putting the sample under pressure in the experimental setup may have induced structural changes. This question was approached in several ways, for example by looking for similar results from the within the bulk insulator to eliminate surface oxidation effects. Care was also taken by ensuring that wherever possible the measurements were obtained as far from any possible source of discharge as possible. In addition experiments were carried out in the absence of any electrical field. (Figure 6.12 & 6.13) To investigate the question as to whether the mere act of placing the sample under pressure was initiating changes, experiments were carried out using exactly the same procedure but without applying any electrical potential across the sample. These tests were carried out for each sample configuration and confirmed that no effects were observed in the absence of an electric field. Figure 7.08 shows a spectrum from a semi-con XLPE interface experiment.

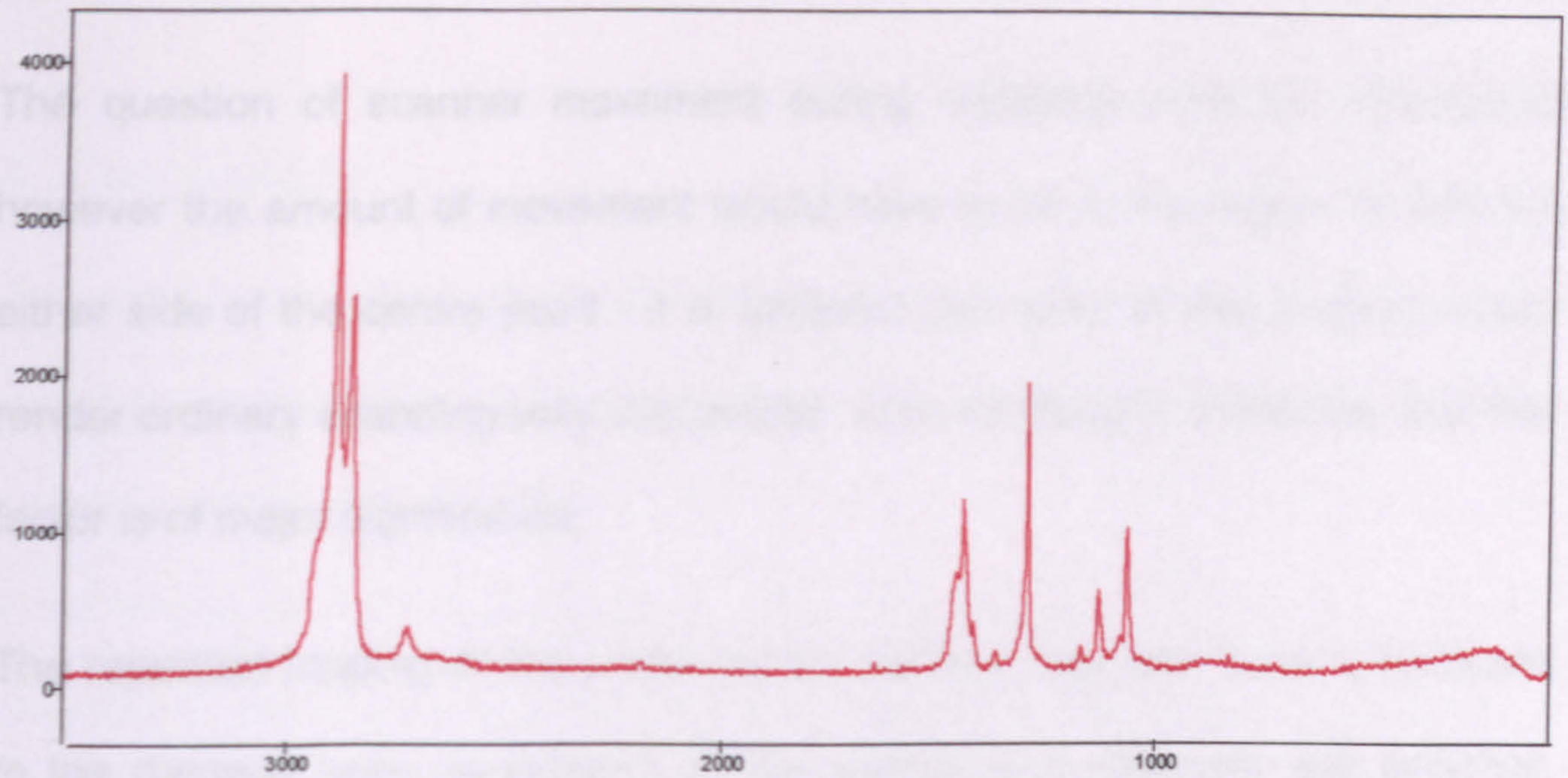

Figure 7.08 Showing a spectrum from a zero field experiment. The spectrum is typical of a LDPE sample showing no spectral developments or signs of fluorescence.

In addition in the case of the plane - plane electrode experiments the semi-con tape was quite soft and sufficient pressure was applied to the samples to ensure that there was close contact between the samples at all points. This was done to exclude atmospheric effects as far as possible.

It should also be noted that the results were repeated in measurements on the cable samples which were subjected to electrical stress testing at a third party site and supplied for experiments to be carried out.

7.5.2. SPM

As outlined in Section 7.4.1 there are several possible factors, which could lead to the damage, seen. When considering these it must be kept in mind that, whilst the damage is roughly the shape of the tip, the damaged area overall is perhaps five times the size of the probe at a point 300 nm up the shaft of the probe. (i.e. the depth of insertion)

The question of scanner movement during charging must be considered however the amount of movement would have to be in the region of 200 nm either side of the centre point - it is believed that 'play' of this amount would render ordinary scanning very impractical. It is not thought, therefore, that this factor is of major significance.

The repeated tapping of the probe on the surface may well have contributed to the damage seen particularly as the sample is a relatively soft polymer. This mode of AFM operation is well known as the preferred method of operation on soft surfaces as it inflicts less damage on the surface as it scans the area. It is therefore thought unlikely that this tapping would lead to the type of 'crazed' damage seen in Figure 6.24, 6.25, 6.27 and 6.29. These images share some similarities with TEM images published [Kaminaga, K *et al.* (1986)] in a paper examining the effect of lamella structure on dielectric breakdown.

It is considered, therefore, that whilst the damage observed is partly the result of the probe touching the surface, the majority of the damage is believed to originate from the intense electrical field surrounding the probe. This field may well have created micro cavities between the lamella forcing them apart leading to the cracks seen in Figure 6.24, 6.25, 6.27 and 6.29; these cracks seem to follow the individual lamella, at least initially, and this is in agreement with the observations of Hozumi, N. *et al.* (1988) where he found that the tree did not grow in the direction of the maximum electrical field but rather along the "..windings of the lamella...".

8. Conclusions

The experiments have demonstrated that significant physical and chemical changes occur in both LDPE and XLPE when subjected to power frequency electrical stresses of the order of $6x10^7$ Vm^{-1}. The most striking feature in the initial stages of stressing (Figure 6.01) is the appearance of a broad band of photoluminescence in the Raman Spectrum, the intensity of which is a function of the stress. At the same time the characteristic Raman bands of unstressed PE, which are attributable to the various modes of CH bond vibration of the polymer chain, become suppressed. If the electrical stress is sufficiently strong the luminescence gradually subsides (Figures 7.01, 7.02) while simultaneously additional broad Raman lines appear (Figure 6.01) at 2640, 1590 and 1330 cm^{-1}. The line at 1590 cm^{-1} is most significant since it indicates the presence of a growing concentration of the unsaturated (C=C) bond. This could arise only from scission of the main chain C-C bonds of polyethylene, a process that would be efficiently triggered if free radicals were present. There are several possible routes for this to occur, especially one involving a repeating cycle of chain decomposition by hydrogen abstraction, radical regeneration and the production of double bond entities (Kagiya *et al* (1979) and figure 3.5). The other new Raman lines are to be attributed to CH_2 deformations with that at 1330 cm^{-1} usually being associated with the amorphous phase (Groenewege *et al* (1965)).

Both luminescence and the double bond development can coexist in a sample as Figure 6.06 strikingly illustrates. In the highest field region on the axis of the point electrode the luminescence has collapsed and C=C bonds have

appeared; but in the surrounding lower field regions luminescence persists without evidence for any C=C bonds.

The results for the semicon electrode system (Figure 6.08 and 6.09) show that the above processes are not restricted to point plane non-uniform field conditions but also occur in uniform fields. The luminescence generated is still highly localized however. This may reflect a local non-uniformity in the semicon electrode surface, which would affect the field or may be due to the inherently non-uniform structure of the semi-crystalline XLPE polymer on a microscopic scale.

The present results complement those given by Uchida and Shimizu *et al* (1991 and 1992) which showed that the concentrations of the C=C group increase markedly in high field regions. Limited IR studies were carried out, which confirm their finding that the C=O group also appears as a result of stressing.

The localized nature of the luminescence, even in the uniform field experiments, supports the work of Laurent (1999) who suggested that ageing is a "highly localized process". The results showing the appearance of the C=C peak in the Raman spectrum and the changes in the C=O peak in the FTIR spectrum also support the mechanisms suggested by Laurent to be involved in the ageing of insulating polymers.

Limited studies with scanning probe microscopy were carried out, the structure of the polymer surfaces was investigated and it was found, that as a result of the electrical stress, the lamella morphology of the polymer is destroyed and in some cases cracks ~10 nm wide appear.

Uchida and Shimizu also proposed that the destruction of the PE structure by hydrogen abstraction and chain scission is initiated by collisions with carriers (electrons) injected at the point electrode and accelerated by the locally intense field. Bamji *et al* (1988) have suggested that injected carriers first generate UV photons by electroluminescence and these are then responsible for the destruction.

Since the present experiments have shown that the fluorescence, Raman peak development and surface structure modification are present in regions well away from the point electrode, electron injection does not seem to be an essential requirement. It is suggested instead that the results support a model based on the concept that the electric field generates mechanical forces strong enough to influence thermally induced bond scission in the polymer. Lewis et al (1996) described a version of this model concentrating on main chain bond scission. It may be extended in an important way by proposing that the mechanical forces first overcome the weaker intermolecular van der Waals bonds so encouraging polymer chain disentanglement by reptation and ductile creep. As a result the crystalline lamellae of PE would disintegrate as tie molecules are pulled out and a fibrillar structure would develop. This concept is supported by the DLAM results as seen in figure 6.07. Those results show the DLAM peak increasing in relative intensity as the stressing time increases; this increase in intensity of the DLAM peak has been shown to be consistent with a decrease in the crystalline proportion of the polymer. (Snyder *et al.* 1986)

Ultimately the increasing mechanical tensions in the fibrils become sufficient to cause chain scissions, free radical production and hydrogen abstraction. An important characteristic of this stage would be the production of molecules with unsaturated C=C bonds continuing disentanglement and tie chain scissions will lead to a void network or craze conducive to tree-like cracking.

The photoluminescence observed on first applying a stress can be related to the filling or populating of the defect sites created during the early mechanical stressing induced by the electrical field. Under continuing electrical stress, as the polymer chains disentangle and the crystallites 'dissolve', these sites would be lost and the luminescence would decline. Moreover, as seen in Figure 6.01 the characteristic vibrational modes of polyethylene side groups are likely to be suppressed when the chains are under strain and undergoing disentanglement by reptation. At the same time the increasing probability of tie chain scissions and free radical activity will cause the concentration of C=C bonds to grow. Removal of the electrical stress at any time would halt the processes, leaving some degree of persistent luminescence corresponding to the structure at that time.

The SPM work has confirmed that structural changes at a gross physical level take place in the polymer long before electrical breakdown occurs. The cracks seen in figures 6.24, 6.25, 6.27 and 6.29, were typical of the damage observed after electrical stressing of the material with the SPM probe. Figure 6.30 shows evidence that the electrical field has "opened" the structure of the material directly beneath the probe, initiated cracks and caused severe lamella distortion and reorganisation. The EFG images shown in section 6

help to support the hypothesis put forward to explain the field induced fluorescence seen and the appearance of new peaks in the Raman spectrum of polyethylene. The evidence of charge, figure 6.31, in the surface layer following application of an electrical field also supports the argument for the presence of charge in defect sites in the polymer.

In terms of observing the initial stages or prebreakdown changes in polymers these results raise some interesting possibilities. The use of electro-luminescence to detect these changes is more sensitive than partial-discharge detection methods. The work of Laurent et al (1999, 1998 1981) and others concentrates on ultra-violet or near ultra-violet – induced luminescence. The work reported in section 6 is concerned with luminescent signals of the same order of magnitude as the Raman signals which are one to two orders of magnitude lower than the UV induced luminescence. It would seem therefore that the method reported here may offer the possibility of earlier detection of prebreakdown changes taking place in the material. In addition as outlined above Bamji *et al* (1988) suggested that injected carriers first generate UV photons by electroluminescence and these are then responsible for the destruction. However these results support structural and chemical changes taking place before the generation of UV photons. This would seem to preclude UV photons as the source of the initial polymer degradation. This is further evidence to support the theory of mechanical forces strong enough to advance thermally induced bond scission in line with the electro-mechanical model of electrical breakdown of Lewis et al.

The Raman Spectrometer is rapidly becoming an extremely useful tool in the investigation of chemical and structural changes in materials and especially as the results complement those of FTIR. There is considerable scope for the extension of this work looking at the DLAM peak and also the Longitudinal Acoustic Mode (LAM) both of these spectral features originate from the conformational structure of the polymer. It should be possible to examine the development of the LAM mode as the electrical breakdown point is approached. Following from the work presented here it is expected that the LAM peak results would complement those of the DLAM investigations in section 6. Mechanical strain induced shifts in the Raman spectrum have also been observed (Meier and Vansweefelt 1995) – this raises the interesting possibility of observing such shifts in the Raman spectrum of electrically stressed polymers. However as these shifts are likely to be extremely small in electrically stressed samples large sample numbers would be required to establish such results.

The Scanning Probe Microscope is fast becoming one of the most innovative and flexible investigative tools available to the researcher. There is the possibility of extending this work using the SPM to observe the surface charges and physical changes in the polymer insulator following the stressing of the material with electrical fields of varying strengths and varying application times. Tian *et al* 1996 carried out some interesting experiments combining both the Raman spectrometer and the Scanning Tunnelling Microscope so as to obtain simultaneous results from exactly the same sample area. It is conceivable therefore that the possibility exists to set up a similar experiment combining both the SPM and the Raman to obtain Raman

Spectra, SPM Topological and EFG images. This could result in the observation of the chemical and structural changes as they occur simultaneously with the development of any electrostatic surface charges.

9. References

Abou-Dakka, M., Bamji, S.S. and Bulinski, A.T. (1997).
Space Charge Distribution in XLPE by TSM using the Inverse Matrix Technique.
IEEE Transactions on Dielectrics and Electrical Insulation. Vol.4, No. 3, pp.314-320.

Amelin, A.V., Pozdryakov, O.F., Regel, V.R., and Sanfirora, T.P. (1971)
Comparison of the Activation Energies for Thermal and mechanical Destruction of Polymers
Soviet Physics – Solid State, Vol.12, pp 2034-2038.

Ania. F, Balta Calleja. F.J, Bayer. R.K, Tshmel. A, Naumann. I, and Michler. G.H, (1996)
Comparative study of size and distribution of lamellar thicknesses and long periods in polyethylene with a shish-kebab structure.
Journal of Materials Science, 31, 4199 – 4206.

Arbab. M.N and Auckland. D.W. (1986)
The influence of vibration on the initiation of trees in dielectrics.
IEE Proceedings, Vol. 133, Pt. A, No. 9.

Artbauer, J. (1996).
Electric Strength of Polymers.
Journal of Physics D, Applied Physics., Vol. 29, pp. 446-456.

Bahder, G., Garrity, T., Sosnowski, M., and Katz, C. (1982)
IEEE Trans. Power Appar. and Syst., PAS-101 (7), pp. 1379-1390.

Banji.S.S (1999)
Electroluminescence – A Technique to Detect the Initiation of Degradation in Polyemeric Insulation.
IEEE Electrical Insulation. Vol. 15, No. 3, pp 9-14

Bamji S S, Bulinski A T and Densley R J, 1988,
Degradation of Polymeric Insulation Due to Photoemission Caused by High Electric Fields
IEEE Trans. Electr. Insul., 24, 91-98.

Bamji.S.S., Bulinski.A.T. and Densley.R.J. (1991).
Degradation Mechanism at XLPE/Semicon Interface Subjected to High Electrical Stress.
IEEE Transactions on Electrical Insulation. Vol.26, No.2, pp. 278-284.

Barclay. A.L., Sweeney. P.J., Dissado.L.A. and Stevens.G.C. (1990)
Stochastic Modelling of Electrical Treeing: Fractal and Statistical Characteristics.
J.Phys.D: Applied Physics., Vol. 23, pp. 1536-1545.

Barlow. A., Hill. L.A., and Maringer. M. F. (1983)
IEEE Trans. Power Appar. and Syst., PAS-102 (7), pp. 1921-1926.

Betteridge, S., Lewis, T. J., and Llewellyn, J. P. (1997)
"A preliminary Study of the Cable Semicon-Insulator Interface using Scanning Probe Microscopy",
Internal Report, BICC Cables Limited, Report Number WTC R/97/395

Bettridge. S. et al. (1997)
Preliminary Measurements on High Voltage Cables using Scanning Probe Microscopy.
Confidential Report BICC - SEECS.

Bhateja. S.K. (1983).
Journal of Applied Polymer Science. Vol.28. pp. 861-872.

Binnig. G., Rohrer, H., Gerber, Ch., and Weibel, E. (1982)
Physical Review Letters. Vol.49, No. 57.

Binnig.G., Quate.C.F and Gerber.Ch. (1986).
Atomic Force Microscope.
Physical Review Letters. Vol.56, No.9, pp.930-933.

Bower, D.I. and Maddams, W.F. (1989)
The Vibrational Spectroscopy of Polymers
Cambridge University Press

Champion, J.V., Alison, J.M., Dodd, S.J. and Stevens, G.C. (1995)
Dynamic bipolar charge recombination model for electroluminescence in polymer based insulation during electrical tree initiation.
J.Phys.D: Applied Physics., Vol. 28, pp. 1693-1701.

Coudray, C. and Blaise, G. (1996).
Charge Trapping Induced Electromechanical Energy
Journal of Applied Physics. Vol. 80, No. 9, pp. 5248-5255.

Crine, J. (1990).
A Model of Solid Dielectrics Ageing.
Proceedings of IEEE International Symposium on EI, pp. 25-27

Crine, J. (1999)
Comparison between Lewis and Crine models for the electrical aging of Dielectric Polymers
IEEE Conference on Electrical Insulation and Dielectric Phenomena, pp508-511.

Crine, J. and Vijh, A. (1985).
A Molecular Approach to Physico-chemical Factors in the Electric Breakdown of Polymers.
Applied Physics Communications, Vol. 5, pp. 139-163.

Dang. C, Parpal. J, and Crine. J. (1996)
Electrical Ageing of Extruded Dielectric Cables - Review of Existing Theories and Data.
IEEE Transactions on Dielectrics and Electrical Insulation. Vol.3 pp237-247.

Digital Instruments Application Note – AFM Part 8

Dissado, L.A. Mazzanti, G., and Montanari, G.C. (1995).
The Incorporation of Space Charge Degradation in the Life Model for Electrical Insulating Materials.
IEEE Transactions on Dielectrics and Electrical Insulation. Vol.2, No. 6, pp.1147-1158.

Dissado. L.A., Fothergill. J.C. (1992).
Electrical Degradation and Breakdown in Polymers.
London: Peter Peregrinus Ltd.

Dissado.L.A and Hill.R.M. (1987)
Self-similarity as a Fundamental Feature of the Regression of Fluctuations
Chem. Phys., 111, pp. 193-207

Dissado.L.A. and Hill.R.M. (1983).
A Cluster Approach to the Structure of Imperfect Materials and Their Relaxation Spectroscopy.
Proc. Roy. Soc. London, 390, pp. 131-180.

Dissado.L.A., Dodd.S.J., Champion.J.V., Williams.P.I. and Alison.J.M. (1997)
Propagation of Electrical Tree Structures in Solid Polymeric Insulation.
IEEE Transactions on Dielectrics and Electrical Insulation. Vol.4 No.3. pp.259-279.

Fan. Z, Takahashi. T. Suzuki. J, Miyata. H. Lemura. S, Itoh. T, Nakiri. T, and Shimuzu. N. (2001)
Relation between Electroluminescence and Degradation in XLPE
IEEE Trans. on Dielectrics and Electrical Insulation, Vol. 8, No. 1, pp 91-96.

Gall. M. J, Hendra. P.J, Peacock. C.J, Cudby. M.E.A, and Willis. H.A. (1972)
Laser-Raman spectrum of polyethylene: Part 1. Structure and analysis of the polymer.
Polymer, Vol. 13, pp104-108.

Gall. M. J, Hendra. P.J, Peacock. C.J, Cudby. M.E.A, and Willis. H.A. (1971)
Laser-Raman spectrum of polyethylene the assignment of the spectrum to fundamental modes of vibration.
Spectrochimica Acta, Vol. 28A, pp. 1485-1496.

Griffith, A.A. (1920)
Phil. Trans. Roy. Soc. (Lond), A221, pp 163-198.

Groenewege, M. P., Schuyer, J., Smidt, J. and Tuijnman, A. F., (1965).
Absorption and relaxation spectra of polyolefins Crystalline Olefin Polymers Part 1,
Interscience Publications, John Wiley and Sons Inc., N.Y.

Guilbault, G.G. (1990).
Practical Fluorescence.
Second Edition, Marcel Dekker, Inc., New York, pp. 51-57.

Hendra. P, Jones. C, and Warnes. G. (1991)
Fourier Transform Raman Spectroscopy.
Ellis Horwood Ltd, Chichester, England.

Hozumi. N, Ishida. M, Okamoto. T, and Fukagawa. H. (1988)
The Influence of Morphology on Electrical Tree Initiation in Polyethylene under ac and Impulse Voltages.
IEEE Trans. on Electrical Insulation. Vol. 25, No. 4, pp 707-714.

Hozumi. N, Okamoto. T, and Fukagawa. H. (1988)
TEM observation of Electrical Tree Paths and Microstructures in Polyethylene.
Japanese Journal of Applied Physics, Vol. 27, No.7, July, pp. 1230-1233.

Jansson. J.F. and Terselius, J. (1979)
Mechano-Chemical Phenomena in Polymers
J. Applied Polymer Science, Applied Polymer Symp., Vol. 35, pp. 455-468.

Jonscher. A.K. and Lacoste. R. (1984)
IEEE Transactions on Electrical Insulation. EI-19, pp. 567-577

Jonsson. J., Ranby. B, Massines. F, Mary. D, and Laurent. C. (1996)
Spectral Features of the Luminescence of PE Subjected to various Excitation Sources
IEEE Transactions on Dielectrics and Electrical Insulation, Vol. 3, No. 6, pp 859 – 865.

Kagiya V T, Takemoto K and Hagiwara M, 1979,
Elementary reactions in polymer degradation
J. Appl. Polymer Sci., 35, 95-104.

Kaminaga. K, Hirato. K, Shin-ichi. I, Kimura. K, Ishino. I, and Nakagawa. H.(1986)
The effect of solid state structure on the dielectric breakdown strength of insulating polymer material.
Conf. Rec.IEEE Int. Sym. On Electrical Insulation. Washington D.C.

Klein. N. (1969).
Advances in Electronics and Electron Physics. Ed. Marton. L.
Academic Press, New York.

Lewis T J, Llewellyn J P, Van der Sluijs M J, Freestone J and Hampton R N, (1996),
A New Model for Electrical Aging and Breakdown in Dielectrics,
IEE International Conference on Dielectric Materials, Measurement and Applications, Conf. Pub. 430, pp 220-224.

Lewis, T.J. (1986)
Electrical Effects at Interfaces and Surfaces.
IEEE Transactions on Electrical Insulation. EI-21, pp. 289-295

Lewis, T.J. (1990).
Charge transport, charge injection and breakdown in polymeric insulators.
Journal of Physics: Applied Physics. Vol. 23, pp. 1469-1478.

Lewis. T.J. (1994)
Nanometric Dielectrics.
IEEE Trans. on Dielectrics and Electrical Insulation. Vol. 1, No. 5.

Liufu. D, Wang. X.S. Tu. D.M, and Kao. K.C. (1998)
High-field Induced electrical aging in polypropylene films
Journal of Applied Physics. Vol. 83, No. 4.

Lloyd Jr. J.M. and Budenstein.P.P. (1977)
On the Formative Stages of Discharge Channels in Solids.
Ann. Rep. CEIDP. 1977, pp. 339-346.

Lustiger A.. and M.M Epstein.. *"Ann. Rep. Conf. Elec. Insulation and Dielectric Phenomenon", pp. 351-357. 1986.*

Lustiger. A. and Epstein. M.M. (1986).
Ann. Rep. Conf. Elec. Insulation and Dielectric Phenomenon, pp. 351-357.

Magonov. S.N. and Whangbo. M.(1996).
Surface Analysis with the STM and AFM.
VCH GmbH.

Mandelkern, L. and Alamo, R.G. (1993)
Use of Raman Spectroscopy in Characterizing the Structure and Properties of Crystalline Polymers
American Chemical Society. Pp.157-190.

Mandelkern, L. (1990)
Acc. Chem. Res. Vol. 23, p380

Mary, D., Albertini, M. and Laurent, C. (1997)
Understanding optical emissions from electrically stressed insulating polymers: electroluminescence in poly(ethyleneterphthalate) and poly(ethylene 2,6-naphthalate) films
J.Phys.D: Applied Physics., Vol. 30, pp. 171-184.

Mason, J. (1981)
Proc. IEE 128A, pp. 193-201.

Masyo, F.R. (1976)
Oxygen Induced Pyrolysis of Polyolefins
Polymer Physics, Polymer Letters Edition Vol. 14, pp. 713-716.

Meier. R.J, and Vansweefelt. H. (1995)
Some comments on the analysis of vibrational bands in strained polymers: polyethylene.
Polymer. Vol. 36 No.20.

Mitsui. T, Kobayashi. T, Shimzu. H, Nagasaki. S, Matsubara. H, Kuno. M, Komatsubara. H and Okada. T. (1984)
Morphological study of Treeing Phenomena in PE and XLPE
IEEE Int. Sym. On Electrical Insulation. Pp 22-26.

Mort, J., and Pfister, G. (1982).
Electronic Properties of Polymers.
J.Wiley and Sons, New York.

Nath. R and Perlman. M.M. (1989).
IEEE Transactions on Electrical Insulation. EI-24 pp. 409-412.

Nielson, J.R. and Woollett, A.H. (1957)
Vibrational Spectra of Polyethylene and Related Substances
J. Chem. Phys. 26, pp. 1391-1400.

Niemeyer.L., Pietronero. L. and Wiersmann. H.J. (1984).
Fractal Dimension of Dielectric Breakdown.
Phys. Rev. Lett., Vol. 52(12), pp. 1033-1036

Noy. A., Vezenov. D.V. and Lieber. C.M. (1997).
Chemical Force Microscopy.
Annual Review of Material Science. Vol.27, pp. 381-421.

Okamoto T., M. Ishida and N. Hozumi. (1988).
"Effect of Agglomeration of Carbon Particles in the Semiconducting Material on the Dielectric Strength of XLPE Insulation".
IEEE Trans. Elect. Insul., 23, 335,

Parpal. J, Crine. J and Dang. C. (1997).
Electrical Ageing of Extruded Dielectric Cables; A Physical Model.
IEEE Transactions on Dielectrics and Electrical Insulation. Vol.4 No.2 pp197-209.

Perlman. M.M. and Haridoss. S. (1986)
Proc. 2nd Int. Conf. Cond. Breakdown in Solid Dielectrics (Erlangen), pp. 494-499.

Raman. C.V. and Krishnan. K.S. (1928).
Nature Vol.121, No.50.

Rasikawan. S, Ishihara. H, Shimuzu. N. (1994)
Comparison between Water-treed and Deteriorated Regions
IEEE Transactions on Dielectrics and Electrical Insulation. Vol.1 No.4 pp597-603..

Reich. L, and Stivala.S.A. (1971)
Elements of Polymer Degradation
McGraw-Hill, New York.

Ritsko. J. J. (1982).
Electronic Properties of Polymers, Chapter 2.
J. Wiley & Son, New York.

Ross. R. and Smit. J.J. (1992).
Composition and Growth of Water Trees in XLPE.
IEEE Transactions on Electrical Insulation. Vol.27 (3), pp. 519-531.

Scarpa. P.C.N. (1995).
Polarisation and Dielectric Behaviour of AC Aged Polyethylene.
PhD Thesis, University of Wales, Bangor.

Shimizu, N., Uchida, K. and Rasikawan, S.(1992)
Electrical Tree and Deteriorated Region in Polyethylene.
IEEE transaction on Electrical Insulation. Vol. 27, No. 3, pp. 513-518.

Sillinsh (1980)
Organic Molecular Crystals
Springer-Verlag, Berlin, Germany.

Smit. J.J. and Guerts. W.S.M. (1984).
IEE Conf. Diel. Mats. Meas. & Applics., IEE. Conf. Pub. 239, pp. 68-71.

Snyder, R.G. (1967)
A revised assignment of the B_{2g} methylene wagging fundamental of the planar polyethylene chain.
J. Mol. Spectroscopy 23, pp. 224-228.

Snyder, R.G., Schotter, N.E., Alamo, R. and Mandelkern, L. (1986)
Observation of a Conformationally Liquidlike component in Crystalline Polyethylene by Raman Spectroscopy.
Macromolecules, 19, 621-626.

Stern.J.E., Terris.B.D., Marnin.H.J. and Rugar. D. (1988).
Deposition and Imaging of Localized Charge on Insulator Surface using a Force Microscope.
Applied Physics Letters. Vol. 53, No.26, pp. 2717-2719.

Strobl. G, and Hagedoorn. W. (1978)
Raman Spectroscopic Method for Determining the Crystallinity of Polyethylene
Journal of Polymer Science: Polymer Physics Edition, Vol. 16., 1181-1193.

Struik. L.C.E. (1978).
Physical Ageing in Amorphous Polymers and Other Materials
Elsevier Press, Amsterdam.

Stucki, F. (1994)
Injection of a Minimal Space Charge as Mechanism for the Initial Phase of Electrical Polymer Degradation.
IEEE Transactions on Dielectrics and Electrical Insulation. Vol.1 No.2 pp 231-234.

Thue, W.A., and Lyle, R. (1983)
IEEE Trans. Power Appar. & Sys., PAS-102, pp. 2116-2123.

Tian, Z.Q., et al.(1996).
Simultaneous STM and Raman measurements on electrochemical interfaces.
Journal of Electrochemical Chemistry, Vol. 401, pp. 247-251.

Uchida K and Shimizu, N, 1991,
The effect of temperature and voltage on polymer chain scission in the High-Field region
IEEE Trans. Electr. Insul., 26, 271-277.

Vansco, G.J., Allston, T.D., Chun, I., L., Liu, G., and Smith, P., (1996)
Surface Morphology of Polymer Films Imaged by Atomic Force Microscopy
Int. Journal of Polymer Analysis and Characterisation Vol.3 pp. 89-105

Wang, X., Tu, D., Tanaka, Y., Muronaka, T., Takada, T., Shinoda, C., and Hashizumi, T. (1995)
Space Charge in XLPE Power Cable under dc Electrical Stress and Heat Treatment.
IEEE Transactions on Dielectrics and Electrical Insulation. Vol.2 No.3 pp 467-474.

Weisendanger, R. (1994)
Scanning Probe Microscopy and Spectroscopy,.
Cambridge Press. ISBN# 0521428475.

Zebouchi, N., Hoang, T.G., and Ai, B. (1997).
Thermoelectronic Breakdown with pressure and Space Charge Effects in Polyethylene
Journal of Applied Physics. Vol. 81, No.5, pp. 2363-2369.

Zeller. H.R., Pfluger. P. and Bernasconi. J. (1984).
IEEE Transactions on Electrical Insulation. EI-19(3), pp. 200-204

Zhurkov S N, 1965,
Kinetic concept of the strength of solids
Int. J. Fracture Mechanics, 1, 311-323.

Zhurkov. S.N and Tomashevskil. E.E. (1966).
Proceedings, Conference on the Physical Basis of Yield and Fracture, Oxford.
Institute of Physics and Physical Society, Conference Series No.1, p.200.

Zhurkov. S.N. and Korsukov. V.E. (1974).
Atomic Mechanism of Fracture of Solid Polymers.
Journal of Polymer Science: Polymer Physics Edition. Vol.12, pp385-398.

Zhurkov. S.N., and Zakrevskyi. V.A. (1972).
Mechanism of Submicrocrack Generation in Stressed Polymers.
Journal of Polymer Science A2, Vol.10, pp. 1509-1520.

Zhurkov. S.N., Novak. I.I. and Vettegren. V.I., (1964).
Dokl. Akad. Nauk SSSR, Vol. 6, p.1431.

Zhurkov. S.N., Tomashevskil. E.E. and Savostin. A. (1964).
Dokl. Akad. Nauk SSSR, Vol. 159, p. 303.

Zhurkov. S.N., Tomashevskil. E.E. and Zakrevskyi. V.A. (1964).
Soviet Physics Solid State, (English Translation), Vol. 6, p. 1508.

Appendices

Appendix A
Investigation of the structural changes in LDPE and XLPE induced by high electrical stress.

Paper presented to the Eighth International Conference, Dielectric Materials, Measurements and Applications, organised by the Institute of Electrical Engineers, Heriott Watt University, Edinburgh, UK. 17-21st September 2000. Pages 403 –407.

Appendix B
The Interpretation of tapping mode images of polymer surfaces in Atomic Force Microscopy.

Paper presented to the 10th International Conference on Electrostatics, organised by the Institute of Physics, Cambridge, UK. 28–31st March 1999. Pages 403-406.

Appendix C
Measuring static charges by scanning probe microscopy.

Paper presented to the 10th International Conference on Electrostatics, organised by the Institute of Physics, Cambridge, UK. 28–31st March 1999. Pages 377-380.

Appendix D
Additional Equipment Constructed.

Appendix D

Appendix D

Additional Equipment Constructed.

During the preliminary work concerned with this thesis equipment was constructed in order to allow the use of Scanning Probe Microscope probes as electrodes. The objective was to use the sharp probe tip to emulate the small scale protrusions found at the interface region between the bulk XLPE insulator and the semi-con layer covering the conductor core. In order to do this a technique and equipment was required that would allow the positioning in the X, Y and Z planes of a fragile probe with the dimensions as shown in figure 1 with an accuracy of +/- 0.5 nm.

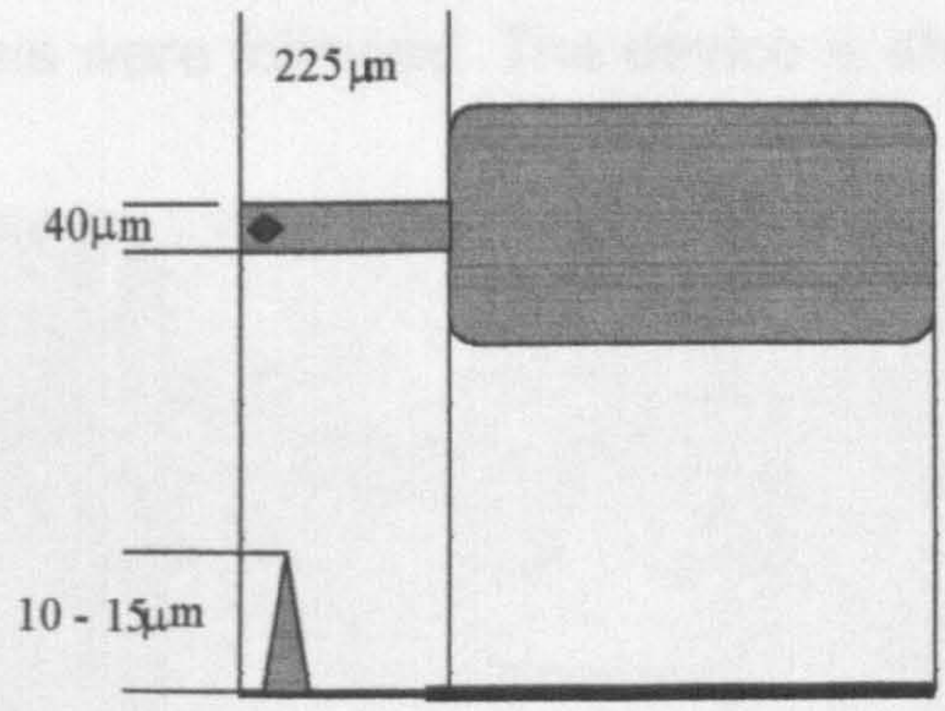

Figure 1 Plan and Elevation of a typical probe assembly.

Any economically available commercial system proved to be unable to handle the positioning of the probe without causing terminal damage to the probe. It was therefore decided to construct a device similar to that used to control the position of the probe in commercial SPM equipment. The design involves the reflection of a laser beam off the top surface of an SPM cantilever probe and the use of a quadrant photodiode to monitor movements of the reflected laser beam due to the deflection of the cantilever (see section 4.2). In addition as the device would have to be computer controlled it would also have to be built

using available PC resources and commercially available analogue to digital and digital to analogue interface boards. The design and programming of the computer control system program was also completed by the author. The system was constructed and met the required specification. In practice the use of this device to apply high local fields to a sample had to be abandoned due to an unforeseen problem. The high voltage applied to the cantilever resulted in the emission of both charge and particles from the sharp edges of the cantilever which is constructed of silicon. These were found to cover the sample surface and ensure that any further experimental investigations using the Raman Spectrometer or the SPM were rendered invalid. At this point this approach was discarded and the experimental techniques as outlined in the main body of this thesis were followed. The device is shown in Figure 2.

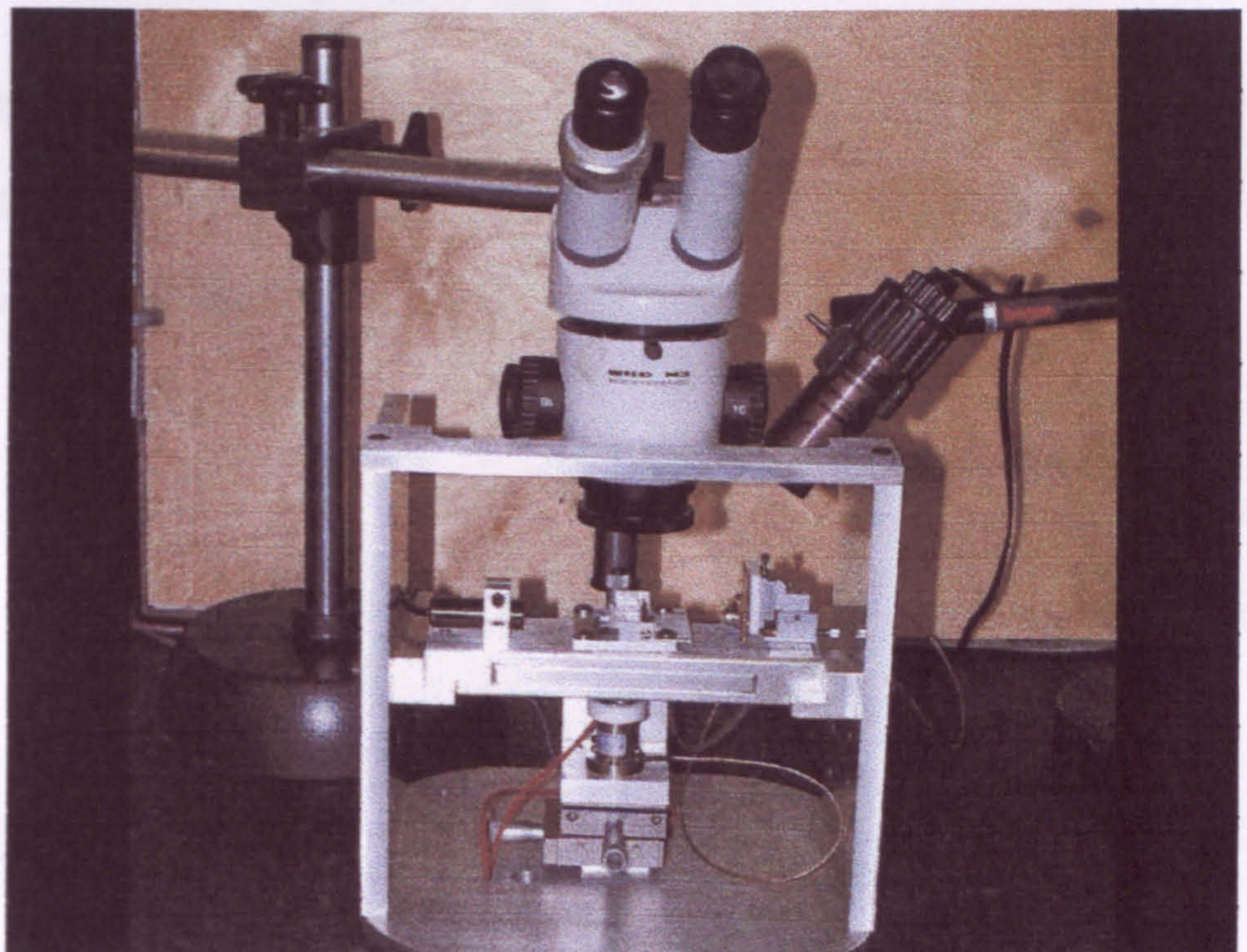

Figure 2 Showing the device constructed to allow the application of high voltages to samples using a SPM probe.

The cantilever probe holder and positioning laser device are shown in detail in figure 3.

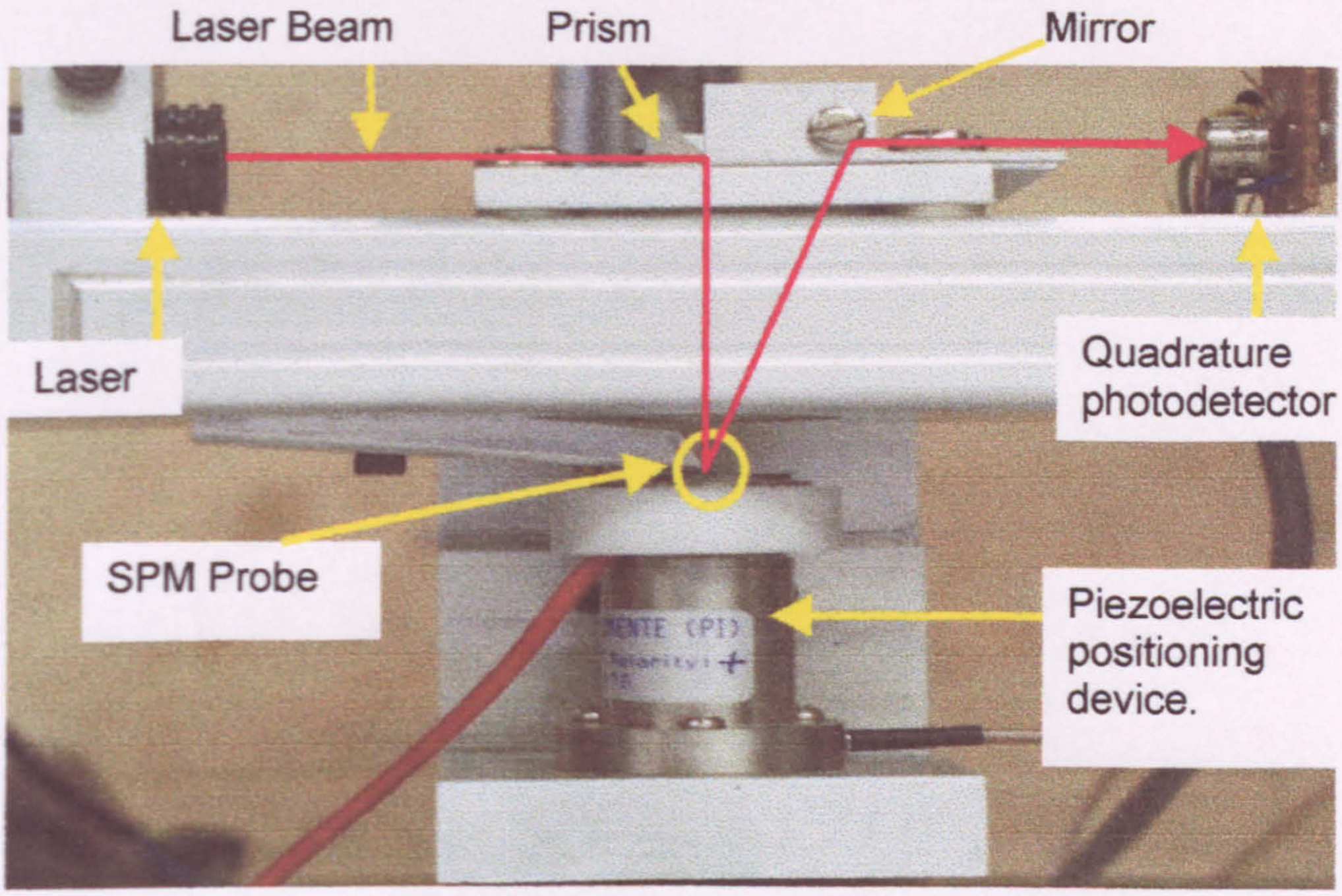

Figure 3 Showing the detail of the device and the laser and general area containing the SPM probe

This can be compared to figure 4.10 in the main body of this thesis. In this case the laser beam was redirected to the back of the cantilever and then back up to the photodetector using a prism directly above the probe tip.